

DELFT UNIVERSITY OF TECHNOLOGY

MASTER THESIS

Control of Subsurface Flow

The Effect of Al-OM Interactions on Hydraulic Conductivity

Author:
Remco VIS

Supervisor:
Prof. Dr. Ir. Timo
HEIMOVAARA

*A thesis submitted in fulfilment of the requirements
for the degree of Master of Applied Earth Science*

in the
Department of Geoscience and Engineering

August 2015

Members of the Graduation Committee:

[Prof. dr. ir. Timo J. Heimovaara](#)

Professor of Geo-Environmental Engineering at Delft University of Technology.

[Dr. Boris Jansen](#)

Assistant Professor in soil chemistry at the Earth Surface Science Research Group of the Institute for Biodiversity and Ecosystem Dynamics at the University of Amsterdam.

[Dr. ir. Leon van Paassen](#)

Assistant Professor Geo-Engineering at Delft University of Technology.

[Dr. Claire Chassagne](#)

Assistant professor at Delft University of Technology in the Department of Environmental Fluid Mechanics.

“In a closed system under constant conditions, chemical reactions reach equilibrium given sufficient time, and the concentrations of reactants and products become constant. However, natural systems are open and receive continual inputs of energy. Many reactions are far from equilibrium. Life on Earth is made possible by the slowness of these reactions”

Edward Tipping (2002)

DELFT UNIVERSITY OF TECHNOLOGY

Abstract

Faculty of Civil Engineering and Geoscience
Department of Geoscience and Engineering

Master of Applied Earth Science

Control of Subsurface Flow

by Remco VIS

Control of subsurface flow is important for sustainable water management. It is, for example, a useful tool for the handling of contaminated sites or the reduction of unwanted seepage. In this thesis, the complexation interactions between DOM and Al are successfully used to reduce the hydraulic conductivity of a sand layer. The complexation of Al and DOM and the resulting floc sizes were first analysed with filtrations and a Malvern Mastersizer. According to the scientific standard, approximately 95% of the organic matter precipitated at Al/C 0.03 (i.e. did not pass through a $0.45\ \mu\text{m}$ membrane). It was found that the mean floc size drastically grows between Al/C 0.02 and 0.03. At high Al/C ratios (> 0.05) these flocs were also formed in a sand layer during constant saturated flow. In the two dimensional laboratory set-up, a narrow (1 cm), dark brown layer grew at the contact front of the Al and DOM solutions. It is thought that hydrodynamic dispersion mixes the solutes and therefore changes the Al/C ratio and that the changed Al/C ratio leads to the immobilisation of Al and DOM. EC measurements showed that the small precipitate layer limits further dispersion of Al, and might therefore limit its own growth. Furthermore it was firmly proven that immobilized Al and DOM cause a significant reduction in hydraulic conductivity. Firstly, the average hydraulic conductivity was reduced to 38% of its original value, after which it was reduced to 23% in a second experimental phase. The local reduction in hydraulic conductivity in the precipitate layer was estimated to be 4 orders of magnitude.

Acknowledgements

During the eight months I have worked on this thesis, it has truly become something I am proud of. That would not have been possible without the people who supported me during this time. There are a few people who I would like to thank explicitly for their invaluable time and expertise.

First of all, I would like to thank the four, very diverse, members of my committee who each in their own way contributed a great deal to this thesis. Especially Timo Heimovaara, who never failed to push me slightly of my trajectory and, in his own charismatic ways, always spiked my interests to think a little different the next time. Boris Jansen who proved himself as the main source of knowledge on soil chemistry and with his open but critical view contributed a lot to the scientific merit of this work. But also Leon van Paassen, who shared his great infectious enthusiasm for everything BioGeo and was always prepared to help despite his full schedule. He also pointed me directly to Claire Chassange, who's knowledge on the behaviour of suspended particles and flocculation made her an invaluable last member of this committee.

Then, I would like to thank André van Turnhout for his advice on modelling and Michael Afansyev for his thoughts on the experimental set-up. I would also like to thank the laboratory support staff at the TU Delft: Han de Visser, Jolanda van Haagen and Marc Friebel, who helped to make the experiments possible. Furthermore I would like to thank Deltares for the use of the Malvern Mastersizer in their laboratories.

And last but not least, I would like to thank my family and girlfriend who tolerated my absence and stories about organic chemistry.

Contents

Abstract	ii
Acknowledgements	iii
Contents	iv
List of Figures	v
List of Tables	vi
Abbreviations	vii
Symbols	viii
1 Introduction	1
1.1 Nature's Way	2
1.2 Organic Matter, an Engineering Tool	3
1.3 Aluminium	3
1.4 Research Goals	4
1.5 Scientific Relevance	4
1.6 Similar Technologies	5
1.7 Thesis Outline	5
2 Theoretical background	7
2.1 Translocation of Al and Fe in Porous Media	8
2.1.1 Theories on Natural Precipitation and Stability	8
2.1.2 Stability of Aluminium and Iron	10
2.2 Movement of Solutes	10
2.2.1 Darcian Flow	10
2.2.2 Advection and Hydrodynamic Dispersion	12
2.2.3 Reduction of Hydraulic Conductivity	14
2.3 Solute Interactions and Precipitation	16
2.3.1 Mono-nuclear Aluminium Solubility	16
2.3.2 Organic Matter	17
2.3.3 Organic Matter Solubility	18
2.3.4 Bimodality of Functional Groups	19
2.3.5 Combined Mobility of Al and OM	20

2.3.6	Colloid Stability	20
2.3.7	The Donnan Model	23
2.3.8	Kinetics of Specific Binding	24
2.3.9	Equilibrium Chemistry of Specific Binding	26
2.3.10	Theoretical Precipitation Rate	29
3	Model	31
3.1	Comsol Formulation	31
3.1.1	Solute Transport	31
3.1.2	Precipitation	32
3.2	Parameters	32
3.3	Boundary Conditions	33
3.4	Solver	34
3.5	Scenarios	35
	Flow.	35
	Solute transport.	35
	Precipitation.	35
3.6	Limitations	35
4	Materials and Methods	37
4.1	Chemicals	37
4.2	2 Dimensional Flow Experiment	38
4.2.1	Set-up in General	38
	Sample ports.	39
4.2.2	Experimental Cycle	39
	Start.	39
	Reaction.	40
	Rinse.	40
	Falling head.	40
4.2.3	Average Falling Head Analysis	41
4.2.4	Local Conductivity Reduction Analysis	42
	Falling head scenario 1:	43
	Falling head scenario 2:	43
	Falling head scenario 3:	44
4.3	Supporting Experiments	44
4.3.1	Titration	44
4.3.2	Filtration	45
4.3.3	Mastersizer	46
4.3.4	Coupling pH and EC to Al/C	47
	Sample preparation.	48
	Correction of the EC data.	48
4.3.5	Predicting EC and Al/C Macro-conditions	50
5	Results and Discussion	51
5.1	Preliminary Experiments	51
5.1.1	Titrations	51
5.1.2	Quantification of Precipitation	53

5.1.3	Floc Size Analysis	53
5.1.4	EC and pH	54
	EC analysis.	55
	pH analysis.	56
5.2	Flocculation in a Porous Medium	59
5.2.1	Visual	59
	First experimental cycle.	60
	Second experimental cycle.	60
5.2.2	Model Results	60
5.2.3	EC and pH, Measurements of Macro Conditions	62
5.2.4	Falling Head	65
	Average conductivity reduction.	65
	Model Analysis	67
6	Conclusion	69
7	Recommendations	71
7.1	The Use of Different DOM Sources	71
7.1.1	On Future Selection of DOM	71
7.2	Improvements for the 2D Laboratory Set-up	72
7.2.1	Continuous Measurements	73
7.2.2	Structural Changes	73
7.2.3	Changes in Flow and Measurement Cycle	74
7.3	Model	75
A	Results From the Floc Size Analysis	77
B	Datasheets	80
C	pH Curve Displacement	82
D	Parameters for NICA-Donnan	83
E	Complementary Model Plots	84
F	Falling Head Data	85
	Bibliography	87

List of Figures

1.1	Introduction to Seepage	1
1.2	Podzol Profile	2
2.5	Donnan potential vs. solubility	25
3.1	Ramp Functions Comsol	32
3.2	Boundary Conditions 2D Model	34
4.2	2D flow set-up	40
4.3	Falling Head	41
4.4	Falling Head Analysis Explanation	43
4.6	pH/EC calibration	49
5.1	Coagulation in a beaker	52
5.2	Floc Size Analysis	55
5.3	pH/EC calibration	56
5.4	EC analysis.	57
5.7	Reactive Flow	61
5.8	Precipitation Predictions	62
5.9	EC, Al/C and DOM Predictions in 2D	63
5.10	Cumulative Outflow of the Falling Head Test	66
5.11	Flow Lines for Conductivity Scenarios	67
7.1	Alternative EC measurements	74
7.2	Propositions for a better Set-up	75
A.1	Floc size analysis	77
A.2	Floc size distribution plots	79
D.1	Parameters for NICA-Donnan	83
E.1	Modelled Flowlines for the Reactive Flow	84
F.1	Falling head: Measured cumulative outflow	85
F.2	Falling head: Measured pressure change over time	86

List of Tables

2.1	Hydrolysis constants aluminium	16
2.2	Devison of directly available organic carbon sources	18
2.3	Elemental composition goundwater and soil humic and fulvic acids	18
2.4	Values for the constant b in the Donnan model	23
3.1	Parameters and Initial Conditions	33
3.2	Boundary Conditions of the COMSOL Model	34
4.1	Average Conditions Flow Model	44
4.2	Dissolved constituents of the DOM stock solution at pH 4.0	45
4.3	EC Correction Factors	47
4.4	Ionic Strength	48
4.5	EC Correction Factors	49
5.1	Precipitated MO Fractions	54
5.2	pH Measurements Reactive Flow	64
5.3	EC Measurements Reactive Flow	65
5.4	Boundary Conditions Flow Model	67
C.1	pH Displacement by Humic Acid Sodium Salt	82

Abbreviations

Al	Aluminium
DOM	Dissolved Organic Matter
DeMi	De- Mineralized
HA	Humic Acid
FA	Fulvic Acid
NICCA	Non Ideal Consistent Competitive Adsorption
NOM	Natural Organic Matter
OM	Organic Matter
SOM	Soil Organic Matter
WHAM	Windermere Humic Aqueous Model

Symbols

κ	Permeability	$[m^2]$
μ	Viscosity	$[Pa \cdot s]$
∇	Nabla operator	$[1/m]$
ϵ	Porosity	$[m^3/m^3]$
ρ	Density	$[kg/m^3]$
θ_w	Volumetric water content	$[m^3/m^3]$
D_m	Molecular diffusivity	$[m^2/s]$
R_S	Solute radius	$[m]$
α_l	Longitudinal dispersivity	$[m]$
α_t	Transversal dispersivity	$[m]$
ψ_D	Donnan potential	$[V]$
V_D	Donnan volume	$[l/kg]$
R	Universal gas constant	$[J/molK]$
F	Faraday's constant	$[coulomb/mol]$
Γ	Electrical conductivity	S/cm

Chapter 1

Introduction

In densely populated low-lying deltas, the control of subsurface flow is vital. These areas deal with a variety of challenges among which: control of contaminated plumes, maintaining optimal groundwater levels for agriculture, reclamation of polluted areas, ensuring the structural integrity of dikes and sustaining clean drinking water (e.g. [Short et al., 2010](#); [Buschmann et al., 2007](#); [Dunbar and Britsch III, 2008](#); [De Graaf et al., 2007](#); [Oude Essink et al., 2010](#)). Even though there is a large incentive to manage water properly, sub surface flow is often handled neither cheaply nor elegantly.

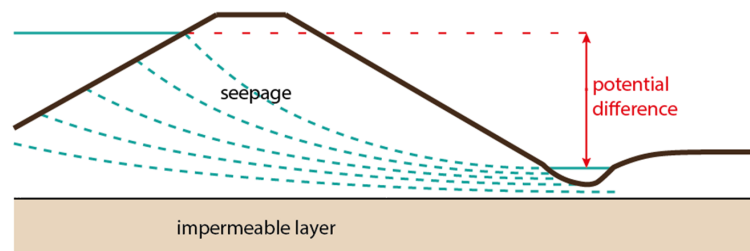


FIGURE 1.1: A cross section showing the seepage through a dike which is build on an impermeable layer. The difference in potential between the two water bodies induces seepage through the dike. Seepage contributes to high water levels beyond the dike and in extreme cases it can destroy the dike by preferential flow an tunneling.

Dikes and dams control large open water bodies but their extent into the subsurface is limited. The potential for flow is the pressure or head gradient between the two sides of, for example, a dike, see figure 1.1. In this case, the potential difference causes a constant (unwanted) subsurface flow called seepage. The resistance to flow is determined by the permeability of the soil. Seepage chooses the path of least resistance and is therefore

concentrated in the more permeable areas in and around large infrastructure. In areas where the head gradient can not be controlled, the movement of fluids and their solutes in the subsurface is primarily determined by permeability. Control of permeability therefore inherently is a great tool for subsurface water management. However, the shear scale of most seepage problems makes rigorous and durable management virtually impossible. Seepage is therefore often only controlled to a short extend with large effort.

1.1 Nature's Way

In nature the permeability of soils is variable in time due to the clogging of pores (much like filling the holes of a sieve) and changing soil structure. Decades of gradual change can lead to orders of magnitude permeability reduction. Pozolization is a good example of such a process and serves as a source of inspiration for this thesis. [Lundström et al. \(2000b\)](#) give a comprehensive review on podzolization, a short introduction will be given here.



FIGURE 1.2: An example of a very distinct podzol from the Lüneberger heide in Germany with a typical grey eluvial horizon and a black illuvial horizon. Source photograph: ([Nikanos](#)).

In the pozolization process, silicates and clay minerals dissociate at low pH which leads to the release of aluminium (Al), iron (Fe) and silicium (Si) in the elluvial horizon (E-horizon). The free Al, Fe, organic matter (OM) and Si move down in the soil until their

solubility product is surpassed or they are adsorbed onto solid surfaces. The solutes then accumulate in what is called an illuvial horizon. The existing pore structure in the illuvial horizon is filled with precipitates, organic matter and adsorbed ions (i.e. Al, Fe and Si). This pronounced illuvial layer in podzols can also be called a hardpan, a name which demonstrates its impenetrable character. Although it is subject to great ambiguity the role of dissolved organic matter in the translocation of Al, Fe and Si in podzols is crucial.

1.2 Organic Matter, an Engineering Tool

Dissolved organic matter (DOM) is extremely versatile: it has by far the greatest capacity to immobilize metals (on weight basis) in soils by adsorption and its state (i.e. solid, dissolved or suspended) is controllable in a variety of ways. DOM, for example, forms soluble complexes with metals and thereby also enhances the solubility of those metals (Ferro-Vazquez et al., 2014). However, when the DOM concentration decreases relative to these metal concentrations precipitation occurs (Jansen et al., 2001, 2005). Furthermore, changes in pH, EC and Eh can also be used to control the solubility of the compounds in a metal-DOM solution (Pott et al., 1984; Sauer et al., 2007). If the behaviour of organic matter in the subsurface can be predicted and manipulated, soil permeability can likely be manipulated as well.

Dissolved organic matter can be extracted from plant litter, manure and other sorts of organic material (Tipping, 2002; Matilainen et al., 2010). The sort and usefulness of the obtained DOM is determined by the composition of the litter itself and the extraction method¹. The properties of the produced DOM can be controlled and the source is cheap. DOM is often categorised into two very general groups: fulvic acids (FA) and humic acids (HA). In reality these groups overlap and classification of DOM is subjective. Relative to the molecular size, the charge and reactivity of HA is larger than that of FA.

¹Organic compounds are dissolved by ionizing the functional groups with NaOH. Afterwards they are purified with HCl. The process of extraction and purification is described by various authors (i.e. Veeken et al., 2000; Miikki et al., 1997). These authors also give inspiration for a great amount of source materials from which DOM can be extracted.

1.3 Aluminium

Aluminium and iron form the most rigid complexes with OM (Tipping, 2002) and due to their high valence (i.e. Fe^{3+} and Al^{3+}) they are able to bind more than one organic molecule at a time. These cations thereby connect several organic molecules to form a larger polymer (Chin et al., 1998; Tipping, 2002). These polymers may then flocculate and become insoluble (Nierop et al., 2002). The stable insoluble polymers are interesting for reduction of permeability (see Scheel et al., 2008a,c,b). Iron, however, may change valence according to the oxidation reduction (redox) potential (Eh) of the solution. Due to oxidation it becomes Fe^{3+} , which is known as rust. Its reduced form is Fe^{2+} . The reduced form is more unstable and unlikely to form precipitated complexes (Nierop et al., 2002). The behaviour of Al^{3+} is comparable to that of Fe^{3+} , but the stability of Al-OM complexes is not negatively dependent on the redox potential of the solution (Duan and Gregory, 2003). It is therefore that Al will be the sole cation discussed in this thesis.

1.4 Research Goals

The goal of this research is to give proof of the principle that permeability can be reduced significantly without great mechanical effort. The hardpan of a podzol and the versatility of dissolved organic matter serve as an inspiration based on which the following research questions are posed:

1. Can aluminium-organic complexes be used to selectively reduce permeability under constant saturated flow?
2. Under which measurable macro conditions (pH, EC, shear) does precipitation take place in a porous medium?

1.5 Scientific Relevance

Organic matter is an important subject in soil science (Kalbitz et al., 2000). The type and concentration of (dissolved) organic matter often determine the availability and solubility of nutrients for plants. Moreover, it has great influence on soil structure and

the formation of soil horizons (Kalbitz et al., 2000; Lundström et al., 2000b; Brady et al., 1996). There is, however, debate about how organic matter influences soil formation (e.g. Lundström et al., 2000a). This debate is fuelled by a great amount of studies that either investigate soil formation in situ (e.g. Lundström et al., 2000a; Gustafsson et al., 2001) or study the solution chemistry in a laboratory (e.g. Jansen et al., 2003; Scheel et al., 2008a; Nierop et al., 2002; Temminghoff et al., 1998). The main subject of interest in these studies is the movement of (heavy) metals (Weng, 2002) or the influence of the stability of DOM in soils on the carbon cycle (Kalbitz et al., 2000). Detailed measurements of physical soil models are missing in these approaches. Hence the consequences of metal-organic interactions to soil permeability are mostly neglected and poorly understood. This knowledge about these physical soil processes, however, will probably help to understand the macro-conditions of soil formation much better. Those macroscopic-conditions or 'environmental factors' are recently believed to be orders of magnitude more important than the characteristics of the organic matter itself (e.g. Scheel et al., 2007; Stosser, 2010). This thesis was built around a physical soil model, it aims to couple the knowledge of solution chemistry to the implications this has for permeability.

1.6 Similar Technologies

(Bio)Chemically enhancing soils by solute and microbial interactions is not exclusive to this thesis (e.g. De Jong et al., 2013). Biogrout, for example, can be used to structurally enhance the subsurface by biochemical hydrolysis of urea $CO(NH_2)_2$ and subsequent precipitation with calcium in the form of calcite ($CaCO_3$) (Leon van Paassen, 2009). There are also examples of research groups that use calcite formation to reduce the permeability of the subsurface (e.g. Mitchell et al., 2013). Calcite, however, is very sensitive to solution acidity. Clogging porous media with biota or their gaseous, dissolved or (after further reaction) solid excrements is also widely studied (e.g. Thullner, 2010). These studies report permeability reductions from two orders of magnitude in earlier studies (Vandevivere and Baveye, 1992) to four orders of magnitude in later studies using different substrates (see Seifert and Engesgaard, 2007; Bielefeldt et al., 2002; Holm, 2000). These reductions in permeability are respectable, but dynamic flow path analysis shows that these bioclogs are susceptible to degradation by shear (Sharp et al., 2005).

Next to that, the dead biomass which is built up out of carbon chains is inherently thermodynamically unstable. The Al-DOM complexation technique discussed in this thesis is a new, and potentially stable (Stosser, 2010; Scheel et al., 2007) tool for hydraulic conductivity control.

1.7 Thesis Outline

This thesis consists of seven chapters. **Chapter 2** is a literature review. This chapter in general gives insight in the movement of organic matter and aluminium in soil solutions. It also demonstrates the discontinuity that exists between the fundamental theory and experimental studies. In section 2.1 the fundamental theory behind flow and the advection, dispersion and diffusion of solutes will be discussed. In section 2.2 the quantifiable theory behind the interaction of dissolved organic matter and metals in simple solutions will be reviewed. In section 2.3 the scientific debate about the role of organic matter in 'real' soil solutions will be discussed. In **Chapter 3**, the theories of chapter 2 are molded into a COMSOL model based on which predictions are made for the outcome of the experiments. **Chapter 4** consists of a detailed description of the materials and methods that were used to set up the two-dimensional flow experiment and all necessary calibrations and prior experiments. In **Chapter 5**, the results of the experiment are given and discussed and compared to the model output. **Chapter 6** is the conclusion in which an answer will be provided to the research questions posed in **Chapter 1**. **Chapter 7** is a short report about what should be done to continue this research in light of the SoSEAL project that will start shortly after this thesis.

Chapter 2

Theoretical background

Foreword. This research aims to significantly reduce sub surface flow by inducing a precipitation reaction between two solutes. An overview will be given about the fundamental theory behind flow, advection, diffusion, dispersion and precipitation of Al and DOM. This is necessary to understand the parameters that can, but also the parameters that cannot be influenced. Figure 2.1 is a graphical representation of the processes that lead to the reduction of permeability.

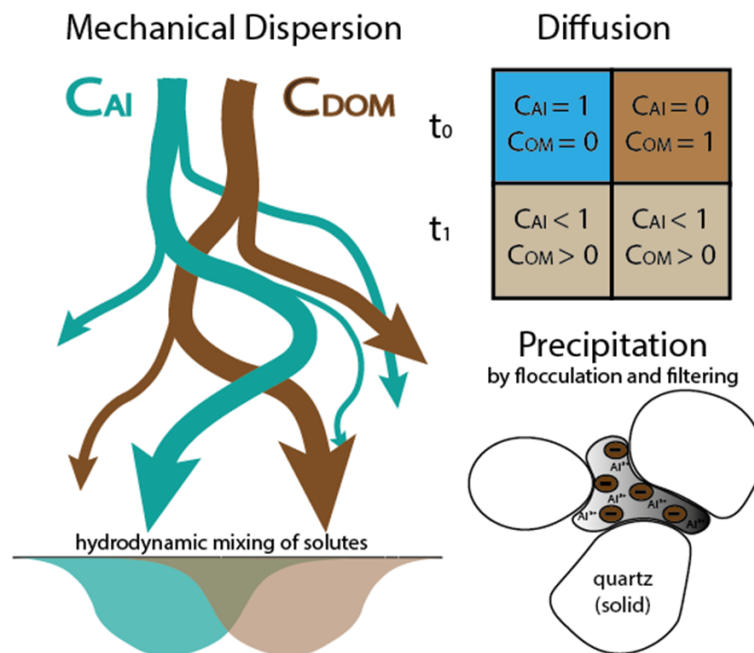


FIGURE 2.1: Mechanical dispersion and diffusion of particles together lead to hydrodynamic mixing. The dissolved aluminium and suspended organic matter flocculate causing precipitation.

2.1 Translocation of Al and Fe in Porous Media

Before diving into a more mathematical approach to translocation and precipitation theories and their fundamentals, it is important to appreciate the practical behaviour of metal organic complexes in the subsurface. The theories that are the result of experimental studies in soil science and waste-water treatment will be discussed here shortly.

2.1.1 Theories on Natural Precipitation and Stability

Impermeable precipitate layers formed by OM, Fe or Al or combinations thereof can be found in several natural environments. Bog iron, for example, is formed in bogs and marshes by the aeration of Fe(II) rich (ground)water. The iron generally precipitates as goethite (FeO(OH)) forming a solid layer. The same process can occur in groundwater solutions (Kaczorek et al., 2004). At places with exceptionally high iron contents (e.g. mine sites, bogs but also enriched soil horizons), the process of iron fixation by oxidation is stimulated by iron fixating bacteria like *T.Ferroxydans* and *L.Ochracea* (Crerar et al., 1979). However the most apparent phenomenon where Fe, Al and OM are incorporated in an impermeable layer is the spodic horizon of a podzol. The formation of spodic horizons is not necessarily bound to the oxidation state of the material, but mostly a function of the concentrations of Al, Fe, DOM and H⁺ and their mobility in the soil. The mobilities of Al, Fe and OM will be discussed in detail, see section 2.3.

The translocation of metals and the stability of organic matter in soils have been important subjects of research for decades. During these decades 6 accepted theories have been developed to explain the solubilization and 'sudden' precipitation of sesquioxides (oxides of Al, Fe and Si) (e.g. Lundström et al., 2000a,b). Most authors believe that the translocation of sesquioxides is governed by interactions with DOM (e.g. some early works Petersen, 1976; De Coninck, 1980; Mokma and Burman, 1987), even though a debate exists about the exact mechanisms (van Hees et al., 2000). The most important theories that describe the translocation and subsequent immobilization of OM and Al in insoluble organo-metallic complexes are:

1. *Classical Fulvate theory*: According to this theory OM dissolves and forms soluble organo-metallic complexes in the soil, it thereby initially also increases the solubility of the associated metals. While moving downward through the soil column, the

complex becomes saturated with Al, which leads to a neutralization of the negative charge of the organic particle. The neutral particle then precipitates (Petersen, 1976; De Coninck, 1980; Sauer et al., 2007).

2. *Low Molecular Weight theory*: LMW theory states that the organic part of the complex is degraded by micro-organisms and that this degradation leads to over saturation of the complex (Lundström et al., 2000b; Sauer et al., 2007).
3. *Co-precipitation*: This theory is more or less complementary to the first two theories. It states that organic matter mainly precipitates due to co-precipitation with metal hydroxides (Gustafsson et al., 2001; Sauer et al., 2007). This kind of aggregate formation is also called sweep flocculation. In this theory precipitation is also governed by changes in the same solution chemistry, but transgression of the metal solubility product is necessary. Organic molecules adsorb to the freshly formed insoluble metal surfaces and by these interactions they become immobilized as well. Changes in pH or total metal concentrations may cause metalhydroxide precipitation and thereafter, DOM readily adsorbs to the freshly formed insoluble phases.¹

These hypothesis are decades old, but apparently correct since they are still widely used to explain translocation and podzolization phenomena in organic rich soils (e.g Sauer et al., 2007; Jankowski, 2014; Bourgault et al., 2015; Banik et al., 2014; Angelico et al., 2014). The first two theories are based on metal-organic (MO) complex translocation. The theoretical mechanism for dissolution of metals in these theories matches well with the data of (Lundström, 1993) and (Sauer et al., 2007) who found that 80 to 85 percent of Al and Fe in an E horizon binds to OM. Lundström et al. (2000b), in a later article, state that in natural environments these soluble organic complexes come into the soil solution in the O and A horizon by degradation of litter and exudation of OM by roots, fungi and microbes. Metal translocation and precipitation by OM complexation is supported by laboratory experiments (Nierop et al., 2002) as well as field studies (Guggenberger and Kaiser, 2003). Nierop et al. (2002) did stepwise titration experiments to give proof of the complexation and precipitation of organo-metallic complexes. In these experiments the Al, Fe(II) and Fe(III) concentrations were simultaneously increased to investigate

¹Three other accepted theories have been formulated next to the three theories described here, these additional theories are summarized in the review article of Lundström et al. (2000a). These theories are not relevant to this thesis.

the competition for binding sites, he concluded that: i) precipitation reactions occurred at an M/C ratio of 0.03 and ii) that Al was dominant at higher M/C ratios. Jansen *et al.* separated the metals and looked at the specific speciation of metal in combination with organic matter and found similar results (Jansen *et al.*, 2004).

2.1.2 Stability of Aluminium and Iron

In a recent study, Grand and Lavkulich (2011) study podzolization and state that: 'In the organic layer, organically complexed Fe forms correlate negatively with soil organic carbon', whereas 'complexed Al did not show the same negative association', which suggests that iron forms less stable insoluble complexes. The group of Temminghoff *et al.* studied metal organic complexation with a wider range of bivalent and trivalent cations in controlled solutions and found that OM preferentially binds with trivalent cations i.e. Al and ferric iron (Fe(III)) (Weng, 2002; Temminghoff *et al.*, 1998). Nierop *et al.* found similar results but also stated that the complexes of ferrous iron (Fe(II)) are soluble regardless of pH and M/C ratio (Nierop *et al.*, 2002), although the organic complex binds stronger with Fe(III) compared to Al (Tipping, 2002). The inherent solubility of the complexes formed with Fe(II), which is apparent from these studies, also makes them less resistant to biodegradation (Boudot *et al.*, 1989; Scheel *et al.*, 2008a; Banik *et al.*, 2014). Therefore, the solubility and stability of Fe-OM precipitates is largely dependent on the oxidation-reduction potential (Eh). In anoxic environments, e.g. deep saturated soils, Fe will be present as Fe(II) either soluble or in an unstable complexes. Moreover, even if stable Fe(III)-OM complexes are formed they are more prone to degradation. Eusterhues *et al.* (2014) argue that microbial populations not only degrade precipitated Fe(III)-OM, but also reduce the Fe(III) bound to the complex to Fe(II). These findings are supported by the data of Banik *et al.* (2014) who studied the Fe and Al contents in three Bh horizons of podzols. Banik *et al.* conclude that Al is stable in these horizons but 'Fe concentrations diminish with progressive wetness'.

2.2 Movement of Solutes

2.2.1 Darcian Flow

The flow of a fluid through porous media has been described by Henry Darcy in 1856. He conducted column experiments where he induced flow through saturated sands at known pressure gradients (Pinder and Celia, 2006; Darcy, 1856). He assumed that the kinetic potential of the fluid was zero², and that its viscosity and density were constant (Pinder and Celia, 2006; Bernoulli, 1738). Based on those assumptions and his experiments he derived the equation that is now well known as Darcy's law:

$$q = -\frac{\kappa}{\mu} \cdot \nabla p \quad (2.1)$$

Darcy's law describes the relationship between q [ms^{-1}] the fluid flux, κ [m^2] the intrinsic permeability of the porous medium, μ [$Pa \cdot s$] the viscosity of the fluid and ∇p [$Pa \cdot m^{-1}$] the pressure gradient. The average velocity of the fluid through the pores u can be derived from q and the porosity ϵ by:

$$u = \frac{q}{\epsilon} \quad (2.2)$$

In this simple equation, Darcy captured the three most important principles of groundwater flow (Pinder and Celia, 2006; Bear, 2012; Ham, 2006): 1) fluid flows from high pressure to low pressure (hence the - sign); 2) the pressure gradient is the driving force behind sub surface flow and 3) intrinsic characteristics of the fluid and the porous medium determine the resistance against flow.

The theory can mathematically be expanded to take spatial variation in viscosity, density and permeability into account. In order to do this, the law of mass conservation is used to solve Darcy's law numerically by means of a partial differential equation over a predefined volume (Pinder and Celia, 2006; Bear, 2012):

$$\frac{\partial M}{\partial t} = M_{in} - M_{out} \quad (2.3)$$

²The assumption that the kinetic potential is zero is often valid in soils because the velocity of water in soil pores is very small. The validity of the assumption can be checked with Reynolds number.

In which the mass of water in the system is defined as the product of the volumetric water content, θ_w [m^3/m^3], the volume over which the partial differential equation is solved [m^3] and the density of the fluid, ρ_w [kg/m^3].³ The mass change (δM) is due to the gradient (δh) which is equal to the pressure head, $\delta\psi$ (because the volume has a fixed location). The in- and outflow of mass can be expressed as the divergence in flux q . Combining all the above terms with a source term Q_m yields the so called groundwater flow equation:⁴

$$Q_m = \frac{\partial}{\partial t}(\rho\epsilon) + \nabla \cdot (\rho u) \quad (2.4)$$

Darcy, however, only described the direction and magnitude of fluid flow in general. Following the migration of fluid particles through the subsurface is more complex.

2.2.2 Advection and Hydrodynamic Dispersion

The movement of groundwater and its solutes can mathematically be described by two fundamental principles: *advection* and *hydrodynamic dispersion*. Therein *advection* is the movement particles in the principal direction of flow. Therefore, if only advective translocation is considered, the concentration change can be defined as (Bear, 2012; Pinder and Celia, 2006)

$$\frac{\partial C_i}{\partial t} = u \cdot \nabla C_i \quad (2.5)$$

In which C_i is the solute concentration [mol/l] and ∇ is the gradient operator in three dimensions. Movement of particles relative to the advective flow is called hydrodynamic dispersion. Due to hydrodynamic dispersion, particles spread rather than moving forward together. Hence, if a cloud of tracer particles is injected into a constant flow, the shape and size of the resulting plume changes together with the concentration of the particles (see figure 2.2). This can be described by Fick's second law (Fick, 1855):

$$\frac{\partial C_i}{\partial t} = \nabla \cdot (D \cdot \nabla \cdot C_i) \quad (2.6)$$

The D in Fick's law refers to the diffusivity. In case of groundwater flow this term has to be modified to the hydrodynamic dispersivity. *Hydrodynamic dispersion* is a combination of two principles: *molecular diffusion* and *mechanical dispersion*. Molecular diffusion

³Since Darcy's law only deals with saturated flow the volumetric water content is always equal to the porosity.

⁴The one dimensional derivation can be found in Appendix A

and mechanical dispersion are the greatest contributors to hydrodynamic dispersion, but [Bear \(2012\)](#) and [Pinder and Celia \(2006\)](#) together list seven other influences on hydrodynamic dispersion. For the sake of simplicity these will be neglected.

Molecular diffusion was first described by Robbert Brown. He observed that suspended particles are always in motion and that this motion is purely driven by the particles themselves ([Brown, 1828](#)). The driving force behind diffusion is the concentration gradient. The speed of the diffusion is governed by the diffusivity, D_m [m^2/s]. This is purely a characteristic of the solute. D_m can be calculated with the Stokes-Einstein Model based on the viscosity of the solvent μ and the radius of the solute R [m] ([Einstein, 1905](#)). The values for D_m at different solutes and solvent combinations can also be found in tables. For water they typically range from $10^{-9}\text{m}^2/\text{s}$ to $5 * 10^{-9}\text{m}^2/\text{s}$ ([Cussler, 2009](#)). Because the diffusivity is so low the transport by molecular diffusion is only important at negligible flow rates.

Mechanical dispersion is a physical process which is dependent on the pathway that particles choose through the porous medium ([Ham, 2006](#)). The movement of a solute due to mechanical dispersion is therefore related to the characteristics of the porous medium and dependent of the Darcian flow velocity (u). Mathematical descriptions of mechanical dispersion are complex; there are multiple theories which describe this process. It is therefore impossible to give a single clear expression for mechanical dispersion within the scope of this thesis. Philip Ham, however, describes this subject at length in the second chapter of his PhD thesis ([Ham, 2006](#)). For this research, the physical soil characteristics that lead to mechanical dispersion are generalized to two parameters: the longitudinal dispersivity α_l [m] and transversal dispersivity α_t [m]. In engineering scenarios it is often assumed that $10\alpha_t \leq \alpha_l$ ([Ham et al., 2004](#); [Bear, 2012](#)). The longitudinal mechanical dispersion α_l can empirically be expressed as a function of the length of the flow path, L [m] ([Bear, 2012](#), and references therein):

$$\begin{aligned} \alpha_l &= 0.017L_s^{1.5} & \text{for } L_s \leq 100m \\ \alpha_l &= 0.32L_s^{0.83} & \text{for } L_s > 100m \end{aligned} \tag{2.7}$$

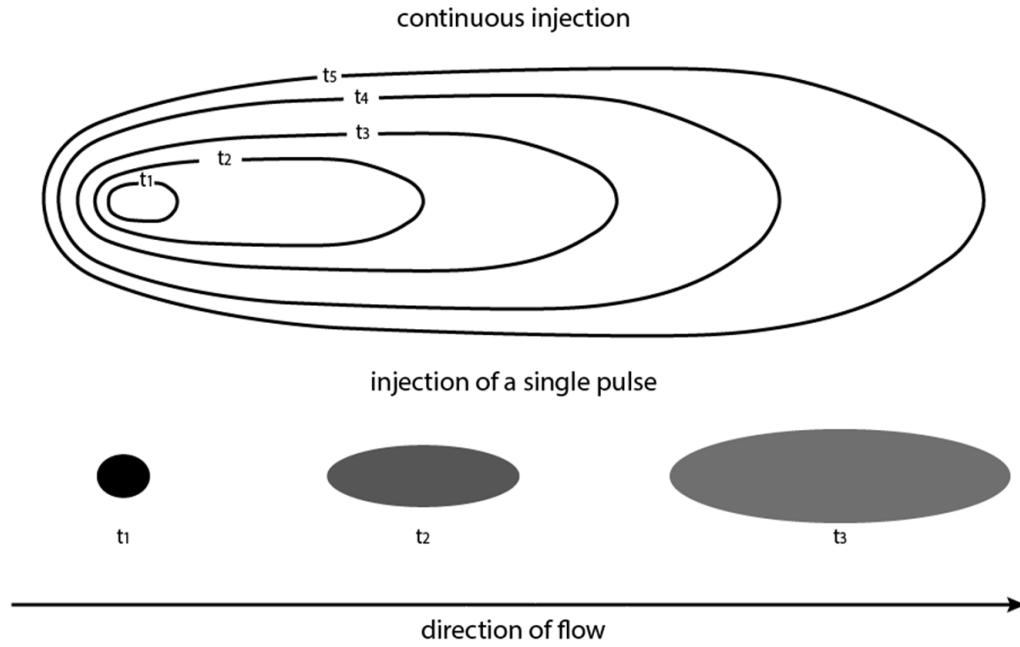


FIGURE 2.2: A graphical representation of hydrodynamic dispersion. The top figure shows a plume that is created at large constant flow. If there were no hydrodynamic dispersion the plume would merely be stretched. With hydrodynamic dispersion, however, there is movement perpendicular to the direction of flow and the lateral extent of the plume is also larger. It is important to realize that, although the principle is the same, the shape of the plume is dependent on the velocity of flow and the properties of the solute and the porous medium. The bottom figure schematically demonstrates the progression of a single pulse in time at constant flow. The shape of the solute concentration as well as the concentration itself changes over time. The largest concentrations are however still found in the center of the plume.

With these assumption the mechanical dispersion can be expressed in terms of α and the Darcy velocity (\vec{u}) according to:

$$D_{\text{MECHANICAL}} = \alpha |\vec{u}| \quad (2.8)$$

Where α changes depending on the evaluated direction. Hydrodynamic dispersion can be expressed as:

$$D_{\text{HYDRODYNAMIC}} = D_{\text{MOLECULAR}} + D_{\text{MECHANICAL}} \quad (2.9)$$

With the use of Darcy's law and Fick's second law (the standard diffusion equation) convection can be coupled to hydrodynamical dispersion in the advection dispersion equation (ADE). The spreading of trace concentrations in porous media can then be

described by the ADE (Pinder and Celia, 2006; Ham, 2006):

$$\frac{\partial C_i}{\partial t} + u \cdot \nabla C_i + \nabla \cdot (D \cdot \nabla C_i) = R_i + S_i \quad (2.10)$$

In the ADE, R_i and S_i are a reaction and a source-sink term respectively. The *molecular diffusivity* in Fick's law is replaced by the hydrodynamic dispersivity ($D_{\text{HYDRODYNAMIC}}$). It can easily be deduced that advection, dispersion and subsequent reactions are coupled processes, hence one cannot be solved without solving the other.

2.2.3 Reduction of Hydraulic Conductivity

The hydrodynamic mixing of solutes may lead to precipitation reactions after which the precipitates can clog the pores as was seen in section 2.1. Reduced porosity will lead to a reduced permeability which influences the permeability. The change in permeability can be related to porosity empirically in the form of (Bear, 2012)

$$\kappa_r = \kappa \cdot \left(\frac{\phi_{act}}{\phi_{max}} \right)^n \quad (2.11)$$

Where ϕ_{act} is the reduced porosity and n is a parameter which is dependent on the characteristics of the porous medium. The Kozeny Carman equation, which is widely used to estimate hydraulic conductivities in soils, can also be used to relate hydraulic conductivity to porosity (Fitts, 2002).

$$K = \left(\frac{\rho_w g}{\mu} \right) \left(\frac{\phi^3}{(1-\phi)^2} \right) \left(\frac{(D_{50})^2}{180} \right) \quad (2.12)$$

This formula also incorporates the mean of the grain size distribution (D_{50}) [m] and the viscosity of the fluid phase, μ , and is dimensionally consistent. Assuming that the fluid phase has a constant viscosity and density the relative permeability based on the Kozeny Carman equation can be written:

$$\kappa_r = \kappa \cdot \frac{\left(\frac{\phi_{act}^3}{(1-\phi_{act})^2} \right)}{\left(\frac{\phi_{max}^3}{(1-\phi_{max})^2} \right)} \quad (2.13)$$

Note: Expressing the relative permeability only as a function of porosity is a crude estimate that may only work at relatively large scale (i.e. several orders of magnitude larger than individual pores). Predicting the reduction of permeability in a fundamental way is a much more diligent task. This is mainly because the shear forces induced by preferential flow paths may break down precipitates but at the same time provide more reactants to stimulate further precipitation. These processes may lead to the development of dynamic preferential flow paths. An experimental example is given by Sharp et al. (Sharp et al., 2005) who use a flat plate reactor with fixed diamond elements as a model of a porous medium and a peristaltic pump to ensure a constant flow rate. With a bulk dye tracer they show that, when the biofilm grows, dynamic preferential flow paths develop after 15 days ⁵.

2.3 Solute Interactions and Precipitation

In this section the source sink term in the ADE 2.10 will be discussed primarily for two species: dissolved aluminium (Al) and 'dissolved' organic matter (DOM). Several models have been developed to describe the mobility of metals in the subsoil which will shortly be discussed. The actual precipitation of complexes can be caused by charge neutralization (a consequence of metal binding) or by flocculation and physical filtering, see figure 2.1.

2.3.1 Mono-nuclear Aluminium Solubility

Aluminium precipitates as aluminium-hydroxide: $Al(OH)_3$. $Al(OH)_3$, which is also known, among others, as the mineral bauxite, is least soluble at pH 6.3 at which $8.3 \cdot 10^{-5}$ M Al is the total aluminium solubility based on mono-nuclear speciation (Duan and Gregory, 2003; Wesolowski and Palmer, 1994). Considering this, the solubility of Al can be written as: ⁶

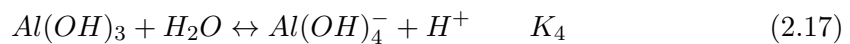
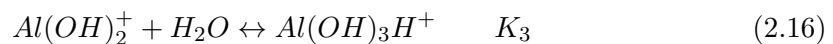
⁵The findings on dynamic flow-paths and permeability are confirmed by the data of Stewart and Fogler (2002) who conducted a similar experiment with a different representation of a porous medium (Stewart and Scott Fogler, 2002). The theory is made comprehensible by Bottero et al. (2013) who modelled the dynamics of preferential flow paths in response to biofilm development and decay, their model shows that the average permeability reaches a 'quasi-constant value' (Bottero et al., 2013). Decay of the clogs, which is in this case biomass lysis, causes shifting numbers and locations of the flow paths.

⁶The formulation of the solubility of aluminium is mainly based on the formulations and constants of ORCHESTRA and the article of Duan and Gregory (2003) (Duan and Gregory, 2003).

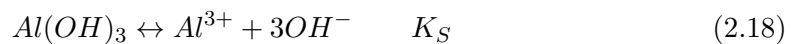
TABLE 2.1: Hydrolysis constants aluminium

pK_1	pK_2	pK_3	pK_4	pK_S
4.95	5.6	6.7	5.6	31.5

The values in this table are from (Duan and Gregory, 2003) and references therein.



To complete the equilibrium a solubility constant for the chargeless metal hydroxide is necessary:



The hydrolysis constants are given in table 2.1. The values of the individual equilibrium constants may vary depending on the literature; there is however general agreement about the total solubility constant pK_S (Wesolowski and Palmer, 1994). When the total aluminium concentration (Al_t) exceeds the sum of solubility of the species at any given pH, $Al(OH)_{3(s)}$ will be formed (see figure 2.3).

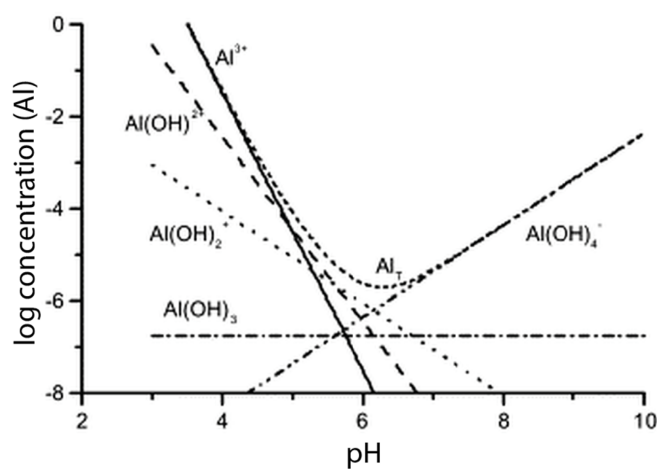


FIGURE 2.3: Solubility and speciation of aluminium as a function of pH based on monomeric hydrolysis of Al^{3+} at 25 degrees Celsius, figure taken from Duan and Gregory 2003 (Duan and Gregory, 2003).

TABLE 2.2: Devision of directly available organic carbon sources

<i>Sort</i>	<i>Pool</i>	<i>tonnes x 10⁹</i>
Unstructured	Seawater	1700
	Groundwater	15
	Surface freshwater	0.5
Structured	Soils	1500
	Terrestrial plants	560

The data are taken from (Moore, 1997; Tipping, 2002, and references therein) and the structural devision was suggested by (Zsolnay, 2003). These are mostly approximate values based on estimates for groundwater and soil volumes and their average carbon concentrations.

2.3.2 Organic Matter

About nine percent of directly available carbon is in organic forms and can be found in the shallow biosphere (Meyers, 1994; Tipping, 2002). This organic matter (OM) can be divided into structured and unstructured OM. Structured OM is solid and has a clear shape (i.e. resembling its origin) and can mainly be found incorporated in sediments or in soils. Unstructured OM can be found in the hydrosphere as, for example, waste water, seawater or soil solutions (Zsolnay, 2003), see table 2.2. According to the International Humic Substances Society (IHSS) 50% of this directly available OM can be classified as humic substances.

The humic substances can be divided further into three subgroups: Fulvic Acids (FA), Humic Acids (HA) and humin (see IHSS). HAs by definition are the subdivision in humic molecules that precipitate at pH 2 or less, whereas FAs stay in solution below pH 2. The extraction methods for DOM therefore depend on target molecules (i.e. HA or FA) and the source material (i.e. structured or unstructured). These methods are systematically given by Tipping in figure 2.1 and 2.2 of his book, see (Tipping, 2002). The source and sort of humic substance greatly determines its elemental composition, see table 2.3. The molecules of humic substances can range in molecular weight from approximately 500 to 5000 g/mol (Thurman, 2012; Stosser, 2010). HA molecules are generally larger and more aromatic than FA molecules (Tipping, 2002).

2.3.3 Organic Matter Solubility

Organic molecules can often be seen without the use of a microscope, hence a solution of DOM is often coloured and frequently looks like a suspension. Dissolved organic

TABLE 2.3: Elemental composition groundwater and soil humic and fulvic acids

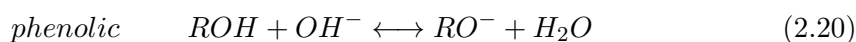
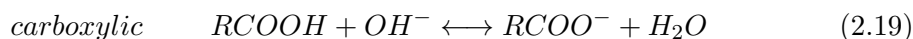
<i>Humic compound</i>	<i>C</i>	<i>H</i>	<i>O</i>	<i>N</i>	<i>S</i>
Soil HA	52.8-58.7	2.2-6.2	32.8-38.3	0.8-4.3	0.1-1.6
Soil FA	40.7-50.7	2.8-7.0	39.7-49.8	0.9-2.3	0.1-2.6
Groundwater HA	65.5	5.2	24.8	2.4	1.0
Groundwater FA	60.4	6.0	32.0	0.9	0.7

Table redrawn from (Tipping, 2002).

matter therefore refers the fraction of OM that passes a 0.45 μm (or 0.10 μm depending on preference and purpose) filter after it is suspended in water (Zsolnay, 2003). In this thesis the 0.45 μm norm is used because practically larger OM fractions travel less easily through porous media. The rest of the OM is then by definition suspended rather than dissolved. This fraction is called particulate organic matter (POM).

When considering a solution the solubility of OM mainly depends on the ionization of its functional groups (Zsolnay, 2003). Hence, the amount of functional groups relative to the size of the organic molecule is inherently also important for the solubility of the OM, independent of its interactions with metal ions (Scheel et al., 2008a). Intrinsic characteristics of the (D)OM like aromaticity and the C/N ratio, to a lesser extent, also influence DOM solubility but to a greater extent the stability of the precipitated complex (Kalbitz et al., 2000; Scheel et al., 2007, 2008a,c,b). Large, stable OM is less likely to become soluble and less prone to decompose.

The pH of the solution plays an important role in the variable solubility because functional groups are ionized in water by OH^- . They then form the polyelectrolytes carboxylate and hydroxylate (Reemtsma et al., 2008; Weng, 2002):



High pH levels result in ionization which will increase the solubility of the organic molecule. The phenolic functional groups are *weak acids* which dissociate at high pH (say 7-9) whilst the carboxylic groups are *strong acids* which dissociate at low pH (say 3-5). The ionic groups (i.e. RCOO^-) that are formed as a result of proton dissociation can interact with coordinated water molecules. This interaction makes the molecule more hydrophilic.

2.3.4 Bimodality of Functional Groups

The type of ligand (i.e. functional group) is very important for the strength and type of bonds. Metal ions can bind to two kinds of functional groups on the organic molecule: *carboxylic groups* and *phenolic groups*. These groups each have their own characteristics, phenolic groups tend to bind metals in a pH range of 7 to 9, whereas carboxylic groups bind metal ions in a pH range of 3 to 5 (Christensen et al., 1998; Milne et al., 2001; Tipping et al., 2011). This is mainly because phenolic groups bind more strongly (inner-sphere) and can therefore less easily dissociate. In other words: at high pH levels the hydrogen ions start to dissociate from the phenolic group, the metals can then easily bind to the organic matter. In this case, even minute concentrations of metal ions can be strongly bound and will only dissociate from the complex if the solution becomes very acidic. Carboxylic groups behave oppositely: they dissociate easily (mostly outer-sphere bonds) and are therefore very prone to changes in pH or metal concentrations.

2.3.5 Combined Mobility of Al and OM

Complexation of Al and DOM happens within minutes after the solutes are mixed (Plankey and Patterson, 1987; Pott et al., 1984; Sauer et al., 2007). It potentially changes the solubility of both OM and Al relative to the single species solubility discussed above (Edzwald and Van Benschoten, 1990; Weng, 2002; Jansen et al., 2003). Jansen et al. (2003) made a DOM from the Oh horizon of a Fimic Anthrosol using nano-pure water. They made separate solutions and adjusted the pH of the solutions to 3.5, 4 and 4.5 respectively. These DOM solutions were used to study the speciation of Al and DOM as a function of the molar Al/C ratio. Jansen et al. accurately demonstrated that the insoluble complexation is dependent on both the Al/C ratio and pH, see figure 2.4. From figure 2.4 it is clear that there is a sudden increase in insoluble complexation at Al/C 0.03. This phenomenon was also observed by Temminghoff et al. (1998), who concluded: 'the almost total coagulation of humic acid occurs over a very small concentration range' (Temminghoff et al., 1998). Weng *et al.* approached complexation from a physiochemical perspective: they measured complexation as a function of the Donnan potential (ψ_D [V]). In their experiments, Weng *et al.* observed the same sudden increase in precipitates at $\psi_D = -0.08$. They state that the Donnan potential can be calculated from the pH and the known concentrations of cations (Weng, 2002). Therefore, in principle the

Donnan potential is based on the same parameters as a simple Al/C ratio but in its formulation the actual DOM concentration is of little importance. The relationships that were found by Jansen *et al.* were later confirmed by Scheel *et al.* (2007, 2008a,c,b), when they did series of experiments to determine the stability of among others Al-OM complexes against biodegradation.

From the experimental studies stated above it is possible to conclude that, at beaker scale, the complexation of DOM and Al can be explained with 4 main parameters: the absolute concentrations of Al^{z+} and DOM and their characteristics (valence, net negative charge), the Al/C ratio, the pH and the electrical conductivity (EC) (Ferro-Vazquez *et al.*, 2014).

2.3.6 Colloid Stability

Older theories state that polyvalent cations can form bridges between humic ions by direct bonds to form aggregates and thereby explain the precipitation of M-OM complexes. Direct bonds, however, cannot solely explain the sudden increases in insoluble complexation found in later experimental studies (e.g. the experiments in Weng, 2002; Jansen *et al.*, 2003; Ferro-Vazquez *et al.*, 2014), more gradual precipitation would be expected. Colloid stability theories can explain these sudden changes in the behaviour of the entire solution (Angelico *et al.*, 2014). Based on these theories, there are two mechanisms that can explain the precipitation of DOM in presence of Al:

1. The stability of the solution may be compromised by an increase in ionic strength which leads to a decreasing zeta potential and a smaller diffuse double layer. Once the solution is unstable the DOM starts flocculating with itself and the larger flocs precipitate (Weng, 2002; Tipping, 2002).
2. Polyvalent cations (Al) and their hydroxides specifically bind to the functional groups of the DOM. This compensates part of the negative charge and in extreme cases reverses the charge. The change of charge can destabilize the solution by reducing the negative electrostatic potential of the organic matter and bringing it close to its isoelectric point (Weng, 2002; Tipping, 2002). This induces flocculation or direct precipitation.

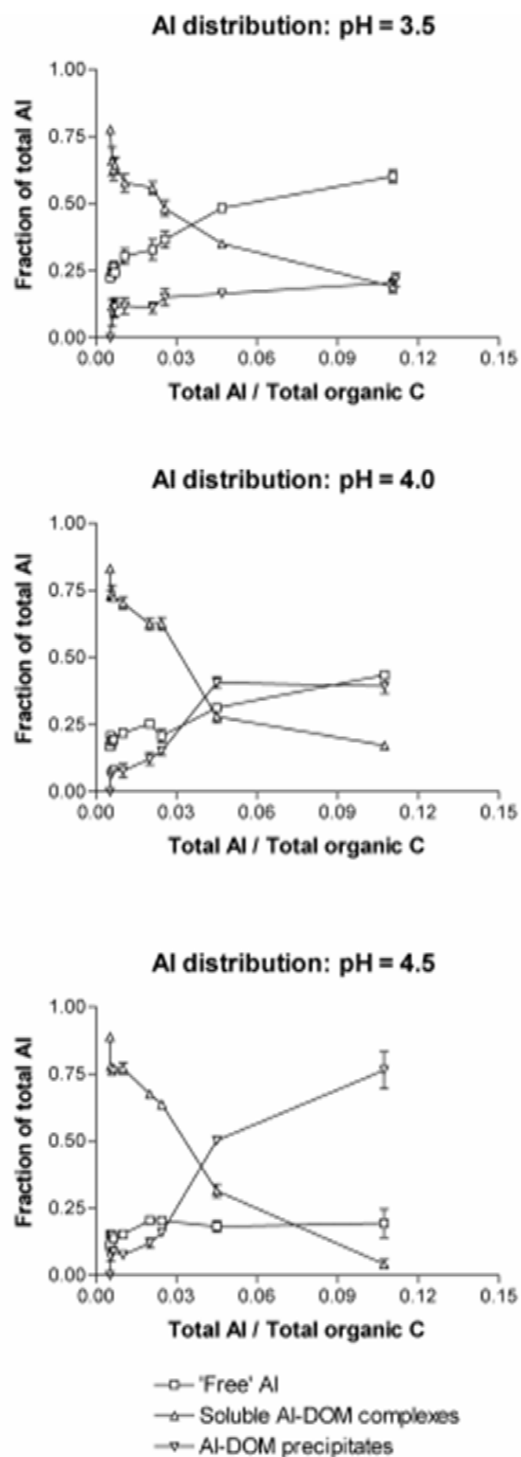


FIGURE 2.4: Figure from Jansen et al. 2003 (Jansen et al., 2003). Fractional distribution of Al over dissolved 'free' Al, soluble complexes and Al-DOM precipitates. The errorbars depict the standard error of the mean.

It is deemed unlikely that the solution becomes unstable solely due to a large ionic strength.⁷ Therefore the bonding interactions between metals (Al) and ligand (OM) are vital if precipitation is to occur. There are four 'specific' bond types described in literature, ordered from weak to strong bonds they are:

1. Adhesion (Stevenson, 1976).
2. Electrostatical binding (coulombic attraction) (Stevenson, 1976; Milne et al., 2001).
3. Specific binding to strong acids (i.e. carboxylic functional groups) or weak acids (i.e. phenolic functional groups) (Van Dijk, 1971; Weng, 2002; Guggenberger and Kaiser, 2003; Tipping et al., 2011; Kinniburgh et al., 1999).
4. Mono-, di- and tridentate binding (in short dendism) (Tipping et al., 2011; Kinniburgh et al., 1999).

The Donnan potential can be used to combine colloid stability with specific binding (Weng, 2002).

2.3.7 The Donnan Model

In the Donnan model the humic particle is seen as a rigid sphere with a certain charge, Q [mol/kg], surrounded by a size variable gel phase, the Donnan volume, V_D [l/kg], which can be calculated from the ionic strength (Christensen et al., 1998; Weng, 2002; Tipping, 2002; Milne et al., 2001).

$$\log_{10}(V_D) = \log_{10}(V_D) \cdot b \cdot (1 - \log_{10}(I)) - 1 \quad (2.21)$$

In which b is a constant dependent on the type and density of the functional groups. Milne *et al.* determined b for 49 datasets and found different values for FAs and HAs see table 2.4. In the Donnan theory it is assumed that the charge on the humic particle

⁷It is necessary to point out that flocculation of 'natural organic matter' (NOM) has been researched extensively by the waste-water industry. This research led to some very interesting articles with regard to the flocculation/precipitation processes that are discussed in this thesis among which (Matilainen et al., 2010) and (Edzwald and Van Benschoten, 1990). (Matilainen et al., 2010) is a review written in 2010 which gives, among other things, a nice overview of the effect of different aluminium macromolecules on the speed and effectiveness of NOM flocculation (see section 3 of the article). (Edzwald and Van Benschoten, 1990) gives a more classical, chemical, overview of this process. It is also from this literature that the notion arose that it is not likely that the solution stability can be compromised merely by an increase in ionic strength in natural waters.

TABLE 2.4: Values for the constant b in the Donnan model

<i>Compound</i>	<i>Mean</i>	<i>Std. dev.</i>	<i>Min</i>	<i>Max</i>
HA	0.51	0.19	0.21	0.84
FA	0.63	0.16	0.29	0.94

Values are derived from Milne et al. (Milne et al., 2001) who fitted the Donnan relation for V_D and ionic strength for 49 datasets; 24 for HA and 25 for FA.

causes a large concentration of counter ions directly around the organic molecule relative to the counter ion concentration in the solution which is theoretically equivalent with the concentration changes between two sides of a Donnan membrane. The relationship between the ion charge within the Donnan volume or gel phase, C_{iD} [mol/l], can be related to the concentration (C_i [mol/l]) and the valence of the ion (Z_i) in the solution with the Boltzmann accumulation factor:

$$C_{iD} = C_i \exp\left(-\frac{Z_i F \psi_D}{RT}\right) \quad (2.22)$$

Where R is the universal gas constant [J/mol K], T is the temperature in Kelvin and F is Faraday's constant [coulomb/mol]. The electro-neutrality of the HA is completely restored within the gel phase which means that the volume of the gel phase is dependent on the difference in ion concentrations and valence inside and outside the Donnan phase. This can be formulated as a charge balance (Milne et al., 2003):

$$\frac{Q}{V_D} + \sum_{i=1}^n Z_i (C_{iD} - C_i) = 0 \quad (2.23)$$

The Donnan theory neatly summarizes the hypothesis that the size of the gel phase is controlled by the Donnan potential and negatively dependent on the counter ion concentration and the valence of that ion.

Although different mechanisms can be thought of it seems Al and HA precipitate by a combination of electrostatic and specific bonds that decrease the negative potential of the over-all particle (Weng, 2002; Companys et al., 2007; Sauer et al., 2007), in a Donnan like way. The findings of Weng et al. (2002) show that a decrease of the Donnan potential can explain the sudden precipitation of HA (Weng, 2002). Based on the data presented in figure 2.5 they also proposed an empirical relationship for percentage of DOC that precipitates:

$$\log_{10}(DOC) = -52.0\psi_D - 1.85 \quad (2.24)$$

Figure 2.5 supports the hypothesis that the charge or Donnan potential of the humic molecule decreases as cations specifically bind to its surface. For the purpose of this thesis it will be assumed that the degree of polyvalent cations chemically bound to HA completely determines the complex its solubility. This is an important assumption that was made knowing that the coupling of precipitation to specific ion binding should be further investigated. With this assumption, however, the precipitation of organic complexes can be based on the chemical equilibria or adsorption kinetics between Al and the functional groups of the HA.

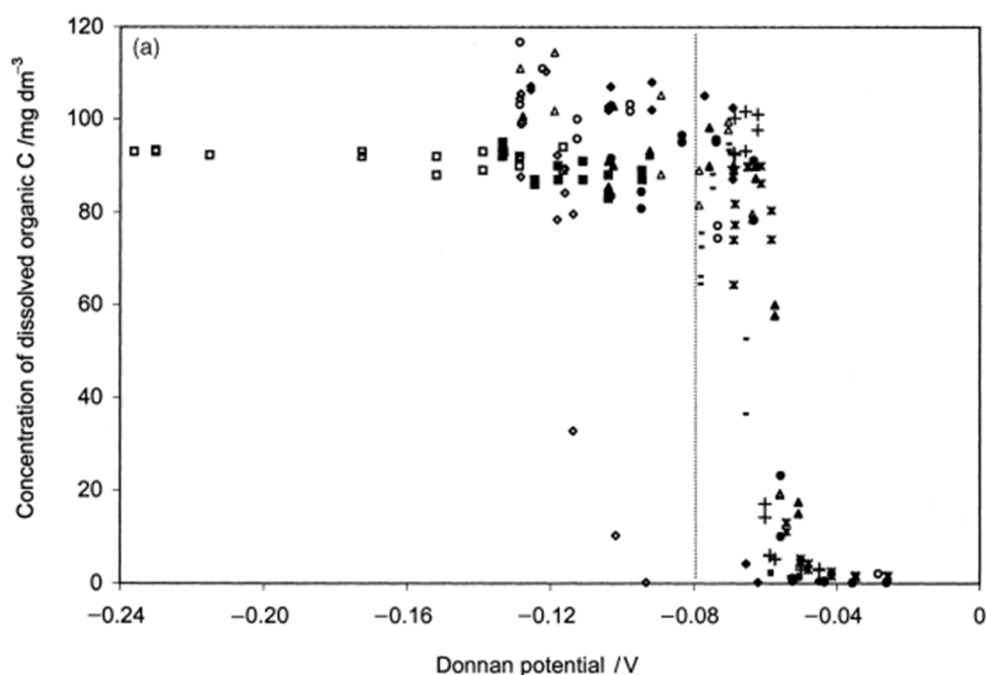


FIGURE 2.5: Donnan potential vs. solubility. The figure was taken from Weng et al. (2002) (Weng, 2002), a plot of calculated Donnan potentials versus DOC concentrations influenced by multiple ions: ■, Na^+pH4 ; □, Na^+pH6 ; ▲, $Ca^{2+}pH6$; ◆, $Al^{3+}pH6$; ◇, $Al^{3+}pH4$; + $Al^{3+} + Ca^{2+}pH4$; * $Al^{3+} + Ca^{2+}pH4$; - $Cu^{2+} + Ca^{2+}pH6$; The dashed line denotes the onset of coagulation.

2.3.8 Kinetics of Specific Binding

To estimate the complexation of OM and Al it is crucial to know its interactions on a 1:1 basis. Although different stoichiometry may occur the simplicity of 1:1 interactions outweigh the profit of describing multi-dendate binding for now. The following subsection on the complexation of organic matter is based on a simple form of the theories

behind the models NICA-Donnan and WHAM (these models are described in a series of articles: [Tipping, 1994, 1998](#); [Tipping et al., 2011](#); [Kinniburgh et al., 1999](#)).

Rate: In a mixed solution of Al and DOM, Al can bind to the functional groups of the DOM as a function of pH. These direct interactions with the organic molecule are called inner-sphere reactions ([Tipping, 2002](#)). They require the displacement of coordinated water molecules (anation) after which a direct bond is formed by sharing a the free electrons of the negatively charged functional group (ligand). In outer sphere reactions the metal adheres to the negative pole of the water molecule leaving the polar bond of the water molecule with the organic complex intact. In each case this is a metal-ligand (M-L) interaction for which the forward reaction rate can be written:

$$Al + DOM = Al \cdot DOM \quad \frac{\partial[Al \cdot DOM]}{\partial t} = k_f[Al][DOM] \quad (2.25)$$

The backwards reaction rate is often written inversely:

$$Al \cdot DOM = Al + DOM \quad \frac{\partial[Al \cdot DOM]}{\partial t} = -k_b[Al \cdot DOM] \quad (2.26)$$

Where k_f , which can range from 10^3 to 10^9 [$m^3/mol \cdot s$] ([Tipping, 2002](#), and references therein), is the rate constant of the forward reaction (i.e. producing complexes) which is very dependent on the solute concentrations and bond types (i.e. forward and backward complexation is faster if the bonds are weak), in reality the stability of a model has to be regarded as well when choosing these constants. The backward reaction constant, k_b [$1/s$], can vary an order of magnitude for aluminium: $10 - 100s^{-1}$ ([Tipping, 2002](#)). Equilibrium chemistry has to be taken into account to explain the bimodality in competition of cations and protons for the ligand.

2.3.9 Equilibrium Chemistry of Specific Binding

Specific binding of HA and metals is classically described as i) an equilibrium between the metals, protons and the functional groups of the HA or ii) in the form of adsorption isotherms in which HA is the solid phase. The latter approach more specifically assumes a solid immobile organic phase and is therefore a less practical approach in this thesis. Considering a solution with known concentrations of metal salts (i.e. $AlCl_3$) and solely strong acids and bases (i.e. NaOH and HCl), the 1:1 binding of a monoprotic ligand

(respectively RCOOH or ROH) with a metal (M) can be described in its simplest form (Tipping, 2002). To write out the equilibrium for this acid producing reaction two assumptions have to be made here: i) that the metal is a cation with a charge equal to or larger than 1 and ii) that the ligand is anionic (e.g. carboxylate or hydroxylate groups). Referring back to equation (2.25) the equilibrium for metal (Al) binding to a ligand (DOM) can be written:



In which K_{AlDOM} is the equilibrium constant this equilibrium constant determines the affinity of the metal to the functional group. K_{AlDOM} and the equilibrium constant for the dissociation of the monoprotic ligand K_{HDOM} are determined by the average type of functional group. K_{AlDOM} is 2.5 or 4.6 for carboxylic and phenolic groups respectively (Tipping, 1998), very slight (0.1) deviations from these values may occur for different types of molecules i.e. HA or FA (Weng, 2002). The equilibrium constant K_{HDOM} is given by:



Depending on the type of carboxylic acid (i.e. size, aromaticity etc.) the dissociation constant K_{HDOM} vary from $-\log(1.7)$ to $-\log(4.95)$ (see www.zirchrom.com). The total mass of the ligands (T_{DOM}) and the metals (T_{Al}) is:

$$T_{DOM} = [DOM] + [H \cdot DOM] + [Al \cdot DOM] \quad (2.29)$$

$$T_{Al} = [Al] + [Al \cdot DOM] \quad (2.30)$$

When regarding the functional groups as the ligand, the charge of a single ligand anion is -1. In this case the charge balance over the former reactions can be written as:

$$z[Al] + (z - 1)[Al \cdot DOM] + [H] + T_B - T_A - [DOM] - [OH] - zT_{Al} = 0 \quad (2.31)$$

Where z denotes the charge of the ion and T_A and T_B are the total concentrations of additional strong acids and bases. To be able to calculate the equilibria of all reactants (Al, H-DOM, DOM, Al-DOM, H and OH) only the self ionization expression of water is missing:

$$K_w = [H][OH] \quad (2.32)$$

To calculate the chemical equilibria a series of substitutions has to be done. The most important value is the complexed DOM to total DOM ratio from which the precipitation of DOM can be derived crudely. This ratio, from here on out called v , can be expressed as a function of pH and metal concentrations by rewriting equations (2.27) (2.28) (2.29), (2.30), (2.31) and (2.32):

$$v = \frac{[Al \cdot DOM]}{T_{DOM}} = \frac{\frac{K_{ALDOM}[Al]}{1 + ([H]/K_{HDOM})}}{1 + \frac{K_{ALDOM}[Al]}{1 + ([H]/K_{HDOM})}} \quad (2.33)$$

At constant pH it is possible to abbreviate the statement:

$$\frac{K_{ALDOM}[Al]}{1 + ([H]/K_{HDOM})} = K_{Al,H} \quad (2.34)$$

In which $K_{Al,H}$ is a dimensionless conditional constant which is dependent on pH. Combining these two equations yields:

$$v = \frac{[ALDOM]}{T_{DOM}} = \frac{K_{Al,H}[Al]}{1 + (K_{Al,H}[Al])} \quad (2.35)$$

This equation is in a mathematical way of thinking closely related to the well known Michaelis-Menten (e.g. Michaelis and Menten, 1913; Monod, 1942) or Langmuir type model in the sense that it describes an asymptotic curve from 0 to 1. Moreover in this particular case the slope of the curve is determined by the equilibrium constants K_{ALDOM} and K_{HDOM} and the pH. It is however important to realise that these equations are only valid if it is assumed there is only one type of functional group and only one metal in the solution. ⁸

Nota bene: Ionic strength. In ideal solutions at very low concentrations activity corrections can be ignored. The activity of an ion is then equal to its concentration: $a_i = C_i$. However in non-ideal solutions i.e. with high concentrations of, especially, polyvalent ions like Al the situation is different: $a_i < C_i$. To be correct, the concentrations of the ions stated in the equilibria above should be adjusted prior to further calculation.

As was swiftly stated above humic ion binding is far more complex than a simple chemical equilibrium, it would for example be impossible to describe the bimodality of functional

⁸This section is partly based on the book of Edward Tipping (2002) (Tipping, 2002), chapters 4 and 5. He and his colleagues were the writers of the WHAM model for humic ion binding. The theory can be supported by the research of Kinniburgh et al. (1998) (Kinniburgh et al., 1999) who, together with his colleagues, published the NICCA-Donnan model.

group characteristics, see 2.3.4. Hence a wide variety of models have been developed in order to correctly predict humic ion binding in complex solutions. The two most widely used models are the i) Windemere Humic Aqueous Model (WHAM) described by Tipping *et al.* in a series of articles (Tipping, 1994, 1998, 2002; Tipping *et al.*, 2011) and ii) NICCA-Donnan (Non Ideal Consistent Competitive Adsorption) described by Kinniburgh *et al.* (Kinniburgh *et al.*, 1999; Christensen *et al.*, 1998; Kinniburgh *et al.*, 1996) and later a consistency formulation was added by Milne *et al.* (Milne *et al.*, 2001, 2003).⁹ The two models both yield excellent results for a wide range of datasets and different ions even though they are fundamentally different (Koopal *et al.*, 2005). Tipping *et al.* describe specific ion binding by equilibrium reactions and add complexity to their model by generating multiple binding sites (Tipping, 1994, 1998; Tipping *et al.*, 2011). These sites potentially have different affinities (i.e. K_i and k_f values) for each ion depending on their nature and can thereby account for differences in functional groups. The approach of Tipping *et al.* will however inevitably lead to a lot of parameters due to the large amount of site types, it therefore requires a lot of assumptions (Milne *et al.*, 2001), Kinniburgh *et al.* (1999) take a seemingly different approach. Their approach is based on the idea that two Gaussian functions can describe the proton affinity distribution over the full pH range (Manunza *et al.*, 1995; Stevenson *et al.*, 1993). At the basis of the formulation of the NICCA-Donnan model an extended form of the Henderson Hasselbach (or Hill) equation is used to describe a similar binding ratio as the ratio v . They inherently assume adsorption rather than chemical equilibria as the main interaction that causes humic ion binding. But however different the approach, generically speaking, the basic equations again have the same mathematical form. Moreover they essentially also separate the affinity distributions of the two functional groups. This is quite comprehensibly described in the general

⁹NICCA-Donnan is also available in ORCHESTRA and WHAM is incorporated in model VII and predecessors.

equation for the bimodal NICCA model:

$$\begin{aligned}
 Q_{it} = & Q_{max1} \cdot \frac{n_i}{n_{H1}} \cdot \frac{(K_{i1}C_{iD})^{n_{i1}}}{\sum_i (K_{i1}C_{iD})^{n_{i1}}} \cdot \frac{\left[\sum_i (K_{i1}C_{iD})^{n_{i1}} \right]^{P_1}}{1 + \left[\sum_i (K_{i1}C_{iD})^{n_{i1}} \right]^{P_1}} \\
 & + Q_{max2} \cdot \frac{n_i}{n_{H2}} \cdot \frac{(K_{i2}C_{iD})^{n_{i2}}}{\sum_i (K_{i2}C_{iD})^{n_{i2}}} \cdot \frac{\left[\sum_i (K_{i2}C_{iD})^{n_{i2}} \right]^{P_2}}{1 + \left[\sum_i (K_{i2}C_{iD})^{n_{i2}} \right]^{P_2}}
 \end{aligned} \tag{2.36}$$

In which C_{iD} [mol/l] is the concentration of an ion in the Donnan gel phase, Q_{it} [mol] is the amount of ions bound to the reactive groups and the subscripts 1 and 2 refer to either the strongly acidic carboxylic groups or the weakly acidic phenolic groups. Q_{max} [mol/kg] is the site density of the organic molecule and K_i the median of the affinity distribution for ion i at a specific site (i.e. nr. 1 or 2). The parameters P and n_i were added by [Milne et al. \(2001, 2003\)](#) and reflect the heterogeneity of humic substances and the non ideality of the solution.

Parameters for NICCA-Donnan can be found in [Appendix D](#). When simply accounting for the concentrations and acidity of a solution only one parameter in the NICCA-Donnan model is unknown: the Donnan potential ψ_D . This value can be derived by measuring solution concentrations and doing a speciation analysis. This can be done with several techniques for example dialysis with a Donnan membrane or Diffusive Gradients in Thin films (e.g. [Jansen et al., 2001](#)). This would purely be done to estimate C_{iD} .

2.3.10 Theoretical Precipitation Rate

From [section 2.3.6](#) and [section 2.3.7](#) can be deduced that precipitation is directly dependent on specific bonding of Al and DOM. Rewriting equations [\(2.25\)](#), [\(2.3.8\)](#) and [\(2.35\)](#) the source sink term of the advection dispersion equation ([\(2.10\)](#)) can be elaborated for the organic complexes:

$$R_{AlDOM} = \frac{\partial [Al \cdot DOM]}{\partial t} = k_f(1 - v)(v \cdot T_{DOM} + K_{Al,H} \cdot v \cdot T_{DOM} \cdot [Al]) - k_b \cdot v \cdot T_{DOM} \tag{2.37}$$

Finally, the change of the Al and DOM concentrations can be found by a mass balance assuming 1:1 interactions these can be written as:

$$R_{DOM} = R_{Al} = -R_{AlDOM} \quad (2.38)$$

To couple the formed precipitate to the porosity it is necessary to know the density of the precipitate, this can be found in literature: precipitated organic matter in illuvial horizons has a density (ρ_{OM}) of 1.4-1.7 g/cm^3 ([Guggenberger and Kaiser, 2003](#); [Adams, 1973](#)).

Chapter 3

Model

To predict the experimental output based on the theory discussed in chapter 2 a two-dimensional model was made in [COMSOL Multiphysics](#). Flow, advection and hydrodynamic dispersion are coupled in this model. The formulation is equivalent to the flow and reaction equations in Chapter 2.

3.1 Comsol Formulation

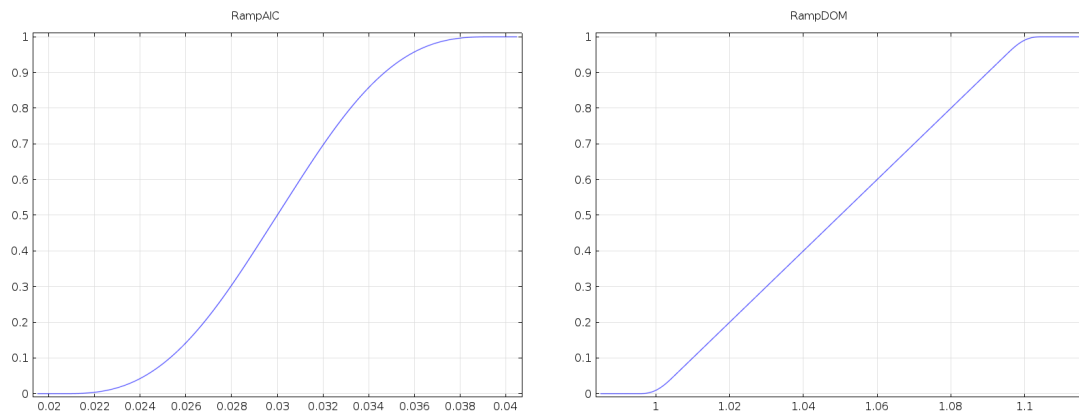
3.1.1 Solute Transport

Flow was calculated from pressure gradients with Darcy's law. Solute transport was described with the ADE. The Darcy's law is formulated exactly like equation 2.1. The ADE, however, is formulated slightly different in COMSOL:

$$P_{1,i} \frac{\partial C_i}{\partial t} + P_{2,i} + \nabla \cdot \Gamma_i + u \nabla C_i = R_i + S_i \quad (3.1)$$

In which $P_{1,i}$ and $P_{2,i}$ are adsorption terms. The dispersive mass change is compressed to Γ_i and can be expressed in the same terms as the ADE in Chapter 2

$$\Gamma_i = D \cdot \nabla C_i \quad (3.2)$$



a) Ramp for the Al/C ratio.

b) Ramp for the DOM concentration.

FIGURE 3.1: Plots of the ramp functions that were used to impose conditional statements on the model without compromising the stability of the solver.

The advection and dispersion, or also the translocation, of a solute (C_i) is summarized to N_i following the equation:

$$N_i = \Gamma_i + u \nabla C_i \quad (3.3)$$

3.1.2 Precipitation

The solute transport for DOM and Al were modelled with equation 3.1. Complexation and precipitation were calculated with a separate PDE, which is equivalent to the ADE. In this PDE the convection and dispersion were assumed to be zero for all solutes. The precipitation of Al·DOM is represented by a source/sink term. The consumption of Al and DOM is expressed as a sink term in the ADE.

In accordance with literature values, it was assumed that no precipitation takes place at Al/C ratios lower than 0.03 (e.g. Jansen et al., 2003; Scheel et al., 2008a). This condition was forced onto the model with a ramp function to ensure the stability of the model (see figure 3.1(a)). Furthermore it was assumed that at very low concentrations of DOM (i.e. 1% of the input concentration) complexation takes place but precipitation does not occur. This effect is represented by a second ramp function (see figure 3.1(b)).

3.2 Parameters

For fluid flow a fitted value of κ was used $3.33 \cdot 10^{-9} \text{ m}^2$ and the standard viscosity of water, $0.001 \text{ Pa} \cdot \text{s}$. The porosity was assumed to be $0.38 \text{ m}^3/\text{m}^3$ and the density of the

TABLE 3.1: Parameters and Initial Conditions

<i>Symbol</i>	<i>Value</i>	<i>Unit</i>	<i>Description</i>
k_f	100	$m^3/mol \cdot sec$	Forward reaction rate constant
k_b	50	$1/sec$	Backward reaction rate constant
K_{AIDOM}	36	$1/mol$	Equilibrium constant for AIDOM formation
K_{HDOM}	$1.6 \cdot 10^{-3}$	$1/mol$	Equilibrium constant for HDOM formation
$C_{DOM,in}$	0.1	$C - mol/liter$	Inlet concentration DOM
$C_{Al,in}$	0.01	$mol/liter$	Inlet concentration Al
$C_{H,in}$	10^{-4}	$mol/liter$	Inlet concentration H
$C_{DOM,init}$	10^{-4}	$C - mol/liter$	Initial concentration DOM
$C_{Al,init}$	10^{-5}	$mol/liter$	Initial concentration Al
$C_{H,init}$	10^{-4}	$mol/liter$	Initial concentration H
Q_{in}	1	$liter/hour$	Flow at the bottom boundary

Model parameters and initial conditions for reactions and flow. The equilibrium constants for the chemical interaction of DOM came from www.zirchrom.com. The source of the rate constants is [Tipping \(2002\)](#). K_{AIDOM} was fitted from the experimental data.

fluid phase constant ($1000 \text{ kg}/\text{m}^3$).

For solute transport anisotropic dispersion was assumed. The dispersivity (D) was calculated according to: $10 \alpha_t = \alpha_l$ [m], as was described in chapter 2, with longitudinal dispersivity (α_l):

$$\alpha_l = 0.017L_s^{1.5} \quad \text{for } : L_s \leq 100m \quad (3.4)$$

The diffusivity of all species was assumed to be isotropic and orders of magnitude lower than the dispersivity: $10^{-9} \text{ m}^2/\text{s}$. Parameters for the reactions can be found in table 3.1.

3.3 Boundary Conditions

The boundary conditions for flow and solute transport can be seen in figure 3.2 and their equations are given in table 3.2. The top boundary flux for flow is controlled by a Neumann boundary condition: $P_w = P_{w,bound}$ [Pa]. For concentrations the top boundary conditions is also controlled by Neumann: $-\mathbf{uN}_i = 0$.

At the bottom a fixed flow is imposed on the system with $q_w = q_{w,in} = constant$ [m/s] (Neumann) and a fixed concentration ($C_i = C_{0,i}$ [mol/m^3]) (Dirichlet), which makes the total flux of a solute over the bottom boundary $q_{Ci} = q_{w,in}C_i$.

TABLE 3.2: Boundary Conditions of the COMSOL Model

	<i>Bottom</i>	<i>Top</i>	<i>Remainder</i>
<i>Flow</i>	$-\phi\rho u = \rho u_{bound}$	$P_w = P_{w,bound}$	$-\phi\rho u = 0$
<i>Solute Transport</i>	$C_i = C_{0,i}$	$-n \cdot N_i = 0$	$-n \cdot N_i = 0$

Specification of the locations can be found in figure 3.2

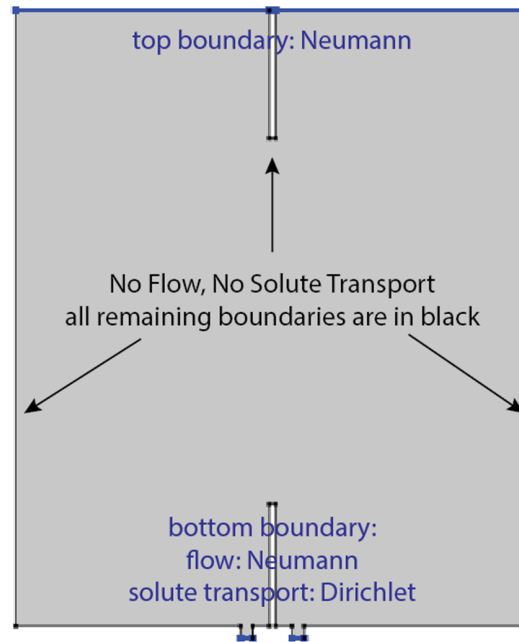


FIGURE 3.2: Boundary conditions for the two-dimensional model for both flow and solute transport. The equations for these boundary conditions can be found in table 3.2.

The rest of the system are Neumann no flow boundary conditions (see figure 3.2), of course in these nodes the boundary condition is only imposed in the direction perpendicular to the boundary. Initially the whole domain has a small concentration of each solute which is 4 orders of magnitude lower than its inlet concentration. This was done to increase the stability of the model. A standard physics controlled mesh was used which is more fine around key areas like inlets, obstacles and boundaries.

3.4 Solver

A time dependent solver was used to calculate both fluid flow and solute transport. The time stepping was controlled by the solver which solves the partial differential equation (PDE) by backward differentiation. The standard backward differentiation formula (BDF) of COMSOL was used as a solver because of the stiffness of the PDE's

that had to be solved. Due to the stiffness of the PDE's the other standard COMSOL solver, the generalized alpha, had trouble converging to an accurate result.

3.5 Scenarios

The tested scenarios can be divided into three categories: 1) flow, 2) solute transport and 3) reactive flow.

Flow. The flow scenarios were used to estimate the local reduction in hydraulic conductivity in the experimental set-up during falling head tests, these scenarios will be discussed in further detail in Chapter 4.

Solute transport. The data of beaker solution experiments (explained in chapter 4 and 5), were used to make an empirical formula. Based on this equation and the solute transport module of the model, the EC values in the thin box experiment were estimated. With this model the Al/C ratios in the thin box experiment have also been predicted.

Precipitation. With the reactions module of the model two scenarios were ran: one with and one without a consumption reaction for Al and DOM in the ADE. This was done because it is unclear how much Al the precipitation reaction consumes. If they were used the Al and DOM sink terms were modelled according to equation 2.38. It was therefore inherently assumed that DOM and Al interact on a 1:1 basis.

3.6 Limitations

The model represents the coupling of the basic theories of four different subjects: flow through porous media, solute transport, colloid stability theories and organic chemistry. All of these theories need further evaluation. The clearest example of this are the chemical equilibria which could be modelled more accurately with Model VII or NICCA-Donnan via ORCHESTRA or PHREEQC. The most important limitation of the model right now, however, is that the reduction in permeability is not coupled to the solute

transport module. Therefore the advection and dispersion of solutes is overestimated at the location of the precipitation layer.

Chapter 4

Materials and Methods

Outline. This chapter revolves around physically reducing the hydraulic conductivity in the subsurface by the complexation reactions described in Chapter 2. The main experiment is a 2 dimensional flow container in which solutes can be mixed at a continuous saturated flow rate. This set-up will be referred to as "the thin box", or simply "the set-up", and will be explained in the second part of this chapter. Firstly, all preliminary, supporting, experiments will be discussed that were necessary to determine the influence of important solution characteristics like pH, EC and Al/C ratio on the precipitation behaviour of the solutes.

4.1 Chemicals

Four main chemicals were used in all following experiments. Humic Acid Sodium Salt (hereafter referred to as humic acid or HA) manufactured by Sigma Aldrich, with CAS number 68131-04-4, was used as a source of OM. The chemical formula for this HA is $C_9H_8Na_2O_{4(s)}$, its structural formula is given in figure 4.1. The molecular weight of this HA is 226.14 gram/mol and therefore a very small HA relative to average HA (roughly 500-5000 gram/mol) (Tipping, 2002; Milne et al., 2001). Furthermore Aluminium was dissolved from: aluminium-trichloride-hexahydrate ($AlCl_3(H_2O)_6(s)$) which is delivered in a large, 1 dm³, container and looks like an off white chunky crystalline powder. The CAS number of this aluminium is 7784-13-6 and it was also manufactured by Sigma Aldrich. Of course aluminium can take many hydrolysed and poly-nuclear forms when

dissolved in water. However, for simplicity all dissolved forms of aluminium will hereafter generally be referred to as Al.¹ Finally an acid: 3M HCl and a base: 1M NaOH were used to control the pH levels of the solution. These strong acids and bases were chosen because their counter ions (Na^+ and Cl^-) would not complicate the consistency of the solution. Moreover the mono valence of these counter ions ensures that their competition for binding sites is practically negligible.

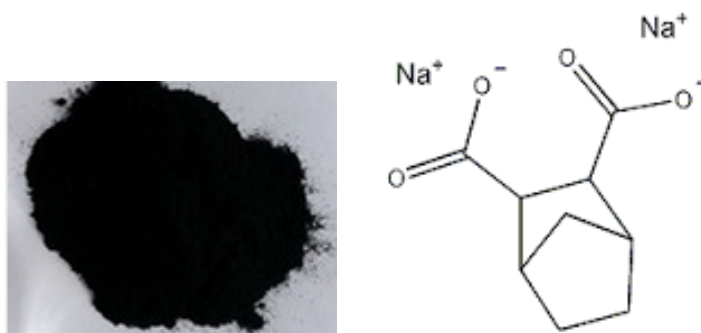


FIGURE 4.1: On the left side a photo of dry humic acid sodium salt on the right side its structural formula. It is a very dark and fine powder that immediately dissolves in water, this particular humic acid has carboxylic functional groups.

4.2 2 Dimensional Flow Experiment

4.2.1 Set-up in General

The set-up is a three dimensional thin box made of perspex and PVC, the inner size of the box is 92 x 42 x 3 cm, the height of the soil layer within the box is 46.5 cm. This was done to approximate two dimensional flow. The thin box will from here on out be referred to as the set-up. The soil is made up of sintered silica sand with a mean grain size of 0.9 mm (course sand) (see figure 4.2). The sand has a relatively low density (2.3 kg/m^3) it was obtained by Michael Afanasyev who used several methods (i.e. a shaking on a shaking table, wetting and a combination of both) to reduce the porosity of the sand as much as possible. He concluded, from unpublished data, that the minimal porosity of this sand was 0.3825 with wetting and shaking. To be sure that the porosity would not change due to settlements during the experiment the sand was carefully dripped into

¹Referring to all dissolved aluminium species as "Al" is a large assumption. However, since this thesis mainly focusses on the physical changes in the soil some of the chemical reactions have to be simplified. Looking at Al as a single species most likely only causes quantitative changes in the outcome of the analysis because aluminium is positively charged in acidic solutions and its affinity for OM is high regardless of its state (Duan and Gregory, 2003; Wesolowski and Palmer, 1994).

the set-up at a shaking table which was continuously shaking up and down at 1.0 G. From the volume (5859 cm³), the weight of the soil (8320.72 gram), the density of the soil and the density of the dry sand the porosity could be deduced. The porosity was 0.3825. Furthermore the sintered sand is, according to its factsheet, non-reactive. Its pH however is 9, this can perhaps partly be explained by the negative surface charge at the outside of silicium-oxide crystals. It is not unlikely that part of the H^+ ions adsorb and are therefore not measured in the solution, unexpected pH levels were however also measured after the first DeMi water flushes.

The two input solutions (Al and HA) were injected at equal rates (0.5 l/h) at the bottom of the set-up 4.2. The HA solution had a concentration of 0.1 C-mol/l and the Al solution 0.01 mol/l which corresponds to Al/C 0.1 this was done to ensure quick precipitation. The input concentration of aluminium was based on its maximum mono-nuclear solubility at pH 4 (see 2.3). These solutions were prepared in two large 20 liter containers and were pumped into the set-up with a two-way pulse pump.² In the middle of the set-up the solutions are allowed to react and at the top they are separated again in such a way that only the non-reactive organic matter could come into the aluminium domain. Hence, at the top there is a separated free flow to two extraction points (one for each constituent) and the weight of the outflow is measured cumulatively with two separate balances.

Sample ports. The pH and EC were measured at 6 locations in the set-up. In order to do this sample ports were made (see figure 4.2). Through these sample ports the solution was extracted in a predetermined order: from 1 to 6. The order was chosen from top to bottom and from the middle to the sides. The volume of water in the sampling tube (2 ml) was emitted after which a 2 ml sample was taken, this process was repeated each hour for each sampling point.

4.2.2 Experimental Cycle

Start. The pH in the set-up was alkaline this was caused by the apparent buffering capacity of the sand. In order to gain knowledge about this buffering capacity and to

²The pulse pump can pump in two directions at equal rate, the rates were calibrated to the pulse speed before the start of the experiment.

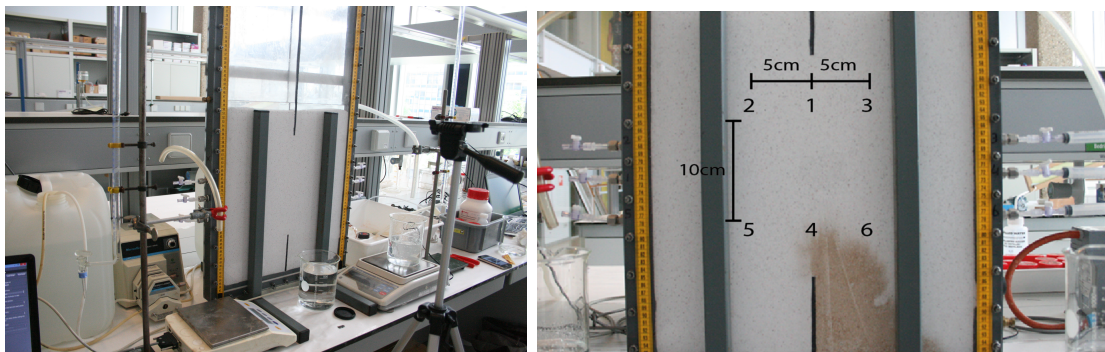


FIGURE 4.2: 2D flow set-up: a 3 dimensional thin box with two injection valves at the bottom and sample ports at the number 1 to 6 samples were taken each hour and the numbers are the order of sampling. The Al solution (colourless) was pumped into the set-up on the left hand side, on the right side a DOM solution (brown) was pumped in at the same rate. The flow is bottom up due to the injections, at the top there is free flow towards outlets at either side of the thin box. The flow through each of the outlets measured cumulatively with two balances. The flow of the 'Al side' and the 'DOM side' are separated by a 10 cm long impermeable plate at the bottom and the top. At the top the impermeable plate is extended, this extension is used for the falling head measurements. The reactants disperse into each others domain in the 30 cm gap in the middle of the container.

reduce the pH in the set-up five liters of pH 4 DeMi water were pumped through the system. During this phase the pH measured at the sampling ports dropped slightly to pH 7. Afterwards a falling head was done (explained hereafter).

Reaction. After the start-up phase the simultaneous injection of Al and DOM could start. The solutions were pumped into the set-up for 7 hours at a rate of 1 l/h. Each hour the flow was stopped for a few minutes to take samples from the sampling ports. Predictions of the flow lines for the reactive flow experiments are in figure E.1.

Rinse. Following the reactive flow, the set-up was rinsed with DeMi water for 1 hour at a rate of 5 liter per hour. This was done to clear the thin box of any non-reacted, soluble, Al or DOM.

Falling head. The falling head was the most important phase. A picture and model representation of the method can be found in figure 4.3. The head at the left side of the set-up was raised 6.5 cm above the head of the right side. The outlet on the left side was closed, therefore the water had to flow through the area where the precipitation just occurred.

The experimental cycle was repeated twice with exception of the start-up.

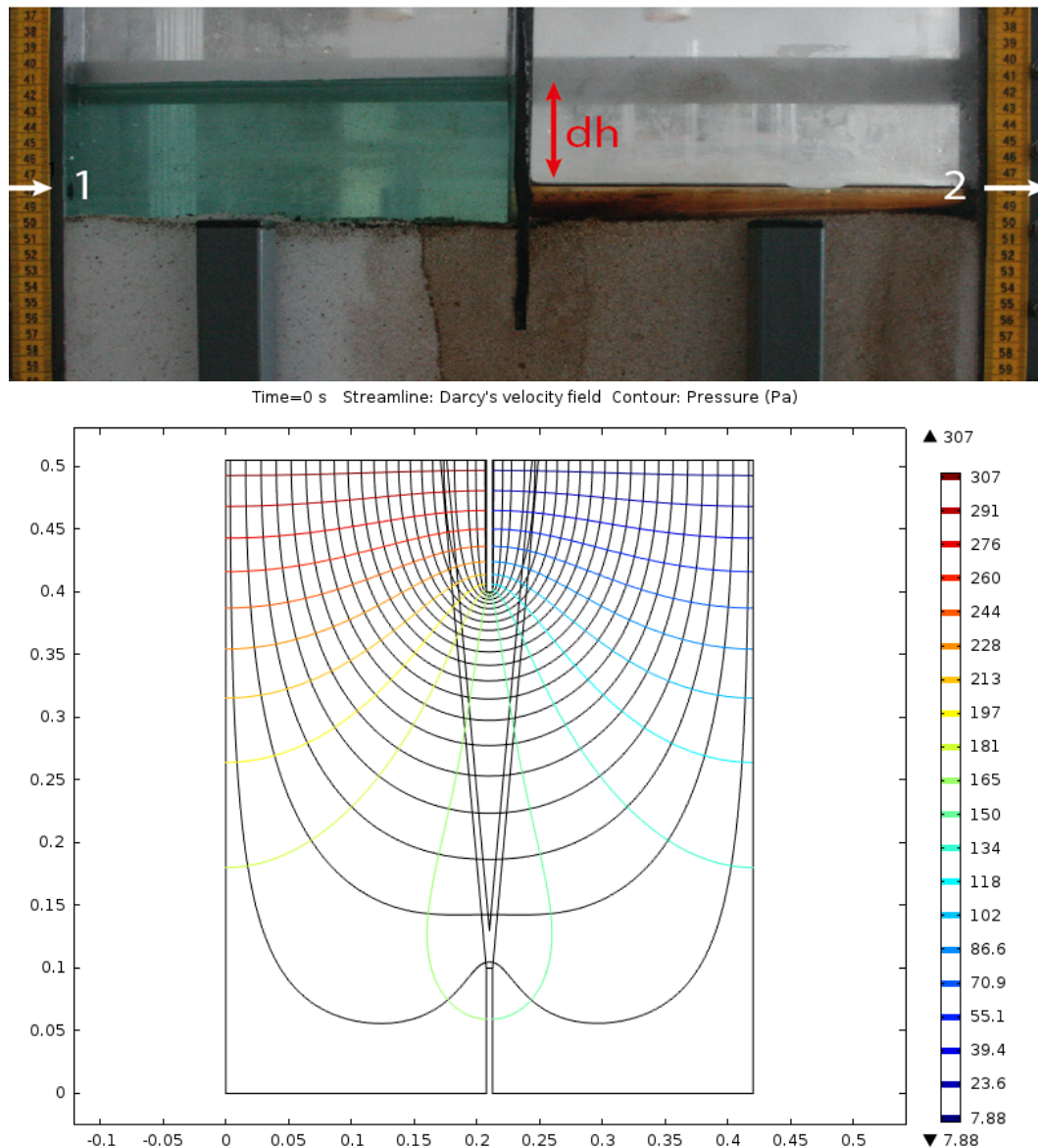


FIGURE 4.3: The top figure is a picture of the last falling head test, the difference in head (dh) is depicted in red. The numbers represent (1) the inlet through which the set-up was filled before the falling head test and (2) the outlet and the outflow opening. The second picture shows the predicted flow lines that are calculated from the pressure contours assuming a homogeneous soil. Predictions of the flow lines for the reactive flow experiments are in Appendix E.

4.2.3 Average Falling Head Analysis

In this particular set-up the hydraulic conductivities can only be compared to one another. This is because there is no objective way to determine the exact length of the flow path (L). The average hydraulic conductivity of the entire set-up was therefore derived

using the following expression:

$$K = \frac{L}{t_1 - t_0} \ln \frac{dh_0}{dh_1} \quad (4.1)$$

In which t is time and dh is the head difference (see figure 4.3). This may however lead to an underestimation of the local conductivity reduction.

4.2.4 Local Conductivity Reduction Analysis

The conductivity reduction in the thin precipitation band is estimated with a numerical model. In order to do this the average outflow was calculated over a set time interval. This has been done for each falling head test according to:

$$Q_{avg} = \frac{Q_{tot350}}{t_{350} - t_0} \quad (4.2)$$

In which t_0 and t_{350} denote the time interval from 0 to 350 seconds. This interval was chosen because it is available in all datasets (see Appendix F for the plotted data). Q_{tot350} is the cumulative outflow $t = 350$ seconds. The average pressure gradient can be calculated from:

$$P_{avg} = \frac{\int_{t_{350}}^{t_0} p(t) dt}{t_{350} - t_0} \quad (4.3)$$

In which $p(t)$ is a function which is fitted to the falling head data (see Appendix F). This function is therefore different for each consecutive falling head experiment (i.e. $P_{FH1}(t)$, $P_{FH2}(t)$ and $P_{FH3}(t)$):

$$P_{FH1}(t) = 10^{2.9-0.0028t} \quad \text{linear norm of residuals : 0.095} \quad (4.4)$$

$$P_{FH2}(t) = 10^{2.9-0.0011t} \quad \text{linear norm of residuals : 0.091} \quad (4.5)$$

$$P_{FH3}(t) = 10^{2.9-0.00066t} \quad \text{linear norm of residuals : 0.191} \quad (4.6)$$

Hence the values for P_{avg} and Q_{avg} are also different for each experimental cycle, these can be found in table 4.1. These values are used as the flow boundary conditions for three numerical simulations. $P_w = P_{avg}$ at the left side of the modelled set-up and $P_w = 0$ at the right side, hence $dP = P_{avg}$. In these simulations the inlets at the bottom of the basin have a no-flow boundary condition ($-\phi \rho u = 0$).

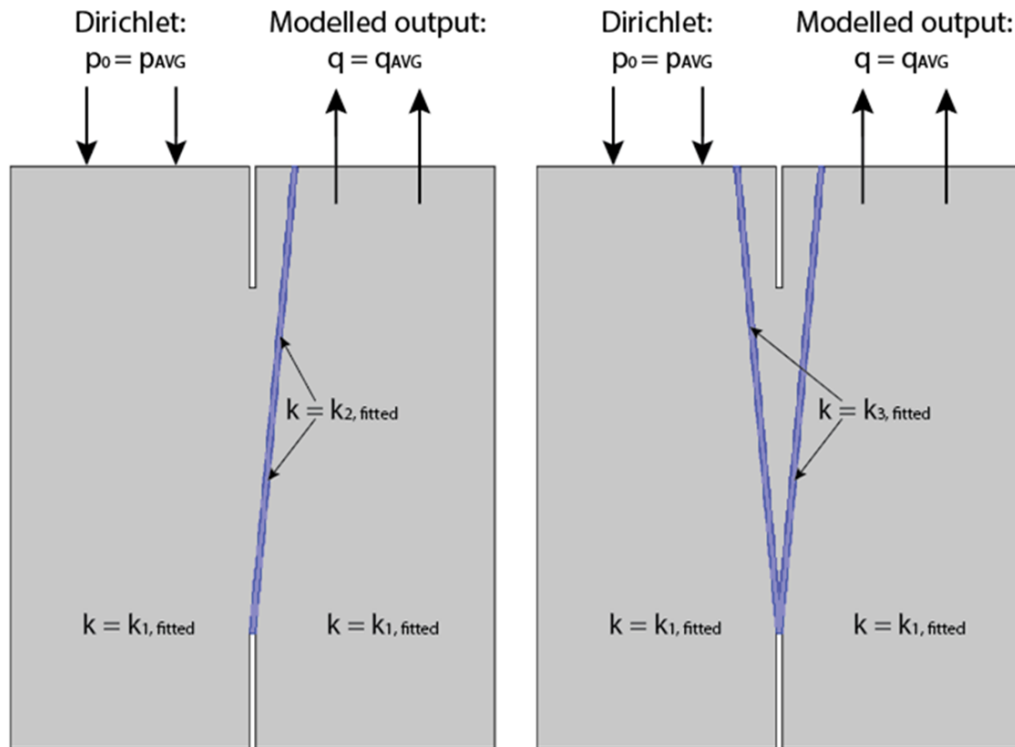


FIGURE 4.4: The geometry of the second (left figure) and third (right figure) modelling scenario. The pressure head on the top left side of the model is p_{avg} , at the right side $p = 0$. Hence the potential difference is p_{avg} , which corresponds to the potential difference in physical soil model. This is different for falling head 1, 2 and 3 respectively (see table 4.1). The κ values were fitted such that the modelled flux over the right boundary (q) was equal to the average experimental flux over that same boundary (i.e. $q = q_{avg}$). In the first scenario it is assumed that $\kappa_1 = \kappa_{2,3}$. The second scenario a simple 0.5 cm wide precipitation layer is included with $\kappa_1 > \kappa_2$. This layer represents the small precipitation band that is visible in the physical experiment. This concept was extended for scenario 3 (right hand figure), in which $\kappa_1 > \kappa_3$.

Falling head scenario 1: In this scenario a homogeneous permeability throughout the set-up is assumed ($\kappa_1 = \kappa_2$). The κ value can be derived from p_{avg} and Q_{avg} (see table 4.1, FH 1). This value can be used as a standard in the other scenarios.

Falling head scenario 2: In this scenario it is assumed that $\kappa_1 < \kappa_2$, and that the value for κ_1 in scenario 1 is still valid for the grey part of the domain (see figure 4.4). The experimental permeability reduction can, again, be estimated from p_{avg} and Q_{avg} (with the values of FH 2). In this scenario changes in κ_2 are assumed to be responsible for the overall reduction in flow. Hence κ_2 is fitted until the Q_{avg} of the model is equal to that of the experiment.

TABLE 4.1: Average Conditions Flow Model

	Δp_{avg} [Pa]	Q_{avg} [m^3/s]	q_{avg} [m/s]	κ_{avg} [m^2]
<i>FH 1</i>	315	$1.29 \cdot 10^{-6}$	$2.05 \cdot 10^{-4}$	$3.33 \cdot 10^{-9}$
<i>FH 2</i>	527	$0.91 \cdot 10^{-6}$	$1.45 \cdot 10^{-4}$	$1.41 \cdot 10^{-9}$
<i>FH 3</i>	616	$0.71 \cdot 10^{-6}$	$1.13 \cdot 10^{-4}$	$9.39 \cdot 10^{-10}$

Δp_{avg} , q_{avg} and Q_{avg} are calculated from the integrated results of the falling head tests. The average permeability, κ_{avg} , is a model fit that results in the same q_{avg} as the physical experiment (at the same Δp_{avg}).

Falling head scenario 3: Similar to scenario 2 this scenario assumes that $\kappa_1 < \kappa_3$ and that the value for κ_1 in scenario 1 is still valid. It should however be noted that the geometric domain of κ_3 is different from the domain of κ_2 (see figure). The permeability reduction is explained by changes in κ_3 .

4.3 Supporting Experiments

4.3.1 Titration

The behaviour of the HA was examined in a range of conditions with two main variables: pH and Al/C ratio.³ This was done to see under which conditions complexation and precipitation would occur. From a theoretical point of view this would be either at high pH levels (less competition for binding sites) or at high Al/C ratios or a combination of both. Hence a stock solution of DOM was made at 0.10 mol/l (prepared on weight basis: 23.50 grams per 9 liters), due to the dissociation of sodium and binding of H^+ ions the stock solution became basic (pH 9.54). Furthermore a stock solution of Al was made at 0.1 mole/l (or 24 grams $AlCl_3(H_2O)_6$ per liter) and pH 4 2.3. ⁴ Samples were taken from the DOM stock solution and the pH was adjusted slightly with 3M HCl in order create the right starting conditions for the following experiments:

1. Gradually changing the pH from 9 to 3 by titration of HCl at three different Al/C ratios (Al/C = 0, Al/C = 0.05 and Al/C = 0.1).

³The Al/C ratio is the ratio of dissolved organic matter in mole-C over dissolved $AlCl_3(H_2O)_6$ in mole-Al

⁴Since the aluminium concentration is three orders of magnitude larger than the proton concentration the pH of the concentrated aluminium stock only marginally affects the end result of the experiments. A concentrated stock does however gives the advantage that changes in the Al/C ratio can be made with marginal volumetric changes.

TABLE 4.2: Dissolved constituents of the DOM stock solution at pH 4.0

<i>DOM [C-mol/l]</i>	<i>Cl mol/l</i>	<i>Na mol/l</i>	<i>H mol/l</i>
0.100	0.0057	0.022	0.0057

Na concentration is derived from the NaDOM input.

2. Changing the Al/C ratio from 0 to 0.2 with steps of 0.01 at three different pH levels (pH 4, 6 and 8).

For each titration experiment 900.0 ml stock solution was used, the beaker was stirred with a magnetic stirrer at rate 250 rpm (the paddle was 2 cm wide). The mixer was turned off for 10 minutes after each titration step to visually confirm changes in floc formation. Series of photos were taken by hand during these ten minutes if any significant changes occurred.

4.3.2 Filtration

Even though the titration experiments gave information over a large range of pH and Al/C conditions they could only yield descriptive data and photographs. In order to quantify precipitation 15 samples were prepared at key Al/C ratios (0, 0.01, 0.03, 0.1 and 0.2) and pH levels (4, 6 and 8). The DOM solution was taken from the stock solution (mentioned before: 4.3.1) and 40 ml was put into 50 ml containers. Then aluminium was added from stock (see: 4.3.1) with a volumetric micropipet (0, 0.4, 1.2, 4 and 8 ml dependent on the target concentration) to reach the preordained Al/C ratios. The headspace in the 50 ml container was filled with de-mineralized water. The samples were shaken and left over the weekend. In the following week the samples were filtered with 0.45 μm filter paper. The total organic carbon content (TOC) was measured for all samples with a TOC-analyzer after filtration (the precision of the TOC analyser is parts per million). These TOC measurements were subtracted from the input concentrations of DOM to calculate the fractions of precipitated organic matter. The same was done for the aluminium and sodium content, these were measured with ICP for a few key samples, mostly as a test, also in parts per million.

4.3.3 Mastersizer

The data of the filtration experiments were expanded by measuring the complete floc size distribution. Particles with a diameter of $0.45 \mu\text{m}$ easily slip through a pore that is orders of magnitude larger. If it is assumed that a filtering mechanism (see figure 2.1) causes the flocs to stabilize in a soil it is more interesting to know the actual floc size rather than the precipitation based on an arbitrary scientific norm. Therefore the floc sizes were analysed with a Malvern Mastersizer 4.5. A full description of the machine, its detailed description and capabilities can be found in the users manual, the most important features will shortly be described here.⁵

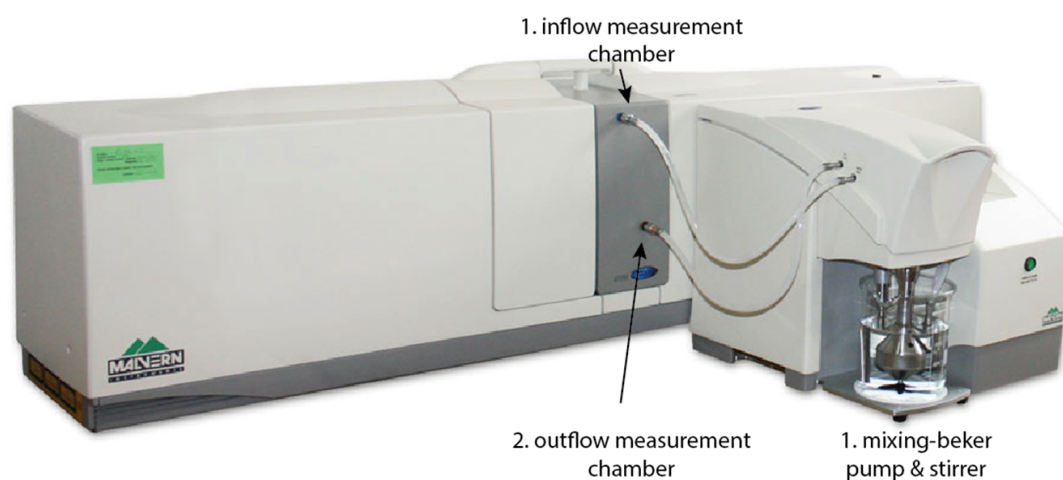


FIGURE 4.5: The Malvern Mastersizer. The injection (1) and extraction (2) tubes through which the solution is brought to the measurement chamber (dark grey) and returned to the mixing vessel (3). In this mixing vessel there is a peristaltic pump and stirring pedals that respectively move and mix the solution.

The solution is pumped from a mixing beaker into the measurement chamber by a peristaltic pump. The mixing beaker is stirred by pedals, the rate of these pedals can be controlled independent of the peristaltic pump that determines the flow through the tubes. Once the particles are in the measurement chamber, a small space in between two glass plates, the Mastersizer estimates floc sizes from blue green and red light scattering. The light comes from a laser which is focussed on the glass. If the target particles are very small ($0.1 \mu\text{m}$) a shadowing effect may occur which inhibits the light from reaching all particles in the right way.

⁵The users manual can be downloaded from the Malvern website after creating an account: www.Malvern.com. In this document a detailed description is given about the workings of the machine and the supporting theory.

TABLE 4.3: EC Correction Factors

<i>OM 1</i>	<i>OM 0.9</i>	<i>OM 0.8</i>	<i>OM 0.7</i>	<i>OM 0.6</i>	<i>OM 0.5</i>
1.14	1.22	1.23	1.23	1.22	1.22
<i>OM 0.4</i>	<i>OM 0.3</i>	<i>OM 0.2</i>	<i>OM 0.1</i>	<i>OM 0</i>	
1.18	1.18	1.19	1.20	1.20	

In this table the correction factors for the EC measurements higher than $2000 \mu S cm^{-1}$ are given. These values were used to adjust the EC data where the curves would not fit due to incompatible calibrations of the high and low EC spectrum measurements.

The samples for the Mastersizer were prepared in exactly the same way as was done for the filtrations. The variation in HA concentrations were not taken into account for this experiment. The obscuring of the solution limits the instrument therefore the highest concentration that could be measured was approximately 0.05 C-mol/l (half the concentration of the input solution). Rather than measuring a range of possible HA concentrations it was assumed that this concentration would not be the key influence on floc size (e.g. [Milligan and Hill, 1998](#)) and that other factors (i.e. relative Al concentration, pH and EC) would most likely be more important. In order to keep the conditions similar to the ones in the thin box experiment no background electrolytes were used. The ionic strength was therefore strongly dependent on the Al concentration (see table 4.4). The concentration of HA, which flocculates with itself, would probably determine the speed of flocculation rather than the resulting floc size. The pH of each sample was adjusted to pH 4.3 (prior to adding Al) in order to be close to the pH range that was expected for the main (2D) experiment. During the experiment the samples were stirred at 3 different rates: 450, 300 and 150 rpm, in this order. Afterwards the rate was increased to 450 again. This order was chosen to show to what extent the flocculation process is reversible. The pumping rate was kept just above the limit, if it would be any lower particles would get stuck in the tubes (see figure 4.5). The velocity of the water determines the shear on the particles and this, in turn, partly determines the size of the weak flocs. The rate was increased to 450 rpm at the end of each measuring cycle to test the reversibility of the flocculation.

4.3.4 Coupling pH and EC to Al/C

The Al/C ratio in the 2D flow experiment may vary from 0 to 0.1. The actual concentrations of the solutes however could be different even at a stable ratio. It is hard

TABLE 4.4: Ionic Strength

<i>Conc. Al</i>	<i>Ionic strength</i>
0	0.067
0.0005	0.069
0.001	0.072
0.0015	0.074
0.002	0.076
0.0025	0.078
0.003	0.081
0.0035	0.083
0.004	0.085
0.0045	0.087
0.005	0.090

The ionic strength was strongly dependent on the Al concentration.

to measure the aluminium and carbon content directly and continuously, therefore EC and pH serve as indirect values. To be able to estimate the concentrations in the main experiment based on pH and EC measurements the pH and EC first had to be calibrated for the entire range of possible mixtures. In order to do the calibration the possible Al concentrations and the possible DOM concentrations were separated into 11 fractions. These are fractions of the input solution 0.1 C-mole/l for DOM and 0.01 mole/l for Al. The fractions served as the axis of a grid (11 x 11) with 121 cross sections at these cross sections the pH and EC was measured.

Sample preparation. The stock DOM solution was brought to pH 4.3 in order to protonate the functional groups of the HA (again in the same range as the main experiment). This was also done to make sure that the pH was of the mixed solution was as close as possible to the predicted conditions for the main (2D) experiment. The stock was then diluted with DeMi water to create the 11 DOM fractions (0,0.1,0.2...1). Then dry aluminium was added to the solutions stepwise ⁶. At each step the pH and EC were measured.

Correction of the EC data. The EC electrodes were calibrated in two ranges: $EC < 2000 \mu S cm^{-1}$ and $EC > 2000 \mu S cm^{-1}$, see figure 4.6. This led to discontinuous measurements which had to be corrected. The corrections were made by fitting a linear trend line through the high EC values ($> 2000 \mu S cm^{-1}$) and the low EC values separately

⁶The steps were made by adding 0.2 grams of dry $AlCl_3(H_2O)_6$. The precision of the scale was mg (two orders of magnitude more precise).

TABLE 4.5: EC Correction Factors

<i>OM 1</i>	<i>OM 0.9</i>	<i>OM 0.8</i>	<i>OM 0.7</i>	<i>OM 0.6</i>	<i>OM 0.5</i>
1.14	1.22	1.23	1.23	1.22	1.22
<i>OM 0.4</i>	<i>OM 0.3</i>	<i>OM 0.2</i>	<i>OM 0.1</i>	<i>OM 0</i>	
1.18	1.18	1.19	1.20	1.20	

In this table the correction factors for the EC measurements higher than $2000 \mu\text{Scm}^{-1}$ are given. These values were used to adjust the EC data where the curves would not fit due to incompatible calibrations of the high and low EC spectrum measurements.

(e.g. [Leon van Paassen, 2009](#)). The trend lines were set to the same interception point so that the formulas would be divisible. The factor resulting from the division of the two trend line formulas was used to scale the exceptionally high values. The scaling factors were calculated per OM fraction, they can be found in table 4.5. If there were not enough data points to fit a regression an average value of the other fractions was used to scale the data. The average correction factor (1.2) was also used to correct the data of the main 2D flow experiment.

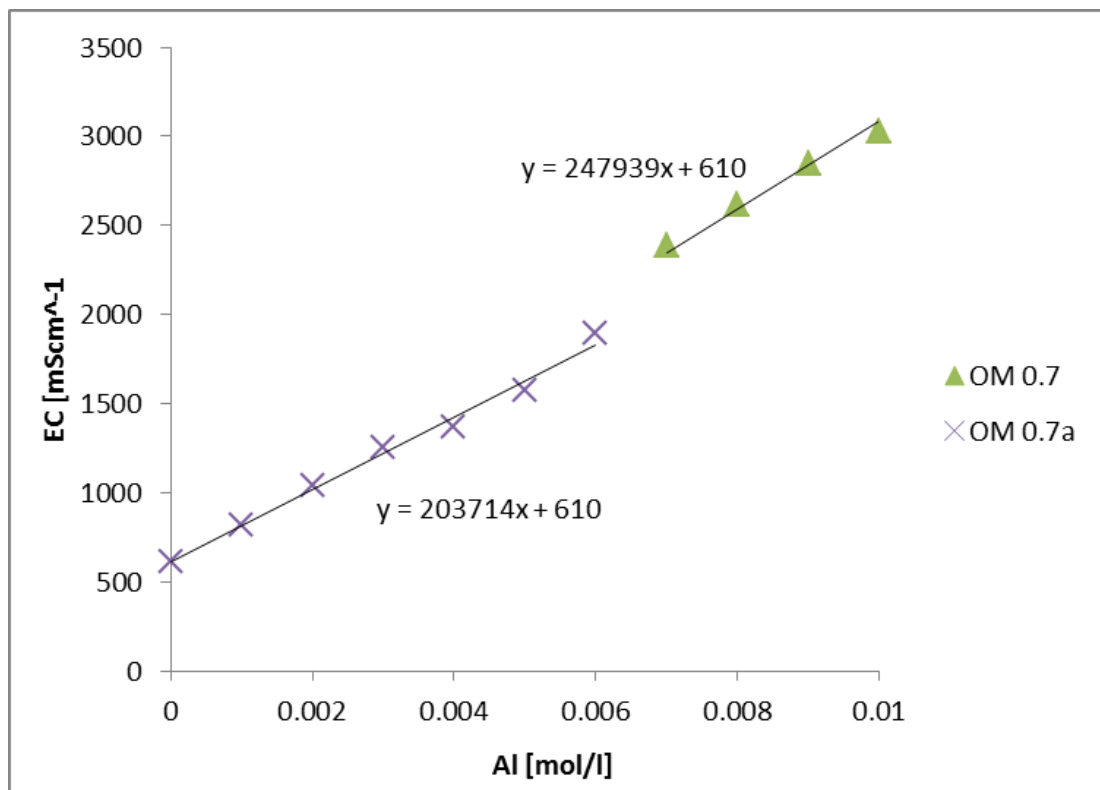


FIGURE 4.6: Raw data of the EC measurements plotted with separate trend lines for the high, $> 2000 \mu\text{Scm}^{-1}$, and low values.

4.3.5 Predicting EC and Al/C Macro-conditions

In order to predict the macroscopic conditions in the main experiment in terms of Al/C and EC, the dispersion of the solutes was evaluated with the reactive flow module of the COMSOL model described in chapter 3. The model predicts the concentrations of Al and DOM at each node, from these concentrations the Al/C ratio could easily be derived. Equation 5.1 was used to estimate the EC values in the main experiment based on the beaker experiments.

Chapter 5

Results and Discussion

Outline. In this chapter the Al/C ratio will be related to precipitation according to the $0.45\mu\text{m}$ scientific standard. Moreover the influence of the Al/C ratio on the actual particle size of the flocculated molecules will be shown. Then the relation of Al and HA concentrations to pH and EC will be discussed after which will be used to explain the results of the main experiment, in this experiment dispersive mixing causes flocculation and precipitation of organic matter ¹.

5.1 Preliminary Experiments

5.1.1 Titrations

The titrations gave superficial insight in the behaviour of the mixed Al-DOM solution. It seemed that with this particular source of organic matter there was very little pH dependence for complexation. Flocculation mostly occurred due to changing Al/C ratios. When precipitation occurred low density, non-crystalline sponge like flocs were observed.

Figure 5.1 represents the visual outcome of the titration experiments with Al/C ratio 0, 0.05 and 0.1. The first set of titrations were a done at constant Al/C ratio. The pH was gradually changed from 9 to 3. No Al was added to the control sample hence the Al/C ratio in this sample was 0. It was expected that, even at $\text{Al/C} = 0$, some

¹Throughout this chapter and in the following chapter it is good to keep the structural formula of humic acid sodium salt in mind. It is important to realize that this particular HA has no phenolic groups and therefore is reluctant to form strong and long range bonds with positively charged ions.

of the organic matter would precipitate as the solution becomes very acidic due to the protonation and subsequent neutralization of functional groups. To check this the solution was given some time to settle but no precipitates were formed, not even at pH 3 (see figure 5.1A). Secondly the Al/C ratio was risen to 0.05 mole/C-mole, see

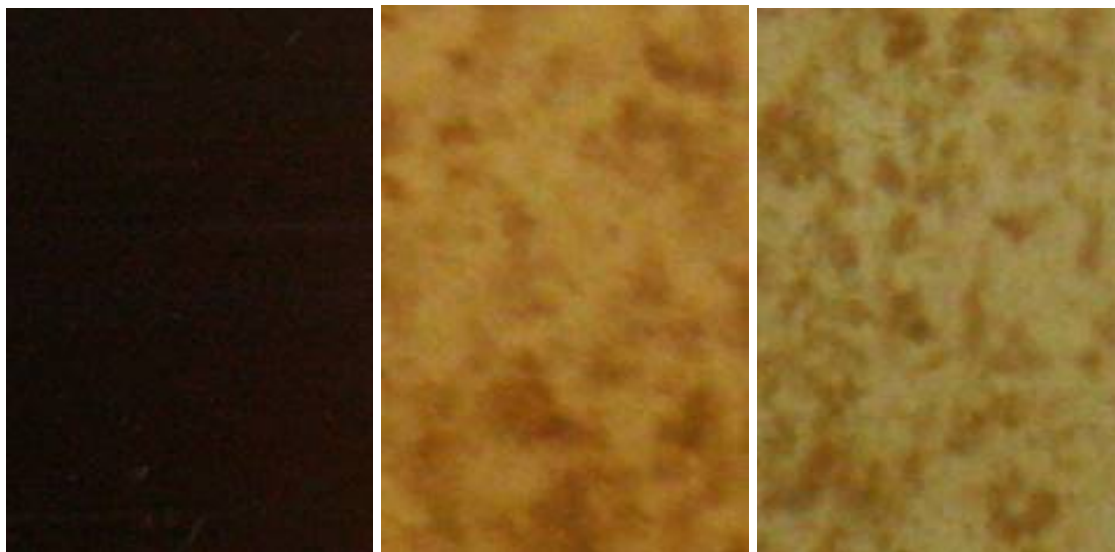


FIGURE 5.1: From left to right: A) Al/C 0, B) Al/C 0.05 and C) Al/C 0.1 after ten minutes of settling at pH 6, this was the remainder of the organometallic complexes in solution. The control samples, which only contain OM (i.e. Al/C 0, fig. A) appear black or very dark brown depending on the solute concentration. It can very easily be seen that the organic matter would not precipitate purely by changes in pH. Carefully looking at Al/C ratio B (0.05) and C (0.1) it is possible to see that some of the larger flocs in the 0.05 beaker were still suspended and that the obscurity of the solution is slightly higher respective to Al/C 0.1, hence also the slightly more brown color. Other pH levels are not included simply because it would be impossible to spot any differences.

figure 5.1B. Referring back to figure 2.4 significant precipitation could be expected at higher pH levels ($\text{pH} > 4.5$) whereas low pH levels ($\text{pH} < 3.5$) would yield very little precipitation. The complexes, however, precipitated regardless of the pH it was therefore impossible to visually confirm a turning point (i.e. the resultant solution all looked like figure 5.1B). The same behaviour was observed at Al/C 0.1, although the obscurity of the solution after precipitation tended to be slightly lower, see figure 5.1C. The differences are marginal but, if anything, it is possible to cautiously state that higher Al/C ratios lead to faster precipitation and thus a clearer solution after 10 minutes.

In the second series of titrations the pH of the DOM solution was set at 4, 6 and 8 the Al/C ratio was changed by adding a concentrated Al solution. In these experiments the resolution for the Al/C ratio was much higher, it could therefore be deduced that the turning point for precipitation lies between Al/C 0.02 and 0.03, rather than at 0.05.

Before Al/C 0.02 the solution would look like 5.1A at any pH. At 0.03 precipitation commenced. At Al/C ratios higher than 0.03 there was no large difference compared to Al/C 0.03 (comparable to the difference between figure 5.1B and 5.1C). The fact that there seemed to be no influence of pH on flocculation is very atypical (e.g. Jansen et al., 2003; Scheel et al., 2008a; Weng, 2002) may be due to the atypical choice of DOM.

5.1.2 Quantification of Precipitation

In table 5.1 the precipitated fractions of the MO complexes are given for several pH levels and Al/C ratios. The pH range was taken into account to prove that there is no significant pH effect on the total amount of precipitates. The concentration of the DOM in the filtrate (measured by the TOC analyser) could be divided by the input concentrations. The rest value of this subtraction is the organic carbon that was left behind in the filter and was thus according to the scientific standard (i.e. particles larger than $0.45 \mu\text{m}$) precipitated. From this table can be deduced that, at least for engineering purposes, there is no significant difference between the pH levels nor is there a real effect of Al/C ratios higher than 0.03. The complexes may simply not be able to bind to more Al because the negative potential of the organic molecule is completely compensated.

The pH independence, that was also found in these experiments, was likely the result of the characteristics of the chosen HA. The Sigma-Aldrich Humic Acid Sodium Salt only has carboxylic functional groups, as said before these groups do not form strong bonds and easily dissociate. The dissociation constant pK_a for NaDOM is 3.48 (Tipping, 2002, and references therein), which means that 50% of the functional groups are dissociated at pH 3.48 in an aqueous solution. A slightly 'phenolic' DOM source is more likely to be affected by changes in pH. This demonstrates that there is only minor competition for binding sites over the entire spectrum making the relative Al concentration the most important factor for complexation.

5.1.3 Floc Size Analysis

In figure 5.2 the mean of the floc size distributions for 3 shear rates are plotted against the Al/C ratio in the solution. In this figure can be seen that the mean floc sizes were dependent on the stirring rate in the mixing jar and the Al/C ratio. The shear stresses

TABLE 5.1: Precipitated MO Fractions

<i>Al/C</i>	<i>pH 4</i>	<i>pH 6</i>	<i>pH 8</i>
0	0.22	0.22	0.22
0.01	0.26	0.27	0.27
0.03	0.93	0.95	0.95
0.06	0.95	0.95	0.96
0.1	0.95	0.95	0.96

The concentration of the DOM in the filtrate was subtracted from the total input concentration and afterwards divided by the total concentration, these fractions (precipitated organic carbon) are given here. The rest value of the subtraction is the organic carbon that was left behind in the filter and was thus, according to the scientific norm (i.e particles larger than $0.45 \mu\text{m}$), precipitated.

caused by increased stirring break the flocs. Higher Al/C ratios led to larger flocs and little to no flocculation occurred at Al/C ratios lower than 0.02. The increase in floc size, however, effectively stopped at Al/C > 0.03 (arguably at 0.04 for the highest rotation speed). In other words between Al/C 0.02 and 0.03 there is a turning point at which the mean floc sizes change the most. It is likely that the complexes reached their isoelectric point at Al/C 0.03 which could either have been due to a severe increase in ionic activity (addition of Al) or by the specific binding of Al to HA ([Angelico et al., 2014](#)).

Next to those findings it was also found that the flocculation of the HA was entirely reversible for all Al/C ratios from which can be concluded that no strong bonds were formed during the flocculation process, see Appendix [A](#).

5.1.4 EC and pH

The effect of precipitation and changing Al and DOM concentrations on the EC and pH were determined. In order to do this a grid of 121 points was made with different Al and DOM concentrations, these concentrations were fractions of the input concentrations for the 2D experiment. At each grid point the EC and pH were measured see figure [5.3](#). With the knowledge that HA and Al are the only dissolved species in a solution their concentrations can be estimated from these figures by measuring the pH and EC of the solution. This can only be done provided that the HA is initially protonated to the same extent as was done in these experiments.

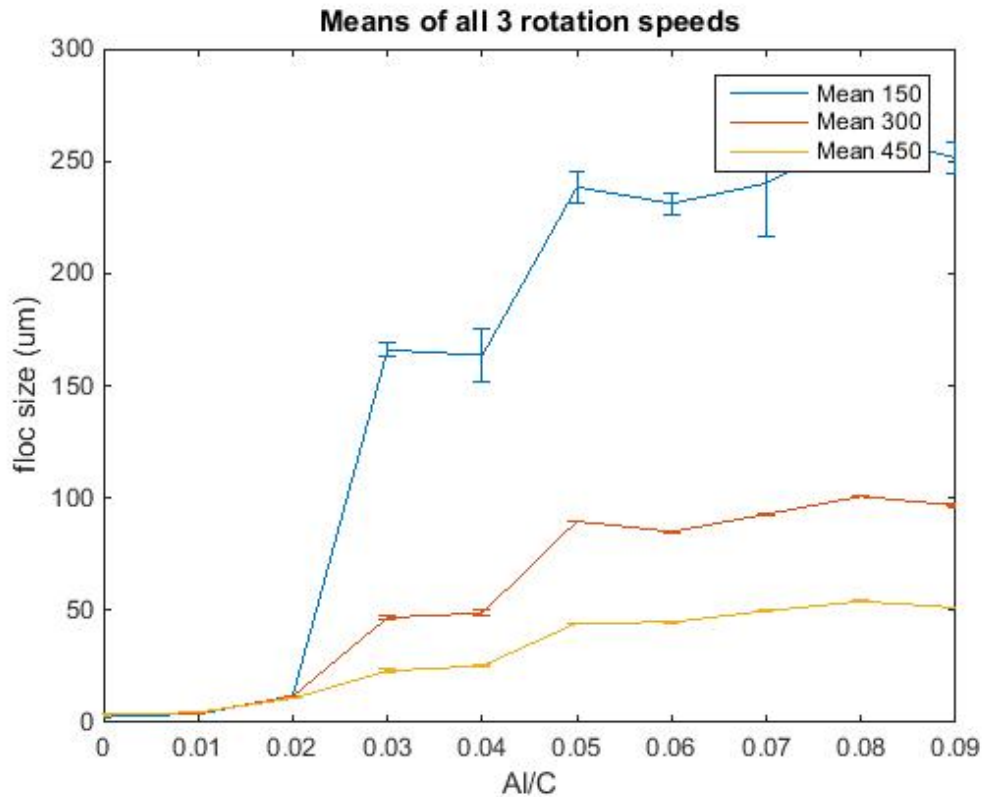


FIGURE 5.2: Flocculation at three different stirring rates (from left to right 150, 300 and 450 rpm respectively). The x-axis contains the molar Al/C ratio, the absolute concentration of organic-C was 0.05 mol/L. The y-axis contains the floc size in μm . For each mean 10 separate measurements were made with small (milliliters) random volumes taken out of the same 900 ml of solution. Additional information about the measurements of the flocculation of HA can be found in Appendix A. This appendix also shows the deviations between the measurements.

EC analysis. In figure 5.4 the EC is plotted against individual HA and Al concentrations and measured combined concentrations. It was found that the calculated sum of the EC values of the individual concentrations is equal to the measured combined EC. Therefore the EC for a mixture of Al and HA solutions can be based on their individual concentrations through an empirical formula:

$$EC_{AlDOM} = EC_{Al} + EC_{DOM} = 10.84 * [DOM] + 187.67[Al] + 10.16 \quad (5.1)$$

In which the HA concentration is given in C-mole/ m^3 and the Al concentration in mol/ m^3 . The formula was rewritten slightly to account for concentrations rather than fractions of a described input solution. The shape of the equation is represented in the surface plot of EC, see figure 5.3. The concentrations of HA and Al can however not be

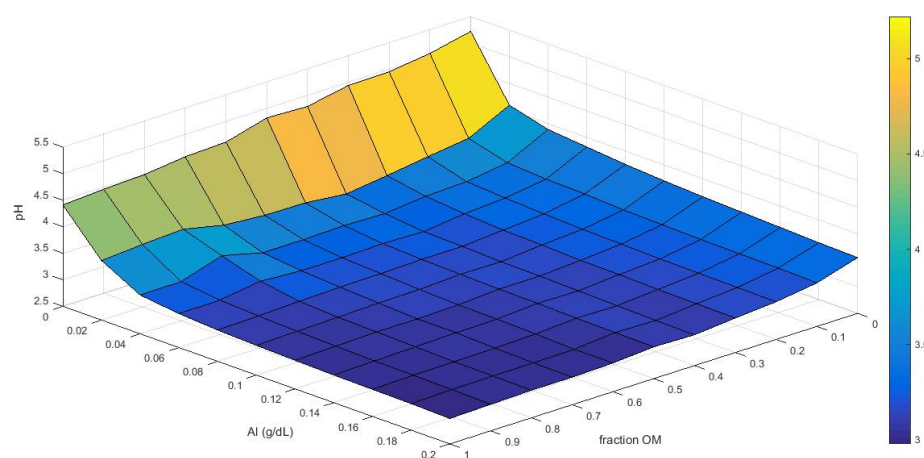
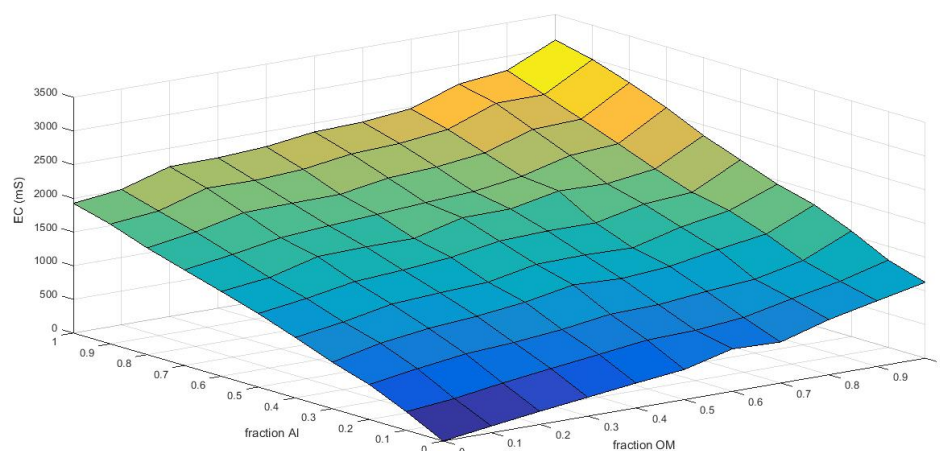


FIGURE 5.3: pH and corrected EC values: Measurements were taken at the 121 intersections of the lines. The x-axis denotes the fraction of OM that will be used in the flow experiment (0.1 C-mole/L), the y-axis contains the Al concentration is the added dry weight of $AlCl_3(H_2O)_6$ per dL. The z-axis is the EC (top) and pH (bottom).

predicted solely based on EC since this equation could yield the same value for several combinations of HA and Al concentrations. Hence a second denominator is necessary.

pH analysis. Furthermore figure 5.3 shows that there are no drastic jumps in pH or EC. The change in H^+ concentration is approximately linearly dependent on the concentration of Al ions, this goes for all HA concentrations. The relationship between the free protons and aluminium can be seen in a log-log plot, see figure 5.5. This figure shows that even at very low HA concentrations the pH is still linearly related to the Al concentration. Even if the Al concentration is large with respect to the HA concentration

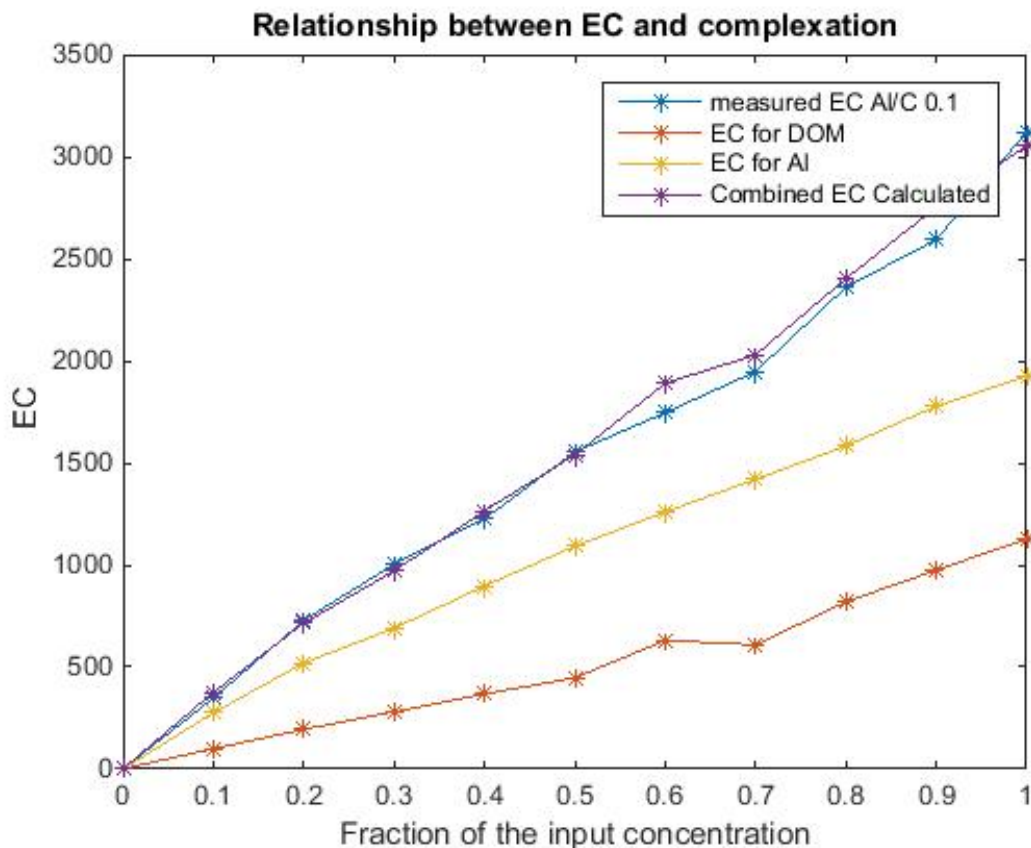


FIGURE 5.4: EC as a function of fractional input concentration of Al and DOM and the measured combined EC. The calculated EC plot is the sum of the Al and DOM EC measurements. Linear trend lines were fitted for the separate effects of Al and DOM on the EC in the form of $y = p1 * x + p2$. The coefficients for Al are $p1 = 1876.7$, $p2 = 101.83$, and for DOM: $p1 = 1083.7$, $p2 = -37.045$.

a reduction in pH still takes place. Based on this information the substitution reaction of Al and H^+ can be written:



Where Al is a Lewis acid (Zumdahl and DeCoste, 2012). In an acidic solution where the carboxylic groups are protonated (i.e. COOH) addition of Al will therefore lead to further acidification. Of course if the solution is alkaline the functional groups will already be dissociated and addition of Al will have less consequence. Figure 5.5 clearly demonstrates that the scale at which acidification occurs is dependent on the concentration of protonated HA. The change in acidity can be explained by three key processes: i) the hydrolysis of aluminium (i.e. organic C concentration = 0), ii) the dissociation of the protonated HA in DeMi water (i.e. Al concentration = 0) and iii) interactions

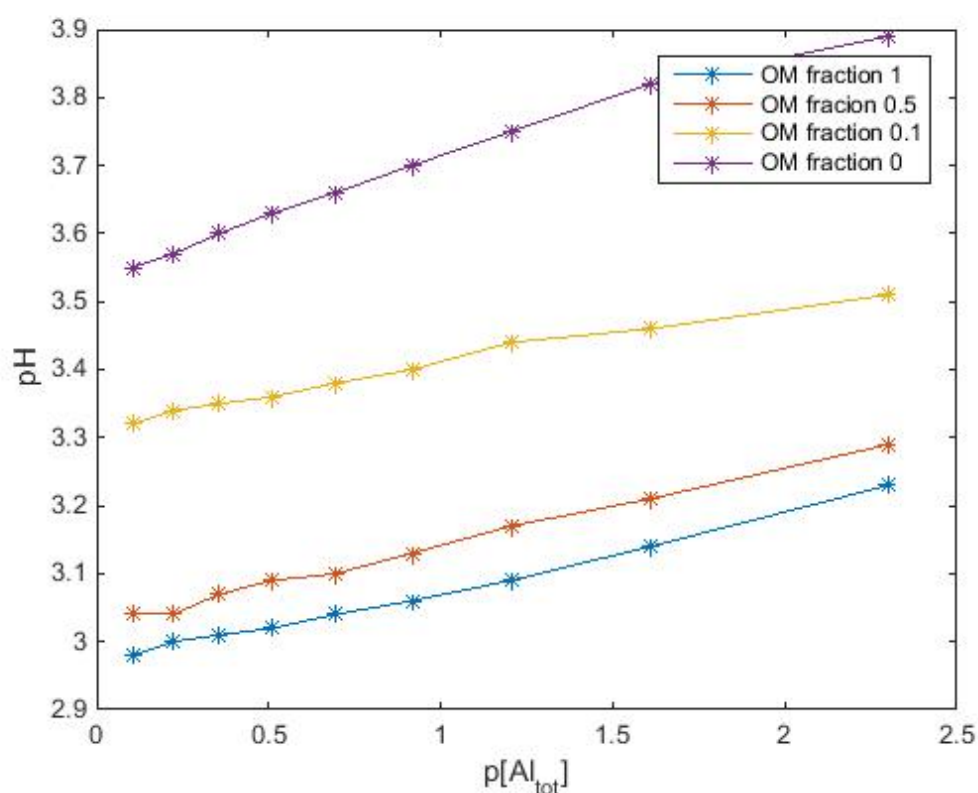


FIGURE 5.5: The pH as a function of the total Al concentration at the outer most and middle DOM concentrations on a log-log scale. The other lines are omitted for clarity. It can be seen that there is approximately linear substitution of Al and H at the HA functional groups. The OM 0 line shows the effect of the hydrolysis of Al on the pH (see section 2.3.1 for the hydrolysis reactions of aluminium).

between Al and HA.² The slope of the OM 0 line in figure 5.5 is comparable to the other lines, this suggests that hydrolysis dominates the acidification regardless of the OM concentration. In figure 5.6 can be seen that this statement is not true. The change in pH can not be explained by summing the hydrolysis and dissociation effects. From figure 5.6 the conclusion could be drawn that the sum of these two effects do not come close to explaining the change in pH in a combined Al-DOM solution. Assuming that Al-DOM complexation is the main cause of the changes in acidity, the extend of complexation can be estimated from the measured change in pH. Of course the calculable deviations due to the hydrolysis of Al and natural dissociation of HA have to be taken into account. It is important to note that the linearity in figure 5.5, even at very large Al/C ratios, suggests that the complexes are not saturated yet.

²Of course the HA source and the extent of the HA protonation (acidity of the DOM solution) respectively determine the shape and steepness of the graph shown in figure 5.5. For example: another source of DOM with more phenolic groups would, perhaps, cause non-linearity.

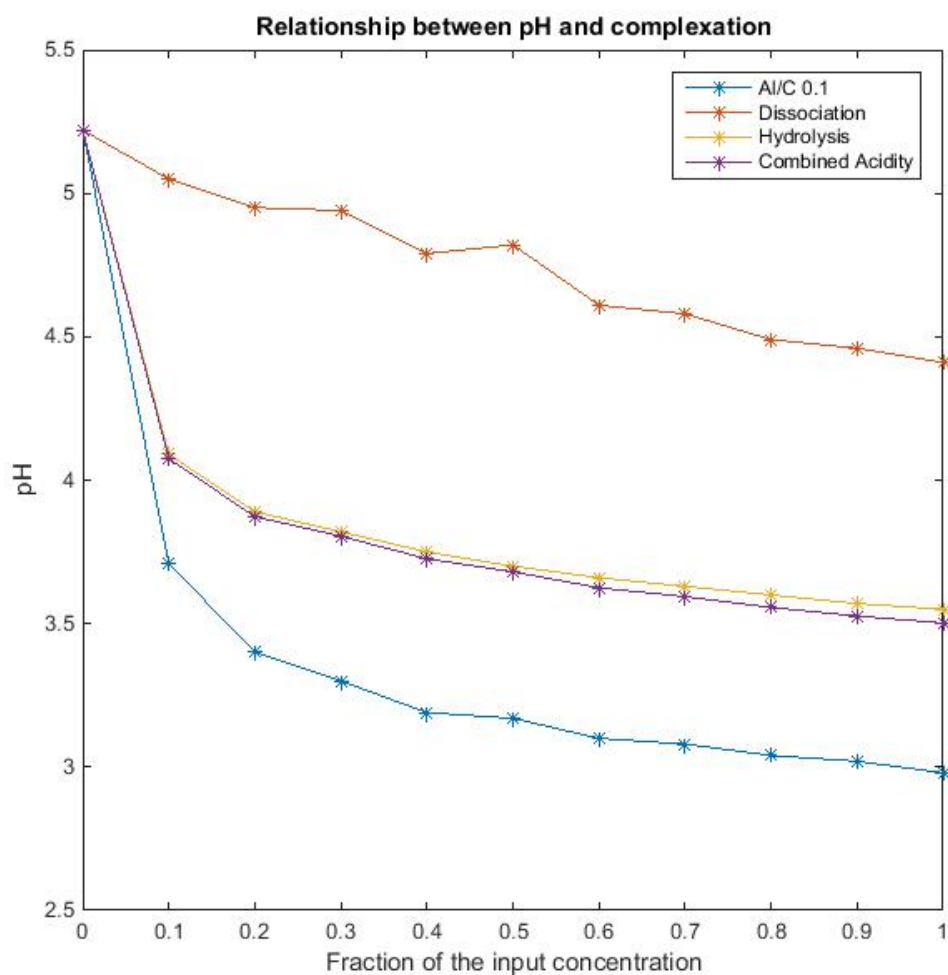


FIGURE 5.6: pH as a function of the fractional input concentration of either DOM or Al or a combination of the two. If there were no complexation the pH would be dependent on the dissociation of hydrogen ions from HA (red) and the hydrolysis of Al (yellow). The combined effect would then be the purple line. The purple line deviates approximately half an order of magnitude from the blue line which is the actual combined acidity at Al/C ratio 0.1.

5.2 Flocculation in a Porous Medium

5.2.1 Visual

First a pulse of HA was sent through the porous medium, this was washed away with a 3 hour high velocity rinse with DeMi water. From this, it could be concluded that the organic matter alone does not precipitate in the pores. After the rinse the HA and Al solutions were injected parallel to each other. On the right hand of the set-up HA was injected (*HA domain*) and on the left side Al (*Al domain*). During this phase of

the experiment the clogging of the pores could easily be recognized as a dark brown layer the dispersion of HA could also be seen very well: figure 5.7. The Al solution was colourless. The experimental cycle was repeated twice as explained in chapter 4.

First experimental cycle. See figure 5.7 (a) and (b). A thin, dark brown band started to grow directly after the solutions dispersed into each others domain. During the 'reactive flow' the band proceeded to grow towards high concentrations of HA (i.e. the right domain in the pictures) which continued until the end of this phase. It could be seen that the HA did not disperse far beyond the precipitate layer. After the reactive flow phase soluble HA and Al was flushed out with DeMi water for one hour, the thin brown band did not fade. This 'rinsing phase' was however far to short hence not all the soluble HA and Al was removed. This became clear during the first falling head test. In this test the left over aluminium solution that was still at the left side of the set-up was pushed far into the right side of the set-up which resulted in a second precipitation band 5.7.

Second experimental cycle. See figure 5.7 (c) and (d). Due to the unfortunate aluminium displacements in the falling head tests the entire HA side became slightly clogged. It was therefore no surprise that during the second reactive flow, some of the flow paths on the 'aluminium side' of the set-up were taken by the HA. This caused the outflow at the Al side to be relatively large during this phase of the experiment and a large amount reactive HA found itself at wrong side of the barrier. In figure 5.7d the effect of these flow path displacements can clearly be seen, the complete top of the set-up became dark brown and a second precipitate line was formed in the sand layer. Visually the third falling head test had roughly the same result as the second one: HA was washed out due to poor prior rinsing. ³

5.2.2 Model Results

Thinking about the system it could be considered that DOM flocculates with itself under the influence of Al. In this scenario the amount of Al that is actually consumed might be

³The same rinsing schedule was used in the second experimental cycle although it was clearly flawed. This was done merely for the sake of continuity, to repeat the cycle in exactly the same way, and because there were simply not enough hours in a day.

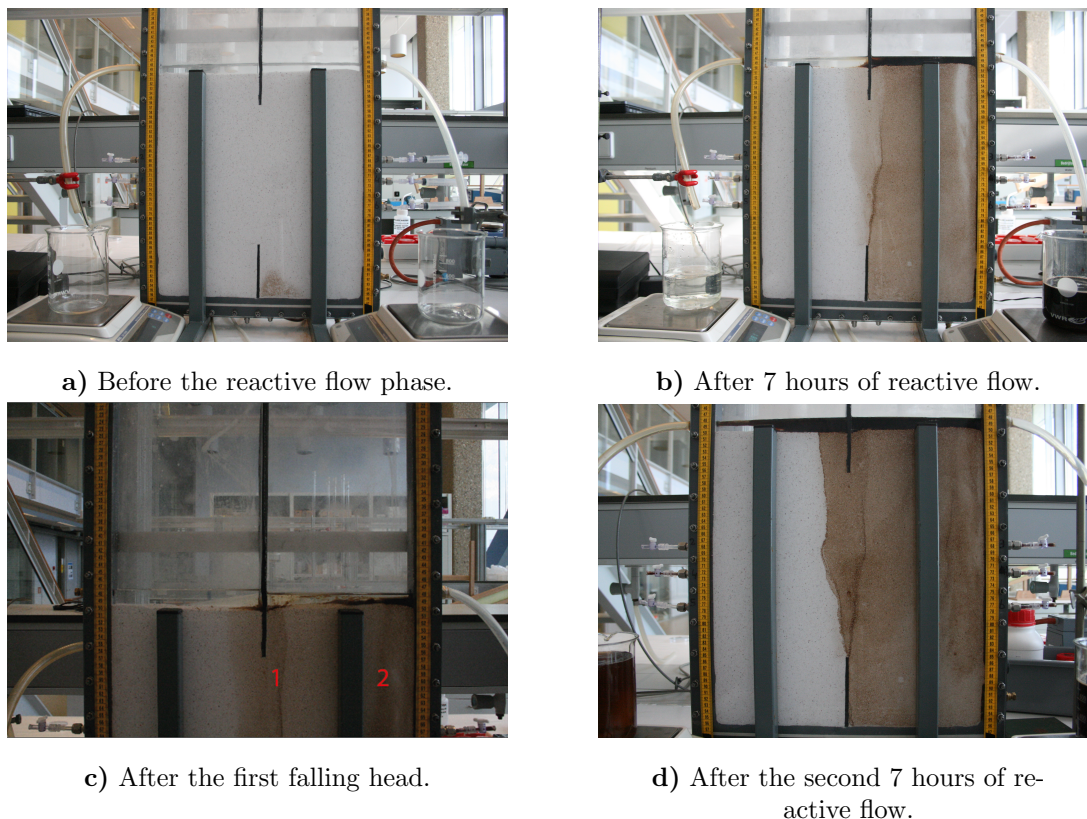


FIGURE 5.7: A clear dark brown layer forms at the boundary of the HA and Al solutions during the first 7 hours of reactive flow. The falling head test pushes the aluminium into the HA domain causing a secondary reaction and precipitation at location 2 in figure c.

very low. Therefore a scenario was modelled in which the Al consumption was neglected. This scenario only considers a source term for Al-DOM in the reactive module. In this case the precipitation band tends to move toward the DOM side of the domain (see figure 5.8). This is because higher DOM concentrations lead to larger amounts of precipitation according to equation 2.37. From the graphics shown in figure 5.8 it can be seen that the location of the precipitate layer can be accurately predicted with the assumption that the Al consumption is very low. If the consumption of Al is high the Al/C ratio will become too small in the DOM domain, the precipitate layer will then be formed in the Al domain.

It is however too optimistic to state that the location of the precipitate layer in the physical model is entirely controlled by the physiochemical processes described in chapter 2 and the COMSOL model. It is far more likely that small defects in the experiment caused preferential flow, for example close to the boundaries of the domain, and thereby

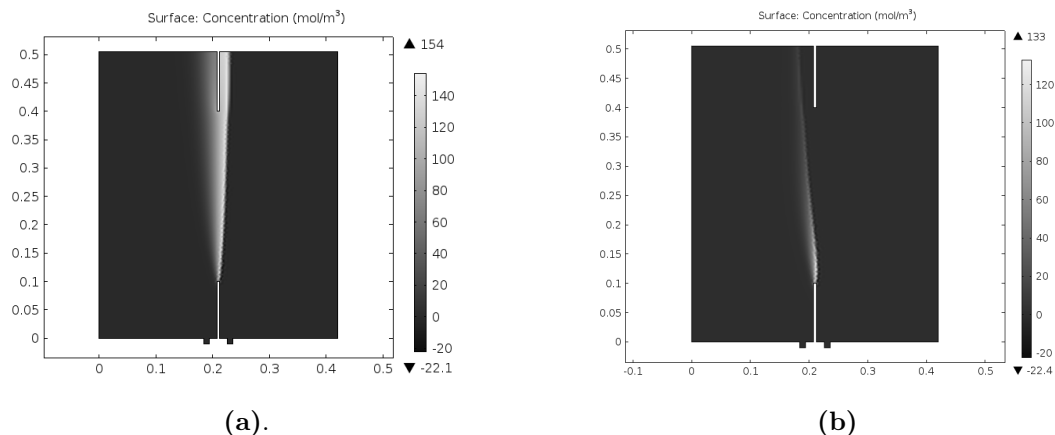


FIGURE 5.8: Precipitation predictions with (b) and without (a) a sink term for aluminium. The white areas depict high precipitate concentrations. Because the porosity is not coupled to the reactions the model overestimates the amount of precipitates, the location of the precipitates is in accordance with the theories in Chapter 2.

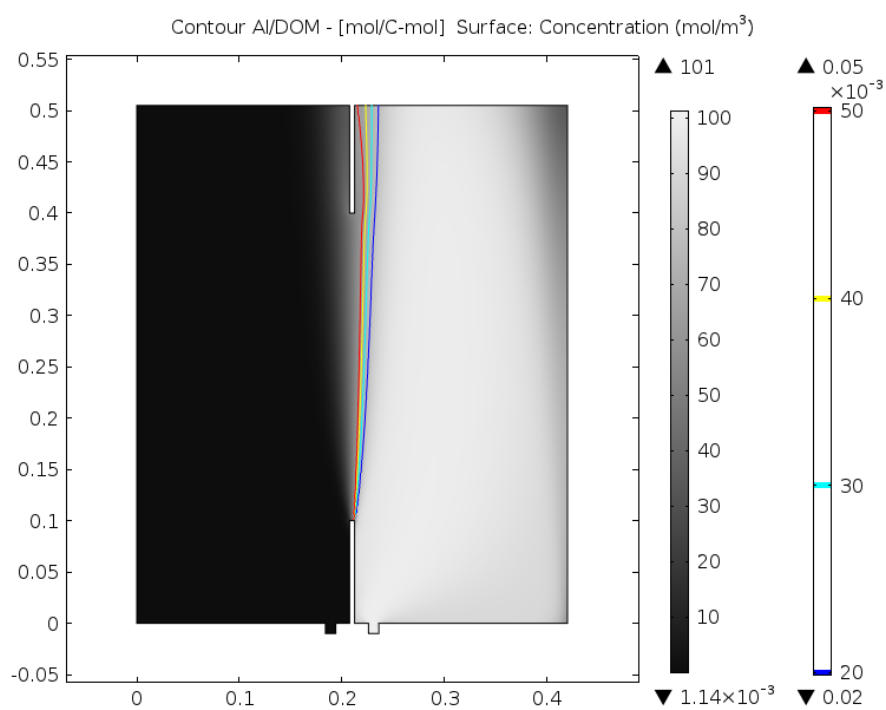
influenced primary location where Al came into contact with DOM. Moreover, the direction of the precipitates also changes in the second phase of the experimental study. Therefore neither of the scenarios can be validated.

5.2.3 EC and pH, Measurements of Macro Conditions

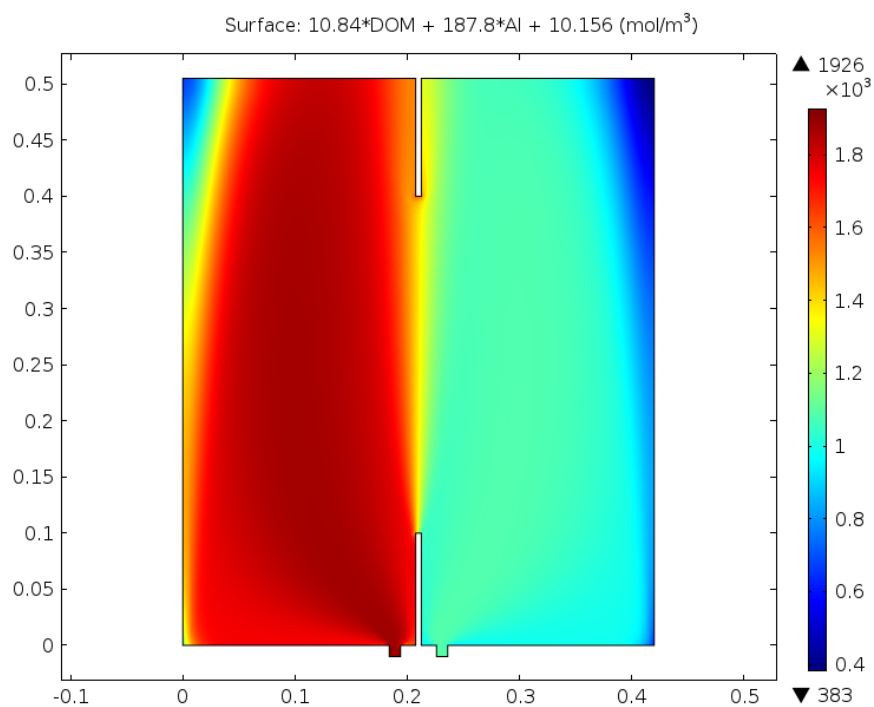
During the reactive flow EC and pH measurements were done each hour over a small grid of six points. It was expected that i) the values within the grid would change gradually and could be interpolated in space (see figure 5.9 (a)), ii) that the Al/C ratio could be deduced from these values to some extent with the pH and EC calibrations (see figure 5.9 (b)) and that iii) the precipitation zone would correspond to estimated Al/C ratios higher than 0.02. In reality the measurements showed in which general area the layer was rather than its formation conditions, these data can be found in table 5.2 and 5.3. In figure 5.9 the model predictions are given based on the parameters found from the solution chemistry experiments in section 5.1.4. For the EC field formula 5.1 was used.⁴

When comparing the predicted EC values from figure 5.9 with the values in 5.3 it can be seen that the measured table values are very high. The model prediction is firmly based on the EC measurements done for the exact same solutions outside of a porous medium, the values should therefore not deviate much. The most likely explanation for this is that some solutes are released by the sand.

⁴In order to give accurate predictions for the pH field based on fundamental chemistry the reactions module of the model has to be expanded.



a) DOM and Al/C ratio.



b) Predicted EC surface.

FIGURE 5.9: Predictions for the DOM concentrations and Al/C ratios in figure a. The contour lines represent the Al/C Domain in which most change can be expected that is: Al/C 0.02 to 0.05. In figure b the calculated EC field is given based on the fitted formula for the solution chemistry data.

TABLE 5.2: pH Measurements Reactive Flow

	<i>2Al</i>	<i>5Al</i>	<i>1HA</i>	<i>4HA</i>	<i>3Mix</i>	<i>6Mix</i>
<i>t1</i>	9.34	4.88	9.22	9.11	9.25	9.32
<i>t2</i>	8.67	4.34	9.02	5.62	9.32	3.92
<i>t3</i>	4.38	4.3	4.23	4.30	4.26	4.25
<i>t4</i>	4.32	4.26	4.21	4.26	4.21	4.23
<i>t5</i>	4.23	4.26	4.19	4.11	4.18	4.2
<i>t6</i>	4.21	4.2	4.21	4.12	4.2	4.12
<i>t7</i>	4.2	4.21	4.18	4.13	4.29	4.15
<i>t8</i>	4.34	4.25	3.79	3.83	3.81	3.83
<i>t9</i>	4.36	4.16	3.80	4.23	3.94	3.97
<i>t10</i>	4.26	4.13	4.24	4.25	4.09	4.13
<i>t11</i>	4.25	4.15	4.15	4.25	4.2	4.08
<i>t12</i>	4.15	4.13	4.19	4.28	4.13	4.13
<i>t13</i>	4.13	4.13	4.25	4.26	4.08	4.13
<i>t14</i>	4.13	4.13	4.09	4.25	4.11	4.12

The pH measurements for the reactive flow phase, each hour at six sample ports. The aluminium side of the set-up is denoted *Al*, the humic acid side *HA* and the mixing zone *Mix*. The *bold values* indicate abnormalities that might indicate complexation.

The results of the pH and EC measurements are in table 5.3 and table 5.2. From the start of the experiment it takes approximately 2 hour for the solutions to reach all sample ports (for the locations see: 4.2). After two hours the precipitation slowly starts and continues to move upwards as the solutions mix there as well. The precipitate band does not change location until a new experimental phase starts. The EC and pH values are also stable after two hours and all sample points seem to fall exclusively in the 'HA zone' or the 'Al zone' because the precipitation band was never really in the middle. It can be seen that with few exceptions the EC values were either very high ($2600 \mu S cm^{-1}$, representative for 0.01 M Al) or very low ($900 \mu S cm^{-1}$, representative for 0.1 C-mole/l HA). The input solutions were both at pH 4 which in accordance with the pH values for the full unmixed fractions in the calibration experiment. In table 5.2 it is clear that the solutions are initially slightly buffered by the sintered sand. The extremely high pH values (i.e pH 9) are just measurements of DeMi water which has a far lower buffering capacity than the actual input solutions its pH is therefore much more dependent on interactions with the sand.

Although the outcomes of these measurements are quite dull there are some interesting things that could be noted. The pH did drop below pH 4 a few times, these are indicated bold in the table. The low values are likely an indirect result of the falling head test. This test, as said before, resulted in aluminium displacement to the right side of the

TABLE 5.3: EC Measurements Reactive Flow

	<i>2Al</i>	<i>5Al</i>	<i>1HA</i>	<i>4HA</i>	<i>3Mix</i>	<i>6Mix</i>
<i>t1</i>	310	1420	550	470	430	465
<i>t2</i>	1850	2050	570	620	600	1410
<i>t3</i>	2250	2200	840	870	1880	2250
<i>t4</i>	2300	2250	860	850	2250	2250
<i>t5</i>	2250	2250	900	820	2200	2200
<i>t6</i>	2200	2300	820	930	2250	2250
<i>t7</i>	2250	2250	850	840	2250	2200
<i>t8</i>	1840	1970	1520	1100	1940	2150
<i>t9</i>	1860	2130	1240	1050	1520	2050
<i>t10</i>	2150	2250	1060	980	1230	1120
<i>t11</i>	2250	2300	1080	980	1260	1050
<i>t12</i>	2250	2250	1020	960	1200	1030
<i>t13</i>	2300	2250	1010	970	1140	1060
<i>t14</i>	2250	2300	990	960	1160	1040

The EC measurements for the reactive flow phase, each hour at six sample ports. The aluminium side of the set-up is denoted *Al*, the humic acid side *HA* and the mixing zone *Mix*.

set-up. The displacement led to mixing with leftover HA and this in turn likely caused reactions and a minute change in pH (minute relative to the pH changes in the calibration experiments). In the next experimental cycle these low pH values were measured during the first two hours (hours 8 and 9), hereafter the normal steady state took over again and the values returned back to normal.

From the EC values the concentrations of Al and HA can be inferred. It is important to note that the EC values found during the flow experiment at the Al side of the set-up are nearly always higher than the maxima found for just aluminium in the EC calibration ($2350 \mu S cm^{-1}$), a difference of $250 \mu S cm^{-1}$. There could be two reasons for the high EC values: i) minute HA concentrations add up to the measured EC or ii) the sand releases solutes that increase the EC. Figure 5.7 clearly shows that hardly any organic matter penetrates the Al domain and from figure 5.3 can be deduced that quite large amounts of HA are necessary to increase the EC by $250 \mu S cm^{-1}$.

5.2.4 Falling Head

Average conductivity reduction. Falling head tests were done before the first reactive flow phase and then again after each experimental cycle. The outflow of the falling head test was measured cumulatively, see figure 5.10. The change in head per

unit time became significantly smaller each cycle from due to the reduced hydraulic conductivity. The $\log(dh)$ vs time plot is approximately linear which indicates that there is no change in the hydraulic conductivity during the falling head experiment. These changes could have been due to unwanted interferences like for example incomplete saturation (Fitts, 2002; Pinder and Celia, 2006) and outwash or growth of precipitates. Moreover the linearity also shows that the secondary reactions during the falling head tests did not lead to very large changes in average hydraulic conductivity.

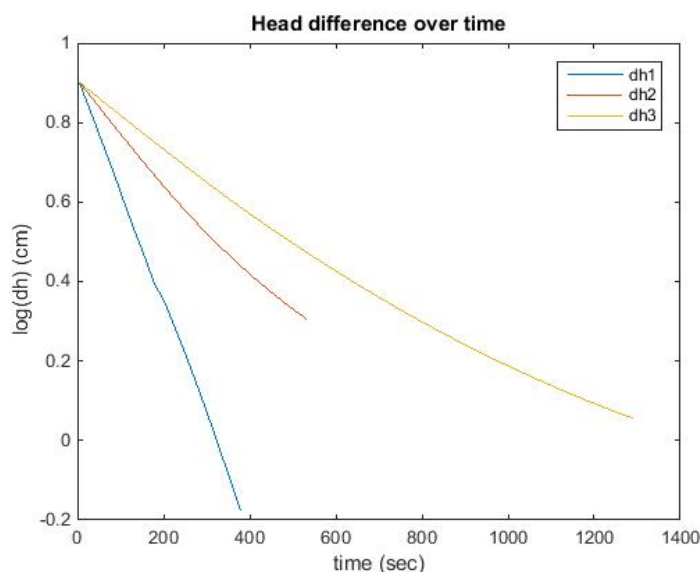


FIGURE 5.10: The results of the first (dh1), the second (dh2) and the third (dh3) falling head tests plotted as the change in head difference between the two sides of the set-up (dh) over time (see 4 for further explanation).

Comparing the conductivities over the whole domain with equation 4.1 is a very simple but robust method to visualize the average change. The conductivities were compared with each other using a mean of 5 data points at the beginning and at the end of each experiment. They could only be expressed relative to one another since the length of the flow path is unknown. Using the data and formula 4.1 the hydraulic conductivities of the second and third falling head could be calculated as a factor of the first one, see the first column of table 5.4. This could be done assuming that changes in the whole domain are responsible for the loss of its conductivity. This table clearly shows that the average hydraulic conductivity of the sand and boundaries in the set-up has been reduced by 77%, due to insoluble Al-DOM complexation. This fact gives proof of principle that this 'engineering tool' works. But the reductions in hydraulic conductivity that are reached with biofouling are around 2 orders of magnitude larger (Seifert and Engesgaard, 2007; Bielefeldt et al., 2002; Holm, 2000). Hence, for engineering purposes, a reduction of 77%

TABLE 5.4: Boundary Conditions Flow Model

	κ_{cal}/κ_1	κ_1/κ_{2-3}
<i>Scenario FH 1</i>	1	1
<i>Scenario FH 2</i>	0.38	$1.10 \cdot 10^{-4}$
<i>Scenario FH 3</i>	0.23	$1.10 \cdot 10^{-4}$

The calculated average conductivity reduction κ_{cal}/κ_1 , and the estimated specific conductivity reduction κ_1/κ_{2-3} .

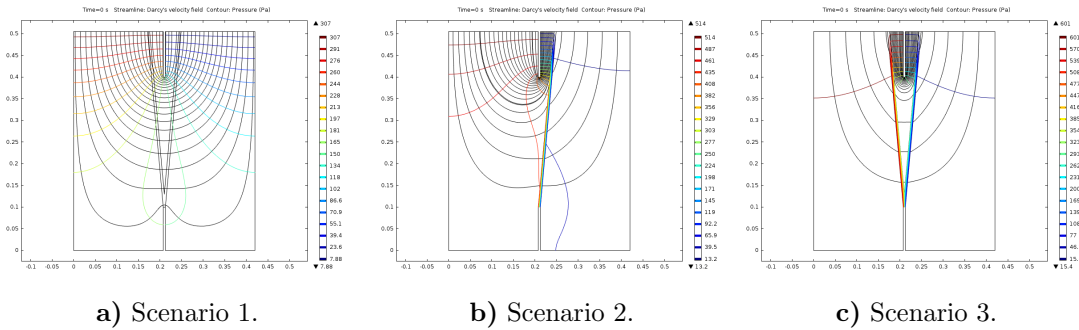


FIGURE 5.11: Modelled flow lines for the three conductivity scenarios.

is far from worthwhile. Local changes in hydraulic conductivities could, however, be much larger than the average 77%. The local changes in κ were estimated with a model.

Model Analysis In section 5.2.1 could be seen that distinct precipitation bands were formed during the reactive flow phases. It is however unlikely that the average reduction in hydraulic conductivity reflects the conductivity reduction in the thin precipitate layer Fitts (2002). Therefore three separate scenarios were modelled. In the second and third scenario (representative of the second and third falling head test) it was assumed that the precipitate layer causes the reduced permeability. Due to this heterogeneous permeability distribution the flow-lines changed drastically (see figure 5.11), as well as the fitted permeabilities (see table 5.4). The conductivity changed with by four orders of magnitude. Moreover, there is virtually no difference between the fitted conductivity reductions for scenario 2 and 3. This notion further approves the assumptions about the physical domains that underlay this analysis (see Chapter 4 for a detailed explanation of the scenarios).

Table 5.4 clearly shows the difference between the assumption that the changed outflow is caused by a homogeneous change in κ and the assumption that this is merely due to the precipitate layer. As said before, the first yields only a 77% reduction whilst the latter shows a reduction of nearly 4 orders of magnitude. In scenario 3 of the modelling

study only the geometry was changed to find a fit. The drastic permeability reduction in the modelling scenarios suggests that the precipitate layer was impermeable relative to the bulk of the sand during the first reactive flow phase of the experiments. This can not entirely be true, because during the second (experimental) reactive flow phase, the DOM solution seemingly easily dispersed through the first precipitate layer. The modelling output may be wrong because there is a far wider precipitation band than can directly be seen, or merely because the geometry is far too simplified. Therefore the truth probably lies somewhere in between the two values.

This range of hydraulic conductivity reduction shown in table 5.4 is comparable or better than other engineering solutions. Moreover the experiment was done over a very short time. It can be expected that further precipitation (e.g. [Weng, 2002](#)) and alteration of the precipitates (e.g. [Scheel et al., 2008a](#)) leads to further reduction of the hydraulic conductivity in longer experiments.

Chapter 6

Conclusion

The average hydraulic conductivity of a silica sand in a three dimensional flow domain has been reduced by 77%. This was achieved by hydrodynamic mixing of an Aluminium ($AlCl_3(H_2O)_6$) and a Humic Acid Sodium Salt ($C_9H_8Na_2O_4$) solution in a silica sand filled thin box. The solutes precipitated subsequent to mixing and thereby reduced the permeability of the sand in the experimental set-up. The reduction in permeability gives proof of principle that Al-DOM interactions can be used as an 'engineering tool' to reduce subsurface flow. Of course, for engineering purposes, the calculated average reduction of 77% is far from worthwhile.

The physical changes that occurred during the hydrodynamic mixing, however, seemed to be concentrated in a small (1 cm wide) precipitation band. By analysing the spatial distribution of EC and pH in the experimental flow domain and using the visual evidence it could cautiously be stated that the precipitation band hampered further advection and dispersion of the solutes. From this information it can be assumed that the hydraulic conductivity changed locally, in the precipitate layer, rather than over the whole flow domain. With a modelling study the local reduction in conductivity was estimated to be 4 orders of magnitude. Although the truth probably lies somewhere in between 77% and 4 orders of magnitude, this range clearly demonstrates the future potential of the technology.

It should also be noted that large differences in hydraulic conductivity between the first and the second falling head test suggests that further reduction of the permeability is possible. Moreover, this was a pilot study in which large changes were achieved in short

time scales (hours), due to these short time scales the full potential of the technology was probably not reached.

The macroscopic conditions at which the interactions between DOM and Al take place were determined for beaker solutions and (laboratory) soil solutions. From titration experiments could be deduced that the HA flocculates with Al, rather than forming crystalline precipitates. This flocculation however ensures that 95% of the HA does not fit through a $0.45 \mu\text{m}$ membrane and can therefore be called particulate. Moreover it was found that the Al/C ratio, and to a far lesser extent the EC and pH of the solution, determine the speed of flocculation and the size of Al-HA flocs at short time scales (minutes) in simple beaker solutions. The onset of flocculation was at Al/C 0.02, at Al/C ratios higher than 0.03 further addition of Al did not lead to a significant increase in floc size. Next to these findings it was observed that the flocculation process was entirely reversible merely by increasing the shear stresses on the flocs.

Flocculation also seemed to be the dominant mechanism for precipitation when Al and HA were mixed in a porous medium made of sintered silica sand. It was shown that the location of the precipitation layer could be predicted based on the processes that apparently govern flocculation in beaker experiments. Therefore it can cautiously be stated that the conditions that determine the amount of precipitation in a beaker also determine the amount of precipitation in a porous medium.

The first precipitates were found to be persistent in the soil. Even though these precipitates were merely weak; low-density; amorphous flocs. The consistency of the flocs suggests that they can coagulate further. At large time scales (i.e. decades) natural soil formation can create hard pans that are orders of magnitude less permeable than their initial soil structure. The amorphous flocs formed during this research may well be one of the first steps towards the creation of such a hard pan. The great future challenge is to bridge the gap of knowledge that exists between the formation of amorphous flocs, their further coagulation and the natural phenomena that cause rigorous permeability reduction. In order to create a viable engineering solution the mechanisms behind further coagulation have to be identified and amplified in order to create impermeable layers at short time scales.

Chapter 7

Recommendations

7.1 The Use of Different DOM Sources

Using Humic Acid Sodium Salt was great for a pilot study and the fact that it has only carboxylic groups makes it a nice reference point for future studies but cheap DOM sources have to be considered. It is however important to be selective when choosing an OM source since the term organic matter is astoundingly broad. Other DOM sources may lead to different flocculation behaviour, for example, the humic acid that I got from Nor Md. Zain only flocculates at higher pH levels ($\text{pH} < 3.5$) and yields far smaller flocs relative to the HA used in the main experiments of this thesis. The HA used in this thesis has very small molecules, its molecular weight is 226.14 g/mol while average DOM has a molecular weight of 500 to 5000. Larger molecules may have very different, perhaps better, precipitation and clogging behaviour. In future research this is an important point to investigate.

7.1.1 On Future Selection of DOM

For now the most important characteristic of the organic matter is its ability to precipitate at short time scales in order to clog pores. Qualitatively the flocculation and thereby also the precipitation behaviour of OM can be analysed fairly quickly with the Malvern Mastersizer, as was done in this thesis. With the help of this machine a selection can be made for different DOM sources that effectively precipitate or flocculate with Al at different pH levels. Ideally starting with a wide basis of FA and HA sources that also

irreversible flocculate. The molecular size, functional group type and functional group density are the most important chemical characteristics based on which the selection has to be made. Next to that it is good to consider cheap sources of DOM like extracts from waste water or compost. Another option is to use the dredged OM from harbour floors. Because the flocculation of DOM in river estuaries causes expansive problems in harbours, therefore this source of OM and its precipitation behaviour is already widely studied. The DOM sources should be stored and their structure has to be analysed, most importantly: 1) elemental analysis (CHNSO analysis), 2) average negative charge (membrane dialysis), 3) quantification of functional groups, 4) structure and aromaticity, 5) orientation of functional groups, and finally 6) the type of external bonds (inner sphere, outer sphere, chemical or physical).

7.2 Improvements for the 2D Laboratory Set-up

There were two large issues with the laboratory set-up and the expectations regarding this set-up:

1. Creating a controllable environment within the walls of the set-up is hard. The plexiglass container was not rigid causing narrow gaps at several attachment points. Several do-overs were necessary because sand started to creep into these gaps during the filling of the container. Then when the sand was filled with satisfactory precision the basin was filled with water. At this point it was found that flow still goes via higher conductivity short cuts along the sides of the basin. Moreover the barriers that were designed to separate the flow of Al and DOM were useless because reactive HA found its way to the Al side of the basin anyway. The plates were placed to be able to make a mass balance but this was not possible due to the mixing of the solutes in the outflow.
2. Next to those issues the reactive front seemed to suppress further dispersion of Al and HA causing a very narrow precipitate layer. The EC and pH therefore changed rapidly over an unexpectedly small area (centimeters). There were therefore far too little sample points and interpolation of the data would yield unrealistic results.

The concept of the set-up, however, is still very interesting. It allows seeing the formation of the precipitates as well as measuring the macro-conditions in which they are formed.

In principle only three major changes have to be made: the measurements must be more continuous in time and space, structural changes to ensure a stable environment and changes in the flow regime. The conclusions that were now cautiously drawn from the EC and pH data would be strengthened by higher resolution measurements.

7.2.1 Continuous Measurements

EC measurements have to be done at a far more regular interval in time and space. This is not possible to do by hand with sample ports. Therefore high conductivity pins can be installed at regular spacing (< 1 cm) over the entire width of the set-up at each side of the set-up. The conductivity can then be measured directly from one side of the basin to the other but also indirectly (see figure 7.1). If a known voltage and current is applied the conductivity is the inverse of the resistance of the medium and can easily be calculated for each of the two cases:

Case 1: black

$$\Delta V = \frac{I}{2\pi\Gamma} \left(\frac{2}{\Delta x} - \frac{2}{2\Delta x} \right) \quad (7.1)$$

and

$$\Gamma = \frac{I}{\pi\Delta V} \frac{1}{\Delta x} \quad (7.2)$$

Case 2: brown

$$\Gamma = \frac{I}{V} \frac{1}{\Delta x} \equiv \frac{1}{\Omega m} = S/m \quad (7.3)$$

Next to this a good way to continuously measure pH or solution stability (a measure of zeta potential) has to be found to uniquely define the problem at all times.

7.2.2 Structural Changes

Furthermore the container must be made less wide in order to ensure that the plexiglass does not bend so far that either the volume or the flow is compromised the basin could for example also be 5 x 20 cm. Glass could also be used in order to increase the stiffness of the thin box but this is a far harder material to handle (i.e. drilling holes for sample ports and making watertight connections). Thought has to be put in the lid of the basin, the solids have to be inserted with ease otherwise layering and heterogeneous packing

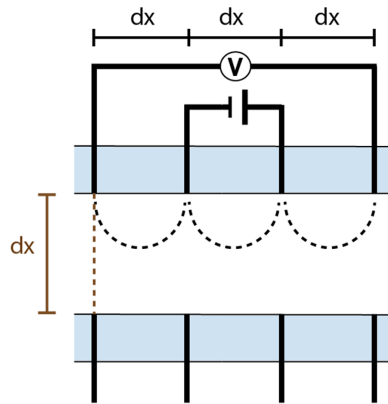


FIGURE 7.1: Alternative EC measurements

or density distributions can cause problems. In order to resolve this problem the basin should have an easily removable lid. The two vertical plates that separate the AI and DOM sides of the basin are of no use, they can best be omitted, dispersive mixing has to be controlled in another way.

For further pilot tests it is better to use glass balls as a porous medium to create a more homogeneous pore size distribution and to reduce chemical variables in the experiment. Later simulations can be done with sudden changes in grain size and clays.

7.2.3 Changes in Flow and Measurement Cycle

To get reliable quantitative data it is important that the flow of solutes is controlled to a larger extent. Figure 7.2 shows the proposal. By generating an under pressure at the extraction points and an overpressure at the sides of the basin by making two extra injection points that pump at 1.5 to 2 times the rate of the solute injection points the flow lines in the middle of the basin can be controlled and pushed inwards. To further reduce boundary effects the in and outlets could be immersed further into the soil. The rinsing phase of the experiment, which is done to remove the solutes and test the resistance of the precipitates, will become more reliable and reproducible with the new method. This is because the solutes will only be concentrated in a narrow band in the middle of the basin, see figure 7.2. During the rinsing phase a lot of solutes will be washed out at first and after a while the concentration of solutes in the effluent will gradually decrease and stabilize. Therefore the EC will likely asymptotically decrease. The rinsing phase of the experiment should run until the EC values of the outflow reach a satisfactory steady state. Measuring these EC values during the rinsing phase will probably also generate

valuable qualitative data depending on whether the simple expectation of asymptotical decrease is met. After this a falling head test can be done in accordance with figure 7.2. The pressure difference can be controlled with burettes outside of the set-up and can best be measured with computer coupled pressure sensors. These sensors can be connected to the set-up with a three way tap.

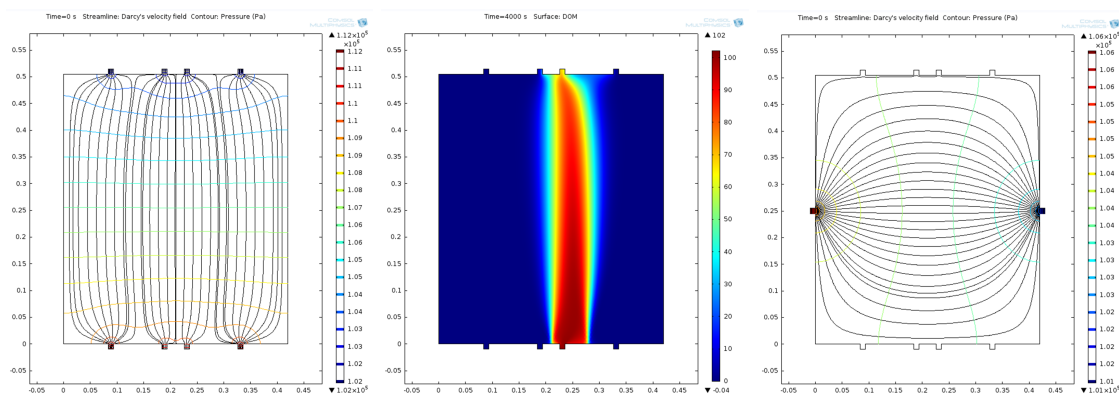


FIGURE 7.2: These figures represent propositions for a better Set-up. The figure on the left and in the middle show the flow lines and solute transport in the reactive flow phase. The figure on the right shows the flow lines for the falling head test.

7.3 Model

In order to increase the theoretical validity of the model the porosity reduction should be coupled to the ADE. This should be validated by comparing the predicted changes in porosity with, for example, CT-scan measurements of the actual porosity change. Next to that it is important to extend the source sink term of the model with a strong physio-chemical equation.

At the moment the model has a reaction module based on equations 2.33, 2.35 and 2.37. Inherent to these equations the assumption is made that precipitation occurs whenever a humic ion is specifically bound to Al and the Al/C ratio is equal to or higher than 0.03 but this assumption may be far too simple. However, in general the model has a very basic definition of ion binding that could easily be expanded to account for, for example, multiple metal solutes (e.g. Tipping, 2002; Kinniburgh et al., 1999). Ideally an adapted form (it only accounts for POM) of the general NICCA model would be used to express specific binding, see equation 2.36, and the Donnan potential formulation for the non-specific ion binding. The inherent reduction in electrostatic negativity that is already empirically coupled to precipitation by Weng (2002) is, in combination with NICCA, the

closest shot at a fundamental description of organic matter precipitation. The theory of [Weng \(2002\)](#) based on the assumption that specific binding causes destabilisation of the solution. All parameters of the NICCA model that can 'easily' be defined can be found in [Appendix D](#). The variables that are not accounted for are the concentrations of solutes inside and outside of the Donnan volume and the Donnan potential. This means that in order to verify a solute transport model, with a precipitation term based on the NICCA-Donnan model, either the speciation of the molecules or the Donnan potential has to be measured at regular intervals.

Appendix A

Results From the Floc Size Analysis

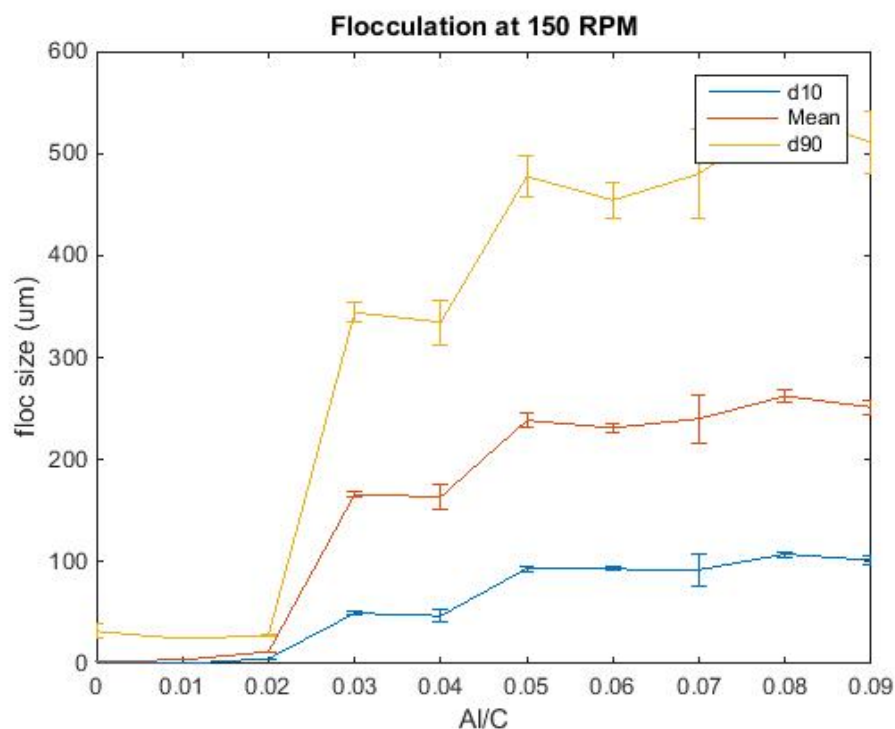
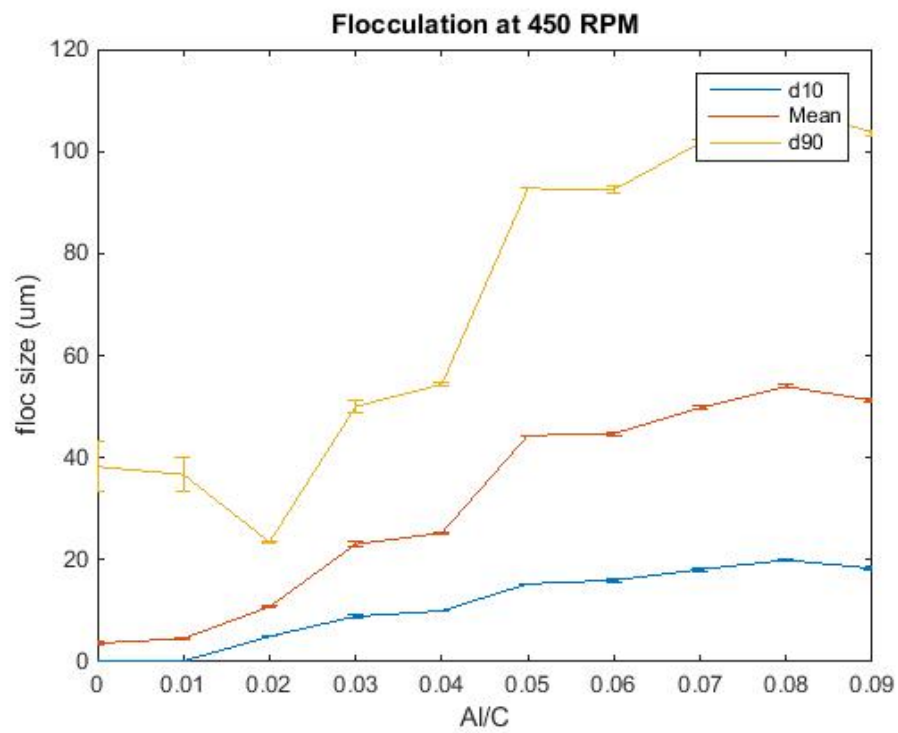
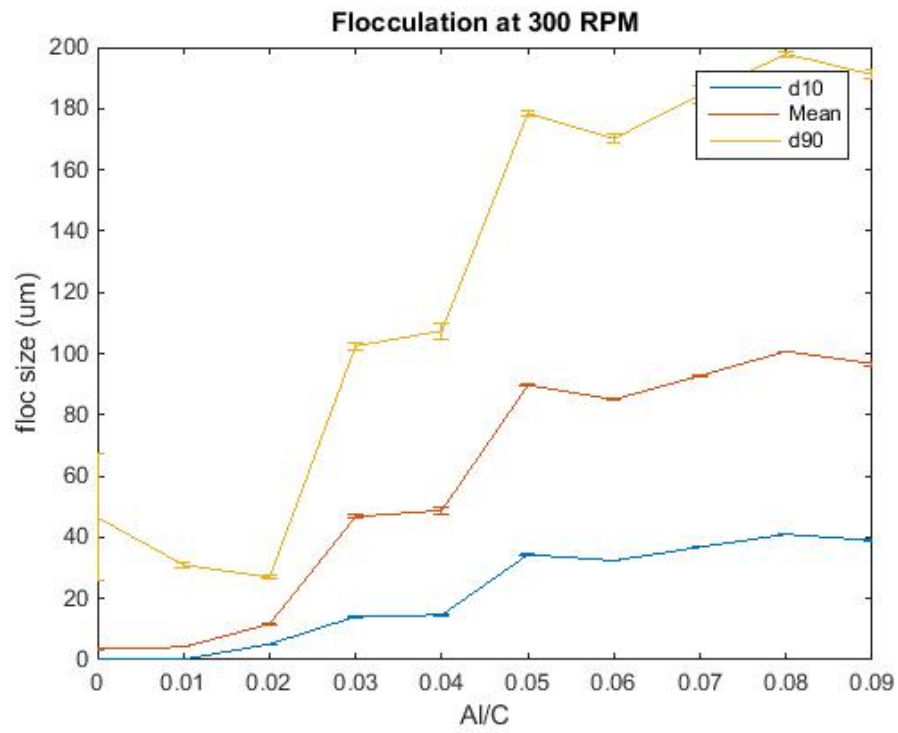


FIGURE A.1: Flocculation at three different stirring rates, from top to bottom 150, 300 and 450 rpm. The d10 and d90 represent the largest 10% and 90% of the flocs respectively. For each mean 10 separate measurements were made with small (milliliters) random volumes taken out of the same 900 ml of solution. The x-axis contains the molar Al/C ratio, the absolute concentration of organic-C was 0.05 mol/L. The y-axis contains the floc size in μm .



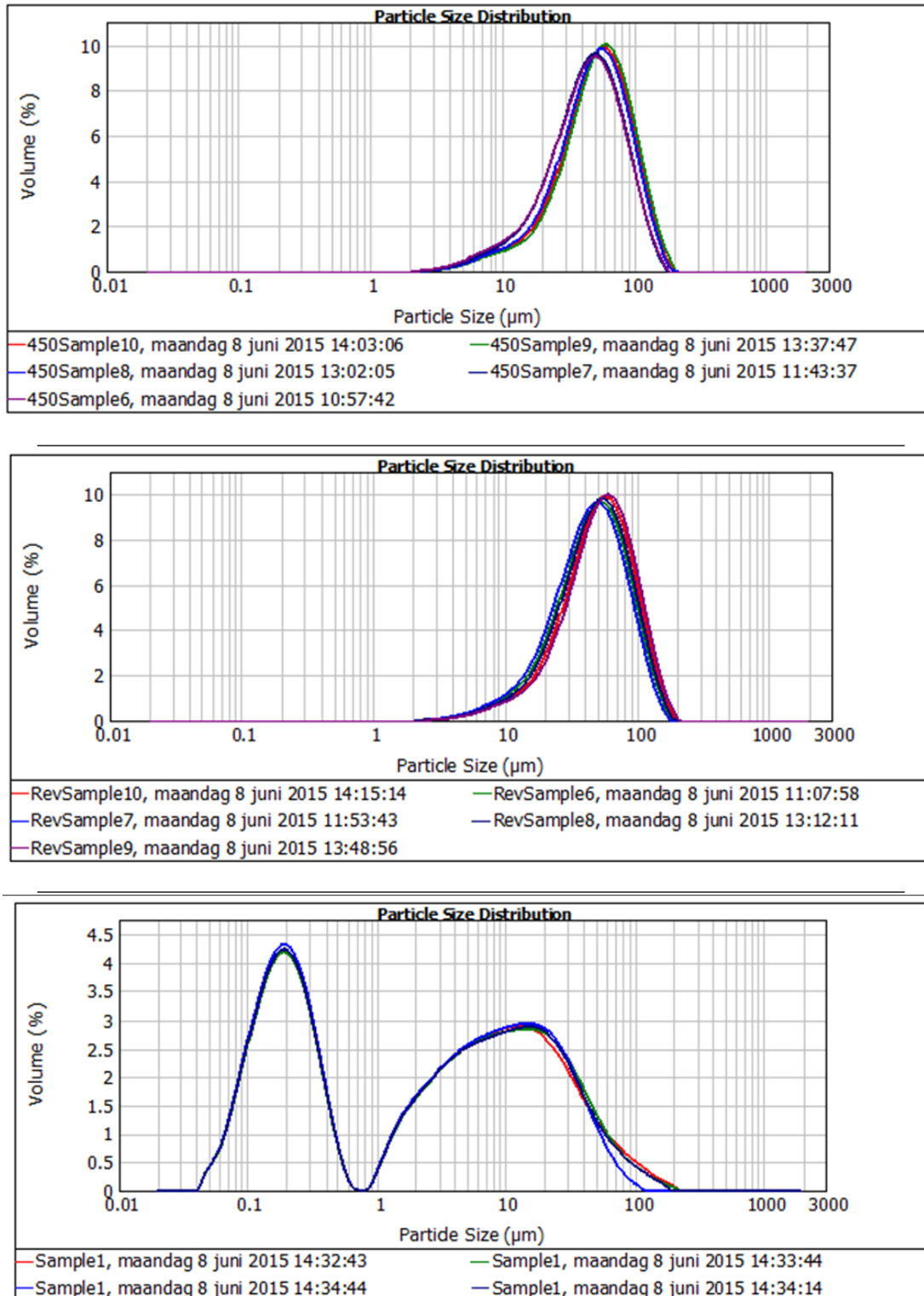


FIGURE A.2: Floc size distribution plots, the top two figures show the floc size distributions for Al/C 0.5-0.9. In an experimental cycle the beaker was stirred at 450, 300 and 150 rpm after which it was again stirred at 450 rpm. The first figure are the samples at the beginning of the measurement cycle at a stirring rate of 450 rpm, the second figure shows the results at the same rotation speed after the whole measurement cycle. The bottom figure shows the curious floc size distribution of the control samples, Al/C 0. The plots were made with Malvern Mastersizer 2000 software.

Appendix B

Datasheets

Datasheets

General fact sheets:

NaDOM: There was no factsheet available on the Sigma Aldrich page for Humic Acid Sodium Salt: www.chemicalbook.com.

Aluminium: A short description of aluminium trichloride hexahydrate could be found on the manufacturers page see the sheet below.

Sand: The factsheet for the grenette sand can be found on the next page.

Product Name:
Aluminum chloride hexahydrate - ReagentPlus®, 99%

Product Number: 237078
CAS Number: 7784-13-6
MDL: MFCD00149134
Formula: AlCl₃ · 6H₂O
Formula Weight: 241.43 g/mol



TEST	Specification
Appearance (Color)	White to Off-White
Appearance (Form) Crystals or Crystalline Solid and/or Chunks	Conforms to Requirements
ICP Major Analysis Confirms Aluminum Component	Confirmed
Titration by AgNO ₃ % Cl	43.4 - 44.7 %

Remarks:
Reviewing Chemist :

Technical Data

Grenette

Omschrijving	Grenette is een sneeuw witte vulstof vervaardigd via een thermische behandeling van zeer zuivere flintstenen. Dit sinterproces verleent aan Grenette bijzondere eigenschappen zoals: de sneeuw witte kleur, kleurbestendigheid, zuurbestendigheid, slijtvastheid, stroefheid, waterdichtheid, hoge weerstand tegen vervuiling, en een laag soortelijk gewicht.																											
Toepassingen	Verfsystemen, kunstharsmortels, sierplijsters, extender en toeslagstof voor thermoplastische en thermohardende kunststoffen.																											
Eigenschappen	<table border="0"> <tr> <td>Kristal soort</td> <td>:</td> <td>hoofdzakelijk cristobaliet</td> </tr> <tr> <td>Witheid</td> <td>:</td> <td>Y > 88</td> </tr> <tr> <td>Hardheid</td> <td>:</td> <td>7 Mohs</td> </tr> <tr> <td>Brekingsindex</td> <td>:</td> <td>1,47-1,55</td> </tr> <tr> <td>Soortelijk gewicht</td> <td>:</td> <td>2,3 kg/dm³</td> </tr> <tr> <td>Stort gewicht</td> <td>:</td> <td>1,1 kg/dm³</td> </tr> <tr> <td>pH</td> <td>:</td> <td>9 à 9,5</td> </tr> </table>	Kristal soort	:	hoofdzakelijk cristobaliet	Witheid	:	Y > 88	Hardheid	:	7 Mohs	Brekingsindex	:	1,47-1,55	Soortelijk gewicht	:	2,3 kg/dm ³	Stort gewicht	:	1,1 kg/dm ³	pH	:	9 à 9,5						
Kristal soort	:	hoofdzakelijk cristobaliet																										
Witheid	:	Y > 88																										
Hardheid	:	7 Mohs																										
Brekingsindex	:	1,47-1,55																										
Soortelijk gewicht	:	2,3 kg/dm ³																										
Stort gewicht	:	1,1 kg/dm ³																										
pH	:	9 à 9,5																										
Kleurbestendigheid	Door het sinterproces is vergeling (oxidatie) uitgesloten. Grenette behoudt dus de witte kleur, ook onder invloed van de weersomstandigheden. Grenette kleurt bovendien niet donker in natte toestand.																											
Chemische Analyse (slechts een indicatie)	<table border="0"> <tr> <td>SiO₂</td> <td>:</td> <td>99,20%</td> </tr> <tr> <td>Fe₂O₃</td> <td>:</td> <td>0,11%</td> </tr> <tr> <td>K₂O</td> <td>:</td> <td>0,04%</td> </tr> <tr> <td>Al₂O₃</td> <td>:</td> <td>0,12%</td> </tr> <tr> <td>CaO</td> <td>:</td> <td>0,50%</td> </tr> <tr> <td>Na₂O</td> <td>:</td> <td>0,06%</td> </tr> <tr> <td>MgO</td> <td>:</td> <td>0,01%</td> </tr> <tr> <td>CaO</td> <td>:</td> <td>0,24%</td> </tr> <tr> <td>Gloeiverleis</td> <td>:</td> <td>0,16%</td> </tr> </table> <p>Vrije basevormende oxiden afwezig</p>	SiO ₂	:	99,20%	Fe ₂ O ₃	:	0,11%	K ₂ O	:	0,04%	Al ₂ O ₃	:	0,12%	CaO	:	0,50%	Na ₂ O	:	0,06%	MgO	:	0,01%	CaO	:	0,24%	Gloeiverleis	:	0,16%
SiO ₂	:	99,20%																										
Fe ₂ O ₃	:	0,11%																										
K ₂ O	:	0,04%																										
Al ₂ O ₃	:	0,12%																										
CaO	:	0,50%																										
Na ₂ O	:	0,06%																										
MgO	:	0,01%																										
CaO	:	0,24%																										
Gloeiverleis	:	0,16%																										
Korrelmaten	<table border="0"> <tr> <td>Grenette nr. 00</td> <td>2,00 - 3,00 mm</td> </tr> <tr> <td>Grenette nr. 0</td> <td>1,00 - 2,00 mm</td> </tr> <tr> <td>Grenette nr. 1</td> <td>0,50 - 1,00 mm</td> </tr> <tr> <td>Grenette nr. 2</td> <td>0,20 - 0,50 mm</td> </tr> <tr> <td>Grenette nr. 4</td> <td>0,02 - 0,25 mm</td> </tr> </table>	Grenette nr. 00	2,00 - 3,00 mm	Grenette nr. 0	1,00 - 2,00 mm	Grenette nr. 1	0,50 - 1,00 mm	Grenette nr. 2	0,20 - 0,50 mm	Grenette nr. 4	0,02 - 0,25 mm																	
Grenette nr. 00	2,00 - 3,00 mm																											
Grenette nr. 0	1,00 - 2,00 mm																											
Grenette nr. 1	0,50 - 1,00 mm																											
Grenette nr. 2	0,20 - 0,50 mm																											
Grenette nr. 4	0,02 - 0,25 mm																											
Verpakking	In PE zakken van 25 kg op éénmalige pallets van 1000 kg met krimpfolie.																											

WAARSCHUWING - Gereedschappen, materialen en straalmiddelen die gebruikt worden voor oppervlaktebehandeling, kunnen gevaarlijk zijn indien ze onoordeelkundig gebruikt worden. Er bestaan diverse nationale voorschriften voor die materialen en straalmiddelen die geacht worden gevaarlijk te zijn tijdens of na gebruik (afvalbeheer), zoals vrij kwarts, carcinogene of toxische stoffen. Deze voorschriften dienen daarom ingezien te worden en te worden nageleefd. Het is belangrijk om te waarborgen dat adequate instructies worden gegeven en dat alle vereiste voorzorgsmaatregelen worden genomen.

TDS. 2014-Grenette (NL) 1/1

Neem contact met ons op voor meer informatie:

Worldwide
Tel: +31 (0)78 6546770
sales.eurogrit@sibelco.com

www.sibelco.eu

Sibelco Europe
PO Box 184
NL-3350 AD Papendrecht
The Netherlands

www.eurogrit.com



Appendix C

pH Curve Displacement

pH Curve Displacement

Due to the substitution of Na^+ by H^+ ions a displacement of the pH curve can be expected. The humic molecules buffer the solution and therefore increase its pH relative to what would occur when adding HCl DeMi water.

TABLE C.1: pH Displacement by Humic Acid Sodium Salt

<i>Weight cum. [g]</i>	<i>HCl cum [mol]</i>	<i>pH DeMi calc.</i>	<i>pH DOM</i>
1073.50	0	6.54	9.04
1083.50	$2 \cdot 10^4$	3.74	7.32
1093.50	$4 \cdot 10^4$	3.43	5.50
1103.50	$6 \cdot 10^4$	3.26	4.19
1113.50	$8 \cdot 10^4$	3.14	3.52

Small dataset for pH displacement.

Appendix D

Parameters for NICA-Donnan

<i>Generic Humic Acid</i>				
Electrostatic Donnan b value in Eq. $\log V_D = a + b \log I$	-0.49			
	low affinity or carboxylic type site		high affinity or phenolic type site	
site density $Q_{\max,H}$ (mol/kg)	3.15		2.55	
heterogeneity p	0.62		0.41	
ion specific parameters	affinity $\log K_1$	non-ideality n_1	affinity $\log K_2$	non-ideality n_2
H	2.93	0.81	8.00	0.63
Ca	-1.37	0.78	-0.43	0.75
Al	-1.05	0.40	8.89	0.30
Fe(III)	5.00	0.30	17.5	0.25
Cu	2.23	0.56	6.85	0.34
Cd	-0.20	0.73	2.37	0.54
Zn	0.11	0.67	2.39	0.27
Ni	-0.26	0.64	1.0	0.55
Pb	1.26	0.60	4.86	0.69

<i>Generic Fulvic Acid</i>				
Electrostatic Donnan b value in Eq. $\log V_D = a + b \log I$	-0.57			
	low affinity site		high affinity site	
site density $Q_{\max,H}$ (mol/kg)	5.88		1.86	
heterogeneity p	0.59		0.70	
ion specific parameters	affinity $\log K_1$	non-ideality n_1	affinity $\log K_2$	non-ideality n_2
H	2.34	0.66	8.60	0.76
Ca	-2.17	0.85	-3.29	0.83
Al	-4.11	0.42	12.16	0.31
Fe(III)	6.0	0.25	36	0.19
Cu	0.26	0.53	8.24	0.36
Cd	-0.99	0.68	0.73	0.50
Zn	-3.84	0.67	-0.73	0.61
Ni	-2.07	0.65	2.03	0.53
Pb	-1.22	0.60	6.87	0.70

FIGURE D.1: Parameters for NICA-Donnan, data from Milne et al. (2001)

Appendix E

Complementary Model Plots

Complementary Model Plots

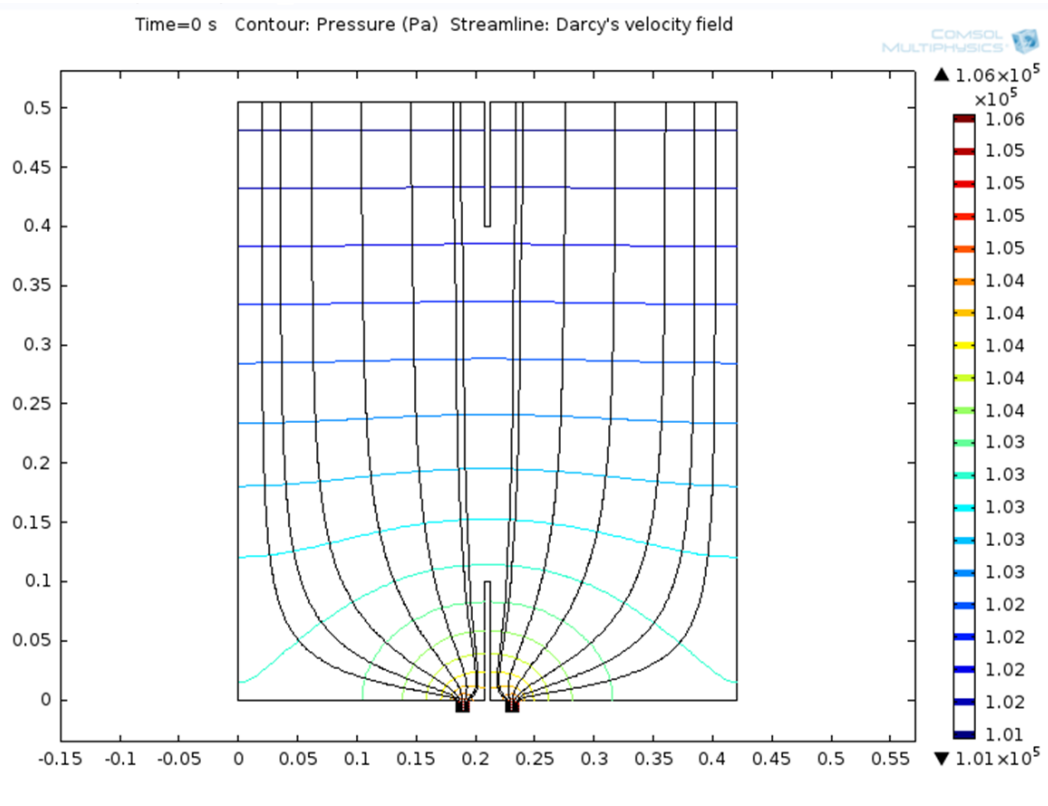


FIGURE E.1: This figure represents the modelled flow lines that are based on the imposed pressure gradients during the reactive flow phase of the experiment.

Appendix F

Falling Head Data

Falling Head Data

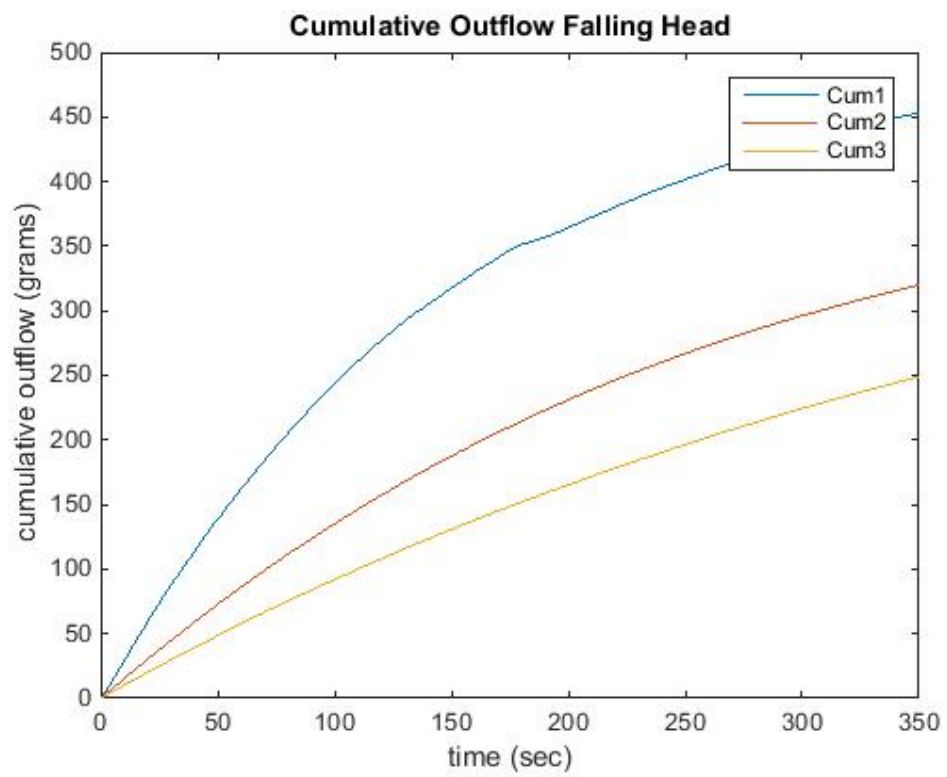


FIGURE F.1: Measured cumulative outflow over time.

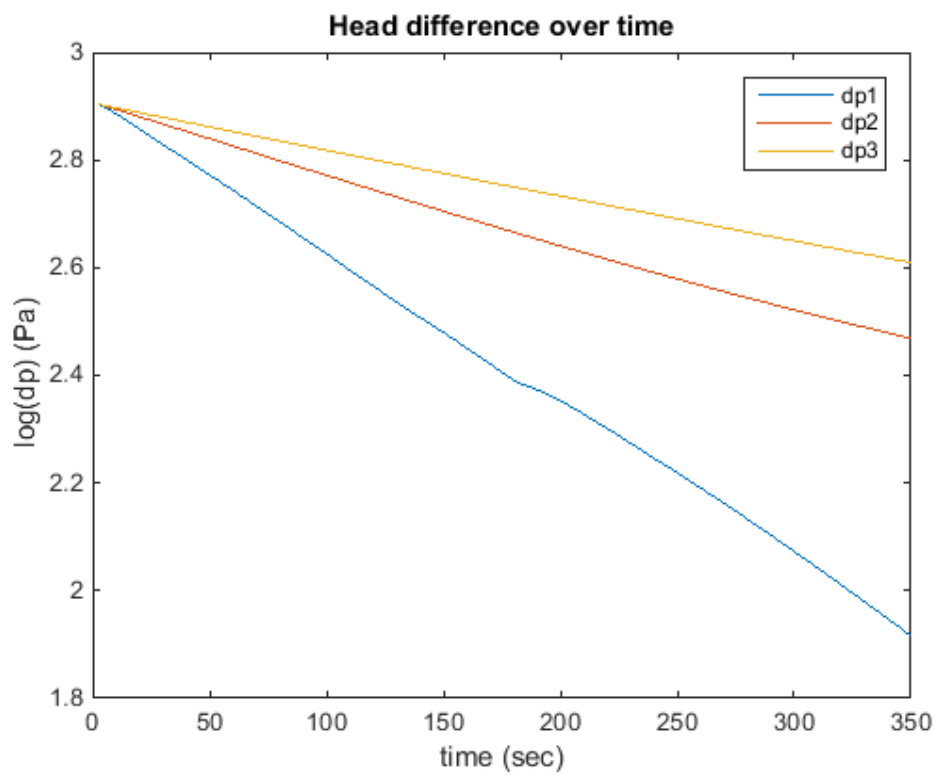


FIGURE F.2: Measured pressure change over time during the falling head tests, dp1, dp2 and dp3 denote the first second and third falling head test respectively.

Bibliography

- Adams, W. (1973). The effect of organic matter on the bulk and true densities of some uncultivated podzolic soils. *Journal of Soil Science*, 24(1):10–17.
- Angelico, R., Ceglie, A., He, J.-Z., Liu, Y.-R., Palumbo, G., and Colombo, C. (2014). Particle size, charge and colloidal stability of humic acids coprecipitated with ferrihydrite. *Chemosphere*, 99:239–247.
- Banik, C., Harris, W., Ellis, R., Hurt, W., and Balboa, S. (2014). Relations of iron, aluminum, and carbon along transitions from udults to aquods. *Geoderma*, 226:332–339.
- Bear, J. (2012). *Hydraulics of groundwater*. Courier Corporation.
- Bernoulli, D. (1738). *Hydrodynamica: sive de viribus et motibus fluidorum commentarii*.
- Bielefeldt, A. R., McEachern, C., and Illangasekare, T. (2002). Hydrodynamic changes in sand due to biogrowth on naphthalene and decane. *Journal of Environmental Engineering*, 128(1):51–59.
- Bottero, S., Storck, T., Heimovaara, T., Loosdrecht, M., Enzien, M., and Picioreanu, C. (2013). Biofilm development and the dynamics of preferential flow paths in porous media. *Biofouling*, 29:1069–1086.
- Boudot, J., Hadj, A. B., Steiman, R., Seigle-Murandi, F., et al. (1989). Biodegradation of synthetic organo-metallic complexes of iron and aluminium with selected metal to carbon ratios. *Soil Biology and Biochemistry*, 21(7):961–966.
- Bourgault, R. R., Ross, D. S., and Bailey, S. W. (2015). Chemical and morphological distinctions between vertical and lateral podzolization at hubbard brook. *Soil Science Society of America Journal*, 79(2):428–439.

- Brady, N. C., Weil, R. R., et al. (1996). *The nature and properties of soils*. Number Ed. 11. Prentice-Hall Inc.
- Brown, R. (1828). Xxvii. a brief account of microscopical observations made in the months of june, july and august 1827, on the particles contained in the pollen of plants; and on the general existence of active molecules in organic and inorganic bodies. *The Philosophical Magazine, or Annals of Chemistry, Mathematics, Astronomy, Natural History and General Science*, 4(21):161–173.
- Buschmann, J., Berg, M., Stengel, C., and Sampson, M. L. (2007). Arsenic and manganese contamination of drinking water resources in cambodia: coincidence of risk areas with low relief topography. *Environmental science & technology*, 41(7):2146–2152.
- Chin, W.-C., Orellana, M. V., and Verdugo, P. (1998). Spontaneous assembly of marine dissolved organic matter into polymer gels. *Nature*, 391(6667):568–572.
- Christensen, J. B., Tipping, E., Kinniburgh, D. G., Grøn, C., and Christensen, T. H. (1998). Proton binding by groundwater fulvic acids of different age, origins, and structure modeled with the model v and nica-donnan model. *Environmental science & technology*, 32(21):3346–3355.
- Companys, E., Garcés, J. L., Salvador, J., Galceran, J., Puy, J., and Mas, F. (2007). Electrostatic and specific binding to macromolecular ligands: A general analytical expression for the donnan volume. *Colloids and Surfaces A: Physicochemical and Engineering Aspects*, 306(1):2–13.
- Crerar, D., Knox, G., and Means, J. (1979). Biogeochemistry of bog iron in the new jersey pine barrens. *Chemical Geology*, 24(1):111–135.
- Cussler, E. L. (2009). *Diffusion: mass transfer in fluid systems*. Cambridge university press.
- Darcy, H. (1856). Les fontanes publiques de la ville de dijon, victor dalmont, paris.
- De Coninck, F. (1980). Major mechanisms in formation of spodic horizons. *Geoderma*, 24(2):101–128.

- De Graaf, R., Van De Giesen, N., and Van De Ven, F. (2007). The closed city as a strategy to reduce vulnerability of urban areas for climate change. *Water Science & Technology*, 56(4):165–173.
- De Jong, J., Soga, K., Kavazanjian, E., Burns, S., Van Paassen, L., Al Quabany, A., Aydilek, A., Bang, S., Burbank, M., Caslake, L. F., et al. (2013). Biogeochemical processes and geotechnical applications: progress, opportunities and challenges. *Geotechnique*, 63 (4), 2013.
- Duan, J. and Gregory, J. (2003). Coagulation by hydrolysing metal salts. *Advances in colloid and interface science*, 100:475–502.
- Dunbar, J. B. and Britsch III, L. D. (2008). Geology of the new orleans area and the canal levee failures. *Journal of geotechnical and geoenvironmental engineering*, 134(5):566–582.
- Edzwald, J. K. and Van Benschoten, J. E. (1990). Aluminum coagulation of natural organic matter. In *Chemical water and wastewater treatment*, pages 341–359. Springer.
- Einstein, A. (1905). Un the movement of small particles suspended in statiunary liquids required by the molecular-kinetic theory Of heat.
- Eusterhues, K., Hädrich, A., Neidhardt, J., Küsel, K., Keller, T., Jandt, K., and Totsche, K. (2014). Reduction of ferrihydrite with adsorbed and coprecipitated organic matter: microbial reduction by geobacter bremensis vs. abiotic reduction by na-dithionite. *Biogeosciences*, 11(18):4953–4966.
- Ferro-Vazquez, C., Nóvoa-Muñoz, J., Costa-Casais, M., Klaminder, J., and Martínez-Cortizas, A. (2014). Metal and organic matter immobilization in temperate podzols: A high resolution study. *Geoderma*, 217:225–234.
- Fick, A. (1855). Ueber diffusion. *Annalen der Physik*, 170(1):59–86.
- Fitts, C. R. (2002). *Groundwater science*. Academic Press.
- Grand, S. and Lavkulich, L. M. (2011). Depth distribution and predictors of soil organic carbon in podzols of a forested watershed in southwestern canada. *Soil Science*, 176(4):164–174.

- Guggenberger, G. and Kaiser, K. (2003). Dissolved organic matter in soil: challenging the paradigm of sorptive preservation. *Geoderma*, 113(3):293–310.
- Gustafsson, J. P., Berggren, D., Simonsson, M., Zysset, M., and Mulder, J. (2001). Aluminium solubility mechanisms in moderately acid bs horizons of podzolized soils. *European Journal of Soil Science*, 52(4):655–665.
- Ham, P. A., Schotting, R. J., Prommer, H., and Davis, G. B. (2004). Effects of hydrodynamic dispersion on plume lengths for instantaneous bimolecular reactions. *Advances in water resources*, 27(8):803–813.
- Ham, P. A. S. (2006). Dispersion controlled natural attenuation: The role of conservative plume characteristics in reactive mixing processes.
- Holm, J. (2000). *Effect of biomass growth on the hydrodynamic properties of groundwater aquifers*. Department of Hydrodynamics and Hydraulic Engineering, Technical University of Denmark.
- Jankowski, M. (2014). The evidence of lateral podzolization in sandy soils of northern poland. *Catena*, 112:139–147.
- Jansen, B., Kotte, M. C., van Wijk, A. J., and Verstraten, J. M. (2001). Comparison of diffusive gradients in thin films and equilibrium dialysis for the determination of al, fe (iii) and zn complexed with dissolved organic matter. *Science of the total environment*, 277(1):45–55.
- Jansen, B., Mulder, J., and Verstraten, J. M. (2003). Organic complexation of al and fe in acidic soil solutions: Comparison of diffusive gradients in thin films analyses with models v and vi predictions. *Analytica chimica acta*, 498(1):105–117.
- Jansen, B., Nierop, K., and Verstraten, J. (2004). Mobilization of dissolved organic matter, aluminium and iron in podzol eluvial horizons as affected by formation of metal-organic complexes and interactions with solid soil material. *European journal of soil science*, 55(2):287–297.
- Jansen, B., Nierop, K., and Verstraten, J. (2005). Mechanisms controlling the mobility of dissolved organic matter, aluminium and iron in podzol b horizons. *European journal of soil science*, 56(4):537–550.

- Kaczorek, D., Sommer, M., Andruschkewitsch, I., Oktaba, L., Czerwinski, Z., and Stahr, K. (2004). A comparative micromorphological and chemical study of “raseneisenstein” (bog iron ore) and “ortstein”. *Geoderma*, 121(1):83–94.
- Kalbitz, K., Solinger, S., Park, J.-H., Michalzik, B., and Matzner, E. (2000). Controls on the dynamics of dissolved organic matter in soils: a review. *Soil science*, 165(4):277–304.
- Kinniburgh, D. G., Milne, C. J., Benedetti, M. F., Pinheiro, J. P., Filius, J., Koopal, L. K., and Van Riemsdijk, W. H. (1996). Metal ion binding by humic acid: application of the nica-donnan model. *Environmental Science & Technology*, 30(5):1687–1698.
- Kinniburgh, D. G., van Riemsdijk, W. H., Koopal, L. K., Borkovec, M., Benedetti, M. F., and Avena, M. J. (1999). Ion binding to natural organic matter: competition, heterogeneity, stoichiometry and thermodynamic consistency. *Colloids and Surfaces A: Physicochemical and Engineering Aspects*, 151(1):147–166.
- Koopal, L., Saito, T., Pinheiro, J., and Van Riemsdijk, W. (2005). Ion binding to natural organic matter: General considerations and the nica–donnan model. *Colloids and Surfaces A: Physicochemical and Engineering Aspects*, 265(1):40–54.
- Leon van Paassen, L. A. (2009). *Biogrout, ground improvement by microbial induced carbonate precipitation*. TU Delft, Delft University of Technology.
- Lundström, U. (1993). The role of organic acids in the soil solution chemistry of a podzolized soil. *Journal of Soil Science*, 44(1):121–133.
- Lundström, U. S., van Breemen, N., and Bain, D. (2000a). The podzolization process. a review. *Geoderma*, 94(2):91–107.
- Lundström, U. v., Van Breemen, N., Bain, D., Van Hees, P., Giesler, R., Gustafsson, J. P., Ilvesniemi, H., Karlton, E., Melkerud, P.-A., Olsson, M., et al. (2000b). Advances in understanding the podzolization process resulting from a multidisciplinary study of three coniferous forest soils in the nordic countries. *Geoderma*, 94(2):335–353.
- Manunza, B., Deiana, S., Maddau, V., Gessa, C., and Seeber, R. (1995). Stability constants of metal-humate complexes: titration data analyzed by bimodal gaussian distribution. *Soil Science Society of America Journal*, 59(6):1570–1574.

- Matilainen, A., Vepsäläinen, M., and Sillanpää, M. (2010). Natural organic matter removal by coagulation during drinking water treatment: A review. *Advances in Colloid and Interface Science*, 159(2):189–197.
- Meyers, P. A. (1994). Preservation of elemental and isotopic source identification of sedimentary organic matter. *Chemical Geology*, 114(3):289–302.
- Michaelis, L. and Menten, M. L. (1913). Die kinetik der invertinwirkung. *Biochem. z.*, 49(333-369):352.
- Miikki, V., Senesi, N., and Hänninen, K. (1997). Characterization of humic material formed by composting of domestic and industrial biowastes: Part 2 spectroscopic evaluation of humic acid structures. *Chemosphere*, 34(8):1639–1651.
- Milligan, T. G. and Hill, P. (1998). A laboratory assessment of the relative importance of turbulence, particle composition, and concentration in limiting maximal floc size and settling behaviour. *Journal of Sea Research*, 39(3):227–241.
- Milne, C. J., Kinniburgh, D. G., and Tipping, E. (2001). Generic nica-donnan model parameters for proton binding by humic substances. *Environmental science & technology*, 35(10):2049–2059.
- Milne, C. J., Kinniburgh, D. G., Van Riemsdijk, W. H., and Tipping, E. (2003). Generic nica-donnan model parameters for metal-ion binding by humic substances. *Environmental Science & Technology*, 37(5):958–971.
- Mitchell, A. C., Phillips, A., Schultz, L., Parks, S., Spangler, L., Cunningham, A. B., and Gerlach, R. (2013). Microbial caco 3 mineral formation and stability in an experimentally simulated high pressure saline aquifer with supercritical co 2. *International Journal of Greenhouse Gas Control*, 15:86–96.
- Mokma, D. and Buurman, P. (1987). Podzols and podzolization in temperate regions. *Soil Science*, 144(1):79.
- Monod, J. (1942). Recherches sur la croissance des cultures bacteriennes. *Herman et cie*, pages 371–394.
- Moore, T. (1997). Dissolved organic carbon: sources, sinks, and fluxes and role in the soil carbon cycle. *Soil processes and the carbon cycle*, 11:281.

- Nierop, K. G., Jansen, B., and Verstraten, J. M. (2002). Dissolved organic matter, aluminium and iron interactions: precipitation induced by metal:carbon ratio, pH and competition. *The science of the total environment*, 300:201–211.
- Nikanos. Bodenprofil heide.
- Oude Essink, G., Van Baaren, E. S., and De Louw, P. G. (2010). Effects of climate change on coastal groundwater systems: A modeling study in the netherlands. *Water Resources Research*, 46(10).
- Petersen, L. (1976). *Podzols and podzolization*. DSR forlag Copenhagen.
- Pinder, G. F. and Celia, M. A. (2006). *Subsurface hydrology*. John Wiley & Sons.
- Plankey, B. J. and Patterson, H. H. (1987). Kinetics of aluminum-fulvic acid complexation in acidic waters. *Environmental science & technology*, 21(6):595–601.
- Pott, J., Aalbers, J., and Elzerman, A. (1984). The influence of pH on the binding capacity of Al and naturally occurring organic matter. *Chemical Geology*, 48:293–304.
- Reemtsma, T., These, A., Springer, A., and Linscheid, M. (2008). Differences in the molecular composition of fulvic acid size fractions detected by size-exclusion chromatography–on line fourier transform ion cyclotron resonance (fticr–) mass spectrometry. *Water research*, 42(1):63–72.
- Sauer, D., Sponagel, H., Sommer, M., Giani, L., Jahn, R., and Stahr, K. (2007). Podzol: soil of the year 2007. a review on its genesis, occurrence, and functions. *Journal of Plant Nutrition and Soil Science*, 170(5):581–597.
- Scheel, T., B., J., Verstraten, J., Kalbitz, K., and van Wijk, A. (2008a). Stabilization of dissolved organic matter by aluminium: a toxic effect or stabilization through precipitation? *European journal of soil science*, 59:1122–1132.
- Scheel, T., Dorfler, C., and Kalbitz, K. (2007). Precipitation of dissolved organic matter by aluminum stabilizes carbon in acidic forest soils. *Soil Chemistry*, 71:64–74.
- Scheel, T., L., H., Ellerbrock, R., Rühlmann, J., and Kalbitz, K. (2008b). Properties of organic matter precipitated from acidic forest soil solutions. *Organic Geochemistry*, 39:1439–1453.

- Scheel, T., Ptirsch., K., Schloter, M., and Kalbitz, K. (2008c). Precipitation of enzymes and organic matter by aluminum - impacts on carbon mineralization. *Soil Science*, 171:900–907.
- Seifert, D. and Engesgaard, P. (2007). Use of tracer tests to investigate changes in flow and transport properties due to bioclogging of porous media. *Journal of contaminant hydrology*, 93(1):58–71.
- Sharp, E., Banks, J., Billica, J., Gertig, K., Henderson, R., Parsons, S., Wilson, D., and Jefferson, B. (2005). Application of zeta potential measurements for coagulation control: pilot-plant experiences from uk and us waters with elevated organics. *Water Supply*, 5(5):49–56.
- Short, M., Higdon, D., Guadagnini, L., Guadagnini, A., Tartakovsky, D. M., et al. (2010). Predicting vertical connectivity within an aquifer system. *Bayesian Analysis*, 5(3):557–581.
- Stevenson, F. (1976). Stability constants of Cu^{2+} , Pb^{2+} , and Cd^{2+} complexes with humic acids. *Soil Science Society of America Journal*, 40(5):665–672.
- Stevenson, F., Fitch, A., and Brar, M. (1993). Stability constants of $\text{Cu}^{(ii)}$ -humate complexes: comparison of select models. *Soil Science*, 155(2):77–91.
- Stewart, T. L. and Scott Fogler, H. (2002). Pore-scale investigation of biomass plug development and propagation in porous media. *Biotechnology and bioengineering*, 77(5):577–588.
- Stosser, E. (2010). Methods for determination of labile soil organic matter: An overview. *Journal of argobiology*, 27:49–60.
- Temminghoff, E., Zee, S., and Haan, d. F. (1998). Effects of dissolved organic matter on the mobility of copper in a contaminated sandy soil. *European Journal of Soil Science*, 49(4):617–628.
- Thullner, M. (2010). Comparison of bioclogging effects in saturated porous media within one-and two-dimensional flow systems. *Ecological Engineering*, 36(2):176–196.
- Thurman, E. M. (2012). *Organic geochemistry of natural waters*, volume 2. Springer Science & Business Media.

- Tipping, E. (1994). Whamc—a chemical equilibrium model and computer code for waters, sediments, and soils incorporating a discrete site/electrostatic model of ion-binding by humic substances. *Computers & Geosciences*, 20(6):973–1023.
- Tipping, E. (1998). Humic ion-binding model vi: an improved description of the interactions of protons and metal ions with humic substances. *Aquatic geochemistry*, 4(1):3–47.
- Tipping, E. (2002). *Cation binding by humic substances*, volume 12. Cambridge University Press.
- Tipping, E., Lofts, S., and Sonke, J. (2011). Humic ion-binding model vii: a revised parameterisation of cation-binding by humic substances. *Environmental Chemistry*, 8(3):225–235.
- Van Dijk, H. (1971). Cation binding of humic acids. *Geoderma*, 5(1):53–67.
- van Hees, P., Lundström, U., Starr, M., and Giesler, R. (2000). Factors influencing aluminium concentrations in soil solution from podzols. *Geoderma*, 94(2):289–310.
- Vandevivere, P. and Baveye, P. (1992). Effect of bacterial extracellular polymers on the saturated hydraulic conductivity of sand columns. *Applied and Environmental Microbiology*, 58(5):1690–1698.
- Veeken, A., Nierop, K., de Wilde, V., and Hamelers, B. (2000). Characterisation of naoh-extracted humic acids during composting of a biowaste. *Bioresource Technology*, 72(1):33–41.
- Weng, L. (2002). *Interactions between metal ions and biogeo-surfaces in soil and water: basis for quantitative risk assessment*. publisher not identified.
- Wesolowski, D. J. and Palmer, D. A. (1994). Aluminum speciation and equilibria in aqueous solution: V. gibbsite solubility at 50 c and ph 3–9 in 0.1 molal nacl solutions (a general model for aluminum speciation; analytical methods). *Geochimica et Cosmochimica Acta*, 58(14):2947–2969.
- Zsolnay, A. (2003). Dissolved organic matter: artefacts, definitions, and functions. *Geoderma*, 113(3):187–209.
- Zumdahl, S. and DeCoste, D. J. (2012). *Chemical principles*. Cengage Learning.